NTNU – Trondheim
Norwegian University of
Science and Technology

Viscoelastic response of hydrogel materials at finite strains

Martin Johannessen Skovly

Civil and Environmental Engineering
Submission date: June 2015
Supervisor: Victorien Emile Prot, KT
Co-supervisor: Bjørn Skallerud, KT

Norwegian University of Science and Technology
Department of Structural Engineering

Department of Structural Engineering
Faculty of Engineering Science and Technology
NTNU- Norwegian University of Science and Technology

ACCESSIBILITY

OPEN

MASTER THESIS 2015

SUBJECT AREA:	DATE:	NO. OF PAGES:
Biomechanical Engineering	June 4, 2015	77+7

TITLE:

Viscoelastic response of hydrogel materials at finite strains

BY: Martin Johannessen Skovly

SUMMARY:
Hydrogel materials are very soft materials consisting of polymer networks and solvent molecules. The materials may exhibit large volume changes depending on its external chemical and mechanical environment and have viscoelastic properties which is common for many polymeric materials. In order to model the material response with the finite element method, a hydrogel constitutive model have been combined with finite viscoelastic theory and the resulting viscoelastic hydrogel constitutive model have been coded in a UMAT-subroutine for analysis with the ABAQUS/Standard finite element modeling software. Material parameters have been extracted from a hydrogel relaxation experiment, and while the experimental data is variable, the constitutive model have successfully been able to mimic the viscoelastic material response shown in the experimental data.

The Neo-Hookean and Yeoh hyperelastic models have also been combined with finite viscoelastic theory in order to model compression experiments performed on acrylic Ugelstad particles. The material models were not able to model the complex force-deflection curve shown in the experimental data and some different hyperelastic models should be considered in order to properly model the material.

The constitutive models have been numerically tested, with finite element creep and relaxation tests, which show that the models are numerically stable at large deformations.

RESPONSIBLE TEACHER: Associate Professor Victorien E. Prot

SUPERVISOR(S): Victorien E. Prot, Bjørn Skallerud

CARRIED OUT AT: Department of Structural Engineering, NTNU

To my always supportive family

Abstract

Hydrogel materials are very soft materials consisting of polymer networks and solvent molecules. The materials may exhibit large volume changes depending on its external chemical and mechanical environment and have viscoelastic properties which is common for many polymeric materials. In order to model the material response with the finite element method, a hydrogel constitutive model have been combined with finite viscoelastic theory and the resulting viscoelastic hydrogel constitutive model have been coded in a UMAT-subroutine for analysis with the ABAQUS/*Standard* finite element modeling software. Material parameters have been extracted from a hydrogel relaxation experiment, and while the experimental data is variable, the constitutive model have successfully been able to mimic the viscoelastic material response shown in the experimental data.

The Neo-Hookean and Yeoh hyperelastic models have also been combined with finite viscoelastic theory in order to model compression experiments performed on acrylic Ugelstad particles. The material models were not able to model the complex force-deflection curve shown in the experimental data and some different hyperelastic models should be considered in order to properly model the material.

The constitutive models have been numerically tested, with finite element creep and relaxation tests, which show that the models are numerically stable at large deformations.

Sammendrag

Hydrogel materialer er svært myke materialer som består av polymerkjeder og væske med oppløste partikler. Materialet responderer med store volumforandringer avhengig av ytre kjemisk og mekanisk miljø, og har viskoelastiske egenskaper som er vanlig for enkelte polymerer. For å modellere responsen til materialet med elementmetoden, har en hydrogel materialmodell blitt kombinert med viskoelastisk teori og den resulterende viskoelastiske materialmodellen har blitt kodet som en *UMAT-subroutine* til bruk med elementmodelleringsprogrammet ABAQUS/*Standard*. Materialparametere har blitt tilpasset til et relaksjonsforsøk av et hydrogelmateriale, og selv om de eksperimentelle dataene er variable, har det blitt vist at materialmodellen klarer å modellere responsen vist i de eksperimentelle dataene.

Neo-Hookean og Yeoh hyperelastiske modeller har også blitt kombinert med viskoelastisk teori for å modellere et kompresjonsforsøk gjort på Ugelstadpartikler av akryl. Materialmodellene klarte ikke å modellere den komplekse kraft-forskyvningsrepsonsen fra eksperimentet og en annen hyperelastisk modell er nødvendig for å modellere materialet.

Materialmodellene har blitt testet numerisk med kryp- og relaksjonstester, ved hjelp av elementmetoden, som viser at modellene er numerisk stabile ved store deformasjoner.

Table of Contents

List of Tables

List of Figures

Abbreviations

H_0	=	Reference configuration
H_1	=	Spatial configuration
$\boldsymbol{X}$	=	Material point vector at H_0
$\boldsymbol{x}$	=	Material point vector at H_1
$\boldsymbol{E}_A$	=	Cartesian basis vector at H_0
$\boldsymbol{e}_A$	=	Cartesian basis vector at H_1
$\boldsymbol{u}$	=	Displacement vector
$\boldsymbol{F}$	=	Deformation gradient
$\boldsymbol{\varphi}(\boldsymbol{X})$	=	Deformation map function
$\boldsymbol{R}$	=	Rotational tensor
$\boldsymbol{U}$	=	Right stretch tensor
$\boldsymbol{V}$	=	Left stretch tensor
J	=	Determinant of $\boldsymbol{F}$, $det(\boldsymbol{F})$
$\boldsymbol{C}$	=	Right Cauchy-Green strain tensor
$\boldsymbol{b}$	=	Left Cauchy-Green strain tensor
$\boldsymbol{E}$	=	Green-Lagrange strain tensor
$\boldsymbol{N}_A$	=	Reference principal directions
$\boldsymbol{n}_A$	=	Spatial principal directions
$\boldsymbol{I}$	=	Identity tensor
δ_{ij}	=	Identity tensor on component form
$\|\|\boldsymbol{x}\|\|$	=	Euclidean norm
I_1, I_2, I_3	=	First, second and third invariant of $\boldsymbol{C}$ and $\boldsymbol{b}$
$\boldsymbol{V}$, $\boldsymbol{v}$	=	Material and spatial velocity
G, κ	=	Shear and bulk modulus
$\boldsymbol{l}$	=	Velocity gradient
$\boldsymbol{d}$	=	Rate of deformation tensor
$\boldsymbol{w}$	=	Spin tensor
$\boldsymbol{Q}$	=	Orthogonal tensor
W	=	Mechanical work
U	=	Strain energy function
$\boldsymbol{P}$	=	First Piola-Kirchhoff stress tensor
$\boldsymbol{S}$	=	Second Piola-Kirchhoff stress tensor
$\boldsymbol{\tau}$	=	Kirchhoff stress tensor
$\boldsymbol{\sigma}$	=	Cauchy stress tensor
$\mathbb{C}$	=	Material tangent modulus
$\mathbb{c}$	=	Spatial tangent modulus
$\mathbb{C}^{\Delta J}$	=	Jaumann tangent modulus
$\mathbb{C}^{ABA}$	=	UMAT tangent modulus
$\bar{\boldsymbol{F}}$	=	Isochoric deformation gradient
$\bar{\boldsymbol{b}}$	=	Isochoric left Cauchy-Green strain tensor

$\boldsymbol{F}_e, \boldsymbol{F}_i$	=	Elastic and inelastic part of the deformation gradient
$\mathbb{I}^{SYM}$	=	Fourth order symmetric identity tensor
$\boldsymbol{r}, \boldsymbol{K}$	=	Local Newton method residual vector and tangent matrix
$\boldsymbol{C}^{ALG}$	=	Algorithmic tangent modulus
η	=	Viscosity
τ	=	Relaxation time
β	=	Material scaling parameter
$\boldsymbol{\pounds}_{\boldsymbol{v}}(\ )$	=	Lie rate
$\lambda^{(0)}$	=	Initial swelling
μ^*	=	Normalized chemical potential
ν	=	Poisson's ratio

Chapter 1

Introduction

Viscoelastic response is a common property of many polymeric materials. While most viscoelastic theories developed are linear with the viscoelastic internal variables close to thermodynamic equilibrium such as Bonet (2001) and Lubliner (1985) the theory developed by Reese and Govindjee (1998) allows large perturbations away from thermodynamic equilibrium described as *finite viscoelasticity* (FV). In this thesis the theory of finite viscoelasticity have been combined with some common finite strain (hyperelastic) material models such as the Neo-Hookean material model and the Yeoh material model as well as the hydrogel material model developed by Kang and Huang (2010).

A hydrogel material is a material consisting of polymer networks and water molecules known to undergo large reversible swelling deformations due to diffusion of solvent molecules in the gel. Due to the materials high sensibility to external change, such as change in pH, pressure and temperature, it may be used in Biotechnology and Medicine for a wide range of applications such as drug delivery and mimicking bio-tissue Galaev and Mattiasson (1999).

Hydrogel materials shows two modes of viscoelastic effects as discussed in Hong et al. (2008), Gentile et al. (2013) and Urayama and Takigawa (2012) with a short time relaxation effect explained by the local rearrangement of the polymer molecules and a long time volume changing effect due to the diffusion of solvent molecules in the gel. This motivates the development of a stable FV hydrogel material model for finite element implementation.

The main goal of this thesis is to implement a stable viscoelastic hydrogel model for finite element modeling which may be used to model and if possible fit the material parameters to experimental data. The Neo-Hookean and Yeoh material models which have been implemented have been used to test the FV model and to model a nano-indentation experiment performed at the NTNU Nanomechanical Lab. The material models described in this thesis have been implemented as user-defined subroutines (UMAT) for use with the ABAQUS/*Standard* finite element modeling software.

1.1 Mathematical notation

The following notation is used in the next chapters:

Small bold letter $\boldsymbol{a}$	=	Vectors and 2-tensors (3x3 matrix) in the *spatial configuration*
Large bold letter $\boldsymbol{A}$	=	Vectors and 2-tensors in the *reference configuration*
$\boldsymbol{a} \cdot \boldsymbol{b}$ (a,b = vector)	=	$a_i b_i$
$\boldsymbol{a} \otimes \boldsymbol{b}$ (a,b = vector)	=	$a_i b_j \boldsymbol{E_i} \otimes \boldsymbol{E_j}$
$\boldsymbol{A} \cdot \boldsymbol{B}$ (A,B = 2-Tensor)	=	$A_{ik} B_{kj} \boldsymbol{E_i} \otimes \boldsymbol{E_j}$
$\boldsymbol{A} \cdot \boldsymbol{b}$ (A = 2-Tensor, b = vector)	=	$A_{ij} b_j \boldsymbol{E_i}$
$\boldsymbol{A} \otimes \boldsymbol{B}$ (A,B = 2-Tensor)	=	$A_{ij} B_{kl} \boldsymbol{E_i} \otimes \boldsymbol{E_j} \otimes \boldsymbol{E_k} \otimes \boldsymbol{E_l}$
$\mathbb{C} = C_{ijkl} \boldsymbol{E_i} \otimes \boldsymbol{E_j} \otimes \boldsymbol{E_k} \otimes \boldsymbol{E_l}$	=	4-tensor

Table 1.1: Mathematical notation of tensors and vectors.

with the Einstein summation convention employed such that

$$\boldsymbol{a} \cdot \boldsymbol{b} = a_i b_i \Longleftrightarrow \boldsymbol{a} \cdot \boldsymbol{b} = \sum_{i=1}^{3} a_i b_i$$

$\boldsymbol{E_A}$ and $\boldsymbol{e_A}$ (A=1,2,3) are the cartesian basis vectors in the reference and spatial configuration defined in chapter 2, $\cdot$ and $\otimes$ is the *inner* and *outer dot product* and the 2-tensor and 4-tensor is tensors which may be represented by a 2-dimensional or 4-dimensional array. The notation chosen with bold upper- or lower-case letters have been chosen to separate tensors in the two configurations and it will be made clear in the following chapters if a mathematical object is a vector or a tensor.

Chapter 2

Theory

In this chapter the basic concepts of Continuum Mechanics, Hyperelasticity and Viscoelasticity are summarized. The content of the sections of Continuum Mechanics and Hyperelasticity are largely based on the lecture notes provided by Professor F. Armero (2014) for his course in *Structural Mechanics* I attended during my year as an exchange student at UC Berkeley and Slaughter (2002). Some other useful resources have been Marsden and Hughes (1994); Ogden (1997); Gurtin (1982) and the website continuummechanics.org made by McGinty (published date unknown). The section about Viscoelasticity are based on the article by Reese and Govindjee (1998) and Tschoegl (2012). This chapter is meant as a brief summary of the theory of the mechanics of viscoelastic materials under finite strains. The cited resources contains a more detailed and rigorous explanation of the contents.

2.1 Introduction to Continuum Mechanics

Continuum Mechanics is the theory describing finite deformations in continua. Mathematically a continuum is defined as a continuous compact metric space while for practical purposes we are describing smooth solids or confined liquids. The continuum mechanics of isotropic solids will be covered in this chapter.

Suppose a 3D-body $\mathbb{B}$ in $\mathbb{R}^3$ where H_0 denotes the undeformed state or the *reference configuration* of $\mathbb{B}$ while H_1 is the deformed state or the *spatial configuration* of $\mathbb{B}$. Introducing the Cartesian coordinate system $\{\boldsymbol{E_1}, \boldsymbol{E_2}, \boldsymbol{E_3}\} \in \mathbb{R}^3$ for the reference configuration allows any point in $\mathbb{B}$ at state H_0 to be described by the vector

$$\boldsymbol{X} = X_1\boldsymbol{E_1} + X_2\boldsymbol{E_2} + X_3\boldsymbol{E_3} = X_A\boldsymbol{E_A} \tag{2.1}$$

where $\boldsymbol{X} \in \mathbb{B}$ is the material points of the continuum. Choosing a different Cartesian coordinate system $\{\boldsymbol{e_1}, \boldsymbol{e_2}, \boldsymbol{e_3}\} \in \mathbb{R}^3$ for the spatial configuration leads to the material points at state H_1 being described by the vector

$$\boldsymbol{x} = x_1\boldsymbol{e_1} + x_2\boldsymbol{e_2} + x_3\boldsymbol{e_3} = x_A\boldsymbol{e_A}. \tag{2.2}$$

For simplicity the basis of the two configuration will be chosen to be similar such that $\boldsymbol{E}_A = \boldsymbol{e}_a$ $(A = a = 1, 2, 3)$ in this chapter.

The deformation of $\mathbb{B}$ is described by the mapping $\boldsymbol{\varphi} : \mathbb{B} \to \mathbb{R}^3$ which transforms a particles position in H_0 to its position in H_1 such that $\boldsymbol{x} = \boldsymbol{\varphi}(\boldsymbol{X})$. The inverse mapping is given by $\boldsymbol{X} = \boldsymbol{\varphi}^{-1}(\boldsymbol{x})$. Further the displacement of a point from H_0 to H_1 is defined as $\boldsymbol{u}(\boldsymbol{X}) = \boldsymbol{x}(\boldsymbol{X}) - \boldsymbol{X}$.

Let the curve C describe the material line passing through the material point $\boldsymbol{X}$. The tangent vector to the curve is then $d\boldsymbol{X}$. Similarly the the tangent to the curve c passing the point $\boldsymbol{x}$ in the spatial configuration has the tangent vector $d\boldsymbol{x}$. It can then be shown the following relation between the two tangent vectors,

$$d\boldsymbol{x} = \boldsymbol{F} d\boldsymbol{X}, \tag{2.3}$$

where $\boldsymbol{F}$ is the *deformation gradient* defined as

$$\boldsymbol{F} = \frac{\partial \boldsymbol{\varphi}}{\partial \boldsymbol{X}} = \frac{\partial \boldsymbol{x}}{\partial \boldsymbol{X}}. \tag{2.4}$$

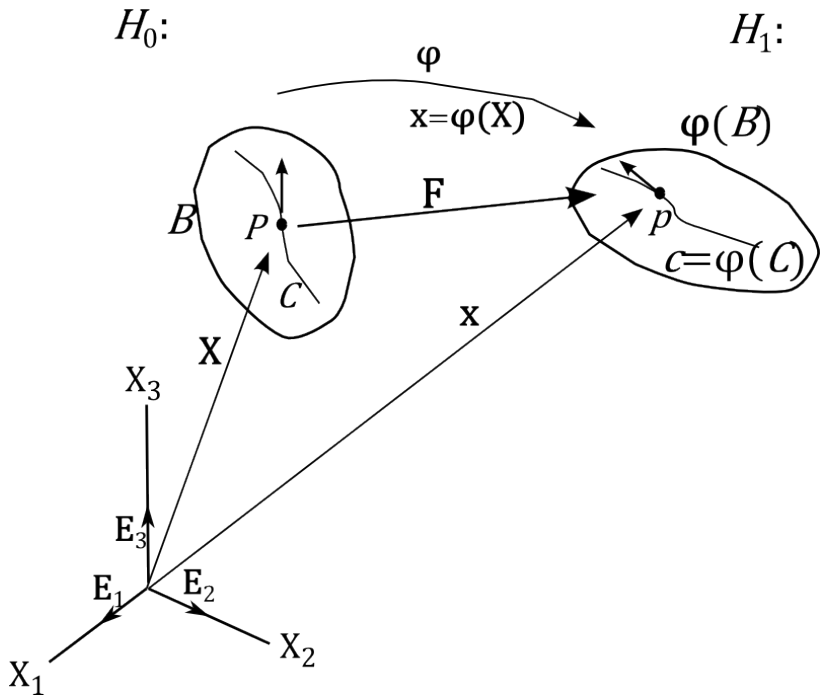

Figure 2.1: Sketch of the deformation of a solid continuum.

2.1.1 Polar Decomposition

According to the Polar Decomposition Theorem the deformation gradient $\boldsymbol{F}$ may be decomposed such that

$$\boldsymbol{F} = \boldsymbol{R} \cdot \boldsymbol{U} = \boldsymbol{V} \cdot \boldsymbol{R} \tag{2.5}$$

with $\boldsymbol{R}$ being the rotational tensor while $\boldsymbol{U}$ and $\boldsymbol{V}$ is the *right* and *left stretch tensors*.

The interpretation of this is that the deformation may be decomposed into a rigid body movement, which produces no strains, and stretching which causes strains in $\mathbb{B}$. Note that $\boldsymbol{R}$ is an orthogonal tensor such that $\boldsymbol{R}\boldsymbol{R}^T = \mathbf{1}$ and the stretch tensors are symmetric.

The right stretch tensor $\boldsymbol{U}$ represents the stretch in the reference configuration H_0, while the left stretch tensor $\boldsymbol{V}$ represents the stretch in the spatial configuration H_1 as shown in figure 2.2.

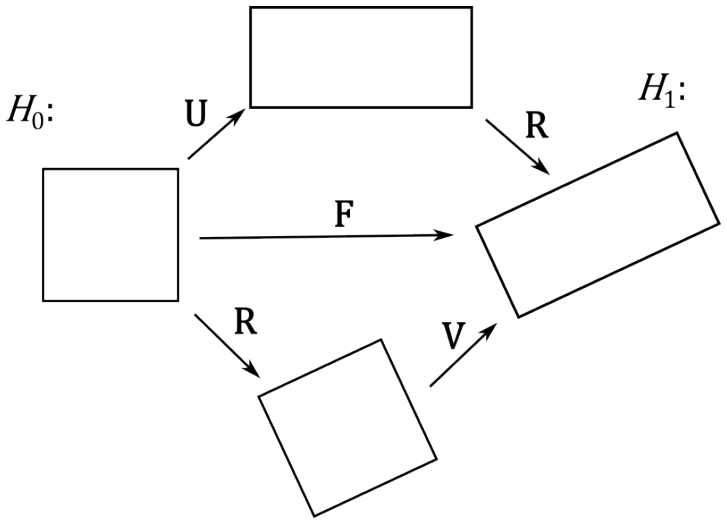

Figure 2.2: Sketch of the Polar Decomposition of the deformation gradient.

The relevance of $\boldsymbol{U}$ and $\boldsymbol{V}$ in terms of strain in the reference and spatial configuration will be described more in depth in the next section.

2.1.2 Volume and area change

Consider the volume dV defined by the three vectors $d\boldsymbol{X}$, $d\boldsymbol{Y}$ and $d\boldsymbol{Z}$ in the reference configuration and the corresponding volume dv defined by the three vectors $d\boldsymbol{x}$, $d\boldsymbol{y}$ and $d\boldsymbol{z}$ in the spatial configuration. dV is then defined as

$$dV = d\boldsymbol{X} \cdot (d\boldsymbol{Y} \times d\boldsymbol{Z}). \tag{2.6}$$

Taking advantage of equation (2.3) the following result is obtained

$$\begin{aligned} dv = d\boldsymbol{x} \cdot (d\boldsymbol{y} \times d\boldsymbol{z}) &= \boldsymbol{F}d\boldsymbol{x} \cdot (\boldsymbol{F}d\boldsymbol{y} \times \boldsymbol{F}d\boldsymbol{z}) \\ = det(\boldsymbol{F})\big(d\boldsymbol{X} \cdot (d\boldsymbol{Y} \times d\boldsymbol{Z})\big) &= det(\boldsymbol{F})dV \\ \Rightarrow\ J = \frac{dv}{dV},\ \ J &:= det(\boldsymbol{F}) \end{aligned}$$

Physically J is the volume change at a point between the reference and the spatial configuration. Another interesting property is that $\boldsymbol{\varphi}$, being a one-to-one mapping of $\mathbb{B}$, implies that the finite volumes must be larger than zero such that

$$J = det\boldsymbol{F} > 0. \tag{2.8}$$

Since $det\boldsymbol{F} > 0$, $\boldsymbol{F}$ is positive definite such that $\boldsymbol{U}$ and $\boldsymbol{V}$ are symmetric positive definite tensors which may be decomposed by the rules of the Spectral Decomposition Theorem. Since $\boldsymbol{F}$ is positive definite, $\boldsymbol{F}$ is also invertible.

The transformation of area from the reference configuration to the spatial configuration (Nanson's formula, Slaughter (2002, chap.3)) may be written as

$$\boldsymbol{n}da = J\boldsymbol{F}^{-\boldsymbol{T}}\boldsymbol{N}dA, \tag{2.9}$$

with $\boldsymbol{n}$ and $\boldsymbol{N}$ being unit normal vectors to the areas da and dA in the spatial and reference configuration.

2.2 Kinematics - Strain and motion

2.2.1 Strain measures

Let dS be the line segment of the curve C passing through $\boldsymbol{X}$ in the reference configuration and ds be the line segment of the corresponding curve c passing through $\boldsymbol{x}$ in the spatial configuration. It may then be shown that

$$(ds)^2 = ||d\boldsymbol{x}||^2 = d\boldsymbol{x} \cdot d\boldsymbol{x} = d\boldsymbol{X} \cdot \boldsymbol{F}^T\boldsymbol{F}d\boldsymbol{X} = d\boldsymbol{X} \cdot \boldsymbol{C}d\boldsymbol{X} = \boldsymbol{N} \cdot \boldsymbol{C}\boldsymbol{N}(dS)^2$$

$$(dS)^2 = ||d\boldsymbol{X}||^2 = d\boldsymbol{X} \cdot d\boldsymbol{X} = d\boldsymbol{x} \cdot \boldsymbol{F}^{-T}\boldsymbol{F}^{-1}d\boldsymbol{x} = d\boldsymbol{x} \cdot (\boldsymbol{F}\boldsymbol{F}^T)^{-1}d\boldsymbol{x} = \boldsymbol{n} \cdot \boldsymbol{b}^{-1}\boldsymbol{n}(ds)^2$$

$$\boldsymbol{N} = \frac{d\boldsymbol{X}}{||d\boldsymbol{X}||} = \frac{d\boldsymbol{X}}{||dS||} \quad \boldsymbol{n} = \frac{d\boldsymbol{x}}{||d\boldsymbol{x}||} = \frac{d\boldsymbol{x}}{||ds||}.$$

With these results we may define the stretch of the continuum in terms of the reference configuration only

$$ds = \sqrt{\boldsymbol{N} \cdot \boldsymbol{C}\boldsymbol{N}}\, dS, \tag{2.11}$$

or in terms of the spatial configuration

$$dS = \sqrt{\boldsymbol{n} \cdot \boldsymbol{b}^{-1}\boldsymbol{n}}\, ds. \tag{2.12}$$

$\boldsymbol{C}$ is the *right Cauchy-Green strain tensor* while $\boldsymbol{b}$ is the *left Cauchy-Green strain tensor*. Using the results from the Polar Decomposition of $\boldsymbol{F}$,

$$\boldsymbol{C} := \boldsymbol{F}^T \cdot \boldsymbol{F} = (\boldsymbol{R} \cdot \boldsymbol{U})^T \cdot (\boldsymbol{R} \cdot \boldsymbol{U}) = \boldsymbol{U}^T \cdot \boldsymbol{U} = \boldsymbol{U} \cdot \boldsymbol{U} \tag{2.13a}$$

$$\boldsymbol{b} := \boldsymbol{F} \cdot \boldsymbol{F}^T = (\boldsymbol{V} \cdot \boldsymbol{R}) \cdot (\boldsymbol{V} \cdot \boldsymbol{R})^T = \boldsymbol{V} \cdot \boldsymbol{V}^T = \boldsymbol{V} \cdot \boldsymbol{V} \tag{2.13b}$$

it is clear that as $\boldsymbol{U}$ is a tensor in the reference configuration $\boldsymbol{C}$ is also a tensor in the reference configuration also called a *material tensor*. Similarly as $\boldsymbol{V}$ is a tensor in the spatial configuration $\boldsymbol{b}$ is also a tensor in the spatial configuration. Such tensors are called *spatial tensors*.

2.2.2 Principal stretches and invariants

As both $\boldsymbol{C}$ and $\boldsymbol{b}$ are positive definite symmetric tensors the spectral decomposition theorem states that the tensors may be expressed as

$$\boldsymbol{C} = \sum_{A=1}^{3} \lambda_A^2 (\boldsymbol{N}_A \otimes \boldsymbol{N}_A) \tag{2.14a}$$

$$\boldsymbol{b} = \sum_{A=1}^{3} \lambda_A^2 (\boldsymbol{n}_A \otimes \boldsymbol{n}_A) \tag{2.14b}$$

and equation (2.13a) and (2.13b) may then be reformulated as

$$\boldsymbol{U} = \sqrt{\boldsymbol{C}} = \sum_{A=1}^{3} \lambda_A (\boldsymbol{N}_A \otimes \boldsymbol{N}_A) \tag{2.15a}$$

$$\boldsymbol{V} = \sqrt{\boldsymbol{b}} = \sum_{A=1}^{3} \lambda_A (\boldsymbol{n}_A \otimes \boldsymbol{n}_A). \tag{2.15b}$$

Realizing that $\boldsymbol{R}$ is the rotation at $\boldsymbol{X}$ such that

$$\boldsymbol{n}_A = \boldsymbol{R} \cdot \boldsymbol{N}_A, \;\; (A = 1, 2, 3)$$

and the fact that the set of vectors $\boldsymbol{N}_A$ are orthogonal leads to the following expression for the rotation tensor

$$\boldsymbol{R} = \sum_{A=1}^{3} \boldsymbol{n}_A \otimes \boldsymbol{N}_A. \tag{2.16}$$

Combining equation (2.15a) and (2.16) leads to the following final expression for the deformation gradient

$$\boldsymbol{F} = \boldsymbol{R} \cdot \boldsymbol{U} = \sum_{B=1}^{3} \sum_{C=1}^{3} \lambda_C (\boldsymbol{n}_B \otimes \boldsymbol{N}_B) \cdot (\boldsymbol{N}_C \otimes \boldsymbol{N}_C) = \sum_{A=1}^{3} \lambda_A (\boldsymbol{n}_A \otimes \boldsymbol{N}_A) \tag{2.17}$$

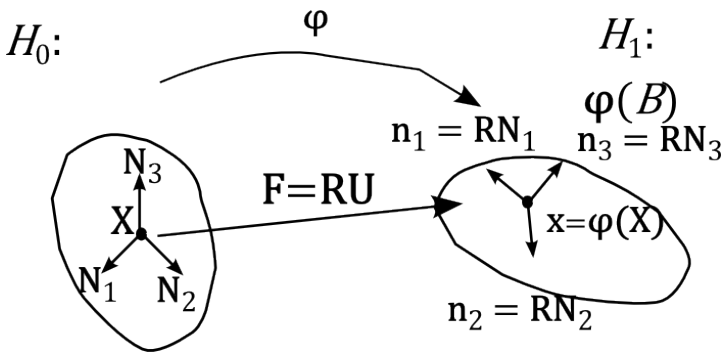

Figure 2.3: Sketch of the reference and spatial principal directions.

The principal stretches can be found by solving for the roots of the characteristic polynomial

$$det\big(\boldsymbol{C} - (\lambda_A^2)\boldsymbol{I}\big) = -(\lambda_A^2)^3 + I_1(\lambda_A^2)^2 - I_2(\lambda_A^2) + I_3 = 0, \tag{2.18}$$

with the invariants defined as

$$I_1 = tr(\boldsymbol{C}) \tag{2.19a}$$

$$I_2 = \frac{1}{2}\Big(tr(\boldsymbol{C})^2 - tr(\boldsymbol{C^2})\Big) \tag{2.19b}$$

$$I_3 = det\boldsymbol{C} = J^2. \tag{2.19c}$$

An important property of the invariants is that $I_A(\boldsymbol{C}) = I_A(\boldsymbol{b})$ which comes from the fact that $\boldsymbol{C}$ and $\boldsymbol{b}$ have the same principal stretches. The invariants in the reference configuration are similar to the invariants in the spatial configuration which is a useful property applied in constitutive theory.

2.2.3 Motion

Introducing time dependence to the change of a particles motion

$$\boldsymbol{x} = \boldsymbol{\varphi}(\boldsymbol{X}, t) \tag{2.20}$$

the *material velocity* may be defined as

$$\boldsymbol{V} := \frac{\partial \boldsymbol{\varphi}(\boldsymbol{X}, t)}{\partial t}\Big|_{\boldsymbol{X}=const.}. \tag{2.21}$$

Noting that $\boldsymbol{X}$ is fixed while $\boldsymbol{x}$ is time dependent, the *spatial velocity* is defined as

$$\boldsymbol{v} := \boldsymbol{v}(\boldsymbol{x}, t) = \boldsymbol{V}\big(\boldsymbol{\varphi}^{-1}(\boldsymbol{x}, t), t\big). \tag{2.22}$$

Both vectors are similar but differs in their depends on $\boldsymbol{X}$ and $\boldsymbol{x}$ respectively although both are defined in the spatial configuration.

The time-derivative of the deformation gradient may be found by applying the chain-rule such that

$$\dot{F}_{iK} = \frac{d}{dt}\frac{\partial x_i}{\partial X_k} = \frac{\partial V_i}{\partial X_k} = \frac{v_i}{x_j}\frac{x_j}{X_k}$$

$$\Rightarrow \dot{\boldsymbol{F}} = \nabla \boldsymbol{v} \cdot \boldsymbol{F}$$

and by defining the *velocity gradient* as $\boldsymbol{l} := \nabla \boldsymbol{v}$ leads to

$$\boldsymbol{l} = \dot{\boldsymbol{F}} \cdot \boldsymbol{F}^{-1} = \boldsymbol{d} + \boldsymbol{w} \tag{2.24a}$$

$$\boldsymbol{d} = \frac{1}{2}(\boldsymbol{l} + \boldsymbol{l}^T) \tag{2.24b}$$

$$\boldsymbol{w} = \frac{1}{2}(\boldsymbol{l} - \boldsymbol{l}^T). \tag{2.24c}$$

The symmetric part, $\boldsymbol{d}$, of $\boldsymbol{l}$ is called the *rate of deformation tensor* while the skew-symmetric part, $\boldsymbol{w}$, is called the *spin tensor*. The rate of deformation tensor and the spin tensor will be used later in describing the constitutive theory in the spatial configuration.

2.2.4 Material and spatial frame indifference

An important concept of continuum mechanics is the change of observer and how it affects, or rather should not affect, the observed deformation in the continuum. Consider two different observers, A and B, observing the following deformation pattern of a body

$$A: \ \boldsymbol{x} = \boldsymbol{\varphi}(\boldsymbol{X}, t) \ \ and \ \ B: \ \boldsymbol{x}^* = \boldsymbol{a}(t) + \boldsymbol{Q}(t) \cdot \boldsymbol{x}$$

where $\boldsymbol{a}(t)$ and $\boldsymbol{Q}(t)$ are an arbitrary translation and rotation from observer A.

To ensure frame indifference the measured deformation observed by the different observers must be similar regardless of $\boldsymbol{a}(t)$ and $\boldsymbol{Q}(t)$. Taking the deformation gradient measured by B

$$\boldsymbol{F}^* = \boldsymbol{Q} \cdot \boldsymbol{F}$$

and applying the polar decomposition such that

$$\boldsymbol{F}^* = \boldsymbol{Q} \cdot (\boldsymbol{R} \cdot \boldsymbol{U}) = (\boldsymbol{Q} \cdot \boldsymbol{R}) \cdot \boldsymbol{U} = \boldsymbol{R}^* \cdot \boldsymbol{U}^*$$

and

$$\boldsymbol{F}^* = \boldsymbol{Q} \cdot (\boldsymbol{V} \cdot \boldsymbol{R}) = (\boldsymbol{Q} \cdot \boldsymbol{V} \cdot \boldsymbol{Q}^T) \cdot (\boldsymbol{Q} \cdot \boldsymbol{R}) = \boldsymbol{V}^* \cdot \boldsymbol{R}^*$$

three requirements for frame indifference is found. As covered earlier $\boldsymbol{U}$ is a material tensor while $\boldsymbol{V}$ is a spatial tensor which imply the following.

A material tensor $\boldsymbol{U}$ is frame indifferent if

$$\boldsymbol{U}^* = \boldsymbol{U} \tag{2.25}$$

and a spatial tensor $\boldsymbol{V}$ is frame indifferent if

$$\boldsymbol{V}^* = \boldsymbol{Q} \cdot \boldsymbol{V} \cdot \boldsymbol{Q}^T. \tag{2.26}$$

Examples of frame indifferent material tensors are the right Cauchy-Green strain tensor $\boldsymbol{C}$ and the second Piola-Kirchhoff stress tensor $\boldsymbol{S}$. Examples of frame indifferent spatial tensors are the left Cauchy-Green strain tensor $\boldsymbol{b}$, the rate of deformation tensor $\boldsymbol{d}$ and the Kirchhoff stress tensor $\boldsymbol{\tau}$.

2.3 Hyperelasticity

Hyperelastic materials are materials undergoing zero internal dissipation during external mechanical work.

Consider a closed process from $t = t_0$ to $t = t_1$ with $\boldsymbol{F}(t_1) = \boldsymbol{F}(t_0)$. The total mechanical work point-wise on a solid as stated by the second law of thermodynamics is

$$W = \int_{t_0}^{t_1} \boldsymbol{P} : \dot{\boldsymbol{F}} \, dt \geq 0. \tag{2.27}$$

Assuming no dissipation leads to

$$W = \int_{t_0}^{t_1} \boldsymbol{P} : \dot{\boldsymbol{F}} \, dt = 0, \quad \boldsymbol{P} = \frac{\partial U(\boldsymbol{F}, \boldsymbol{X})}{\partial \boldsymbol{F}} \tag{2.28}$$

where $\boldsymbol{P}$ is the *first Piola-Kirchoff stress tensor* and $U(\boldsymbol{F}, \boldsymbol{X})$ is the *strain-energy function*.

Equation (2.28) may be modified to include the other frame indifferent material and strain tensors such that

$$W = \int_{t_0}^{t_1} \boldsymbol{\tau} : \boldsymbol{d} \, dt = \int_{t_0}^{t_1} \boldsymbol{P} : \dot{\boldsymbol{F}} \, dt = \int_{t_0}^{t_1} \boldsymbol{S} : \dot{\boldsymbol{E}} \, dt = 0 \tag{2.29}$$

where $\boldsymbol{E}$ is the *Green-Lagrange strain tensor* defined as

$$\boldsymbol{E} = \frac{1}{2}(\boldsymbol{C} - \boldsymbol{I}). \tag{2.30}$$

The second Piola-Kirchoff stress tensor may be expressed in terms of the strain energy function as

$$\boldsymbol{S} = \frac{\partial \breve{U}(\boldsymbol{E}, \boldsymbol{X})}{\partial \boldsymbol{E}} = 2\frac{\partial \tilde{U}(\boldsymbol{C}, \boldsymbol{X})}{\partial \boldsymbol{C}}. \tag{2.31}$$

Note that $U(\boldsymbol{F}, \boldsymbol{X}) = \hat{U}(\boldsymbol{U}, \boldsymbol{X}) = \tilde{U}(\boldsymbol{C}, \boldsymbol{X})$.

2.3.1 Elasticity tensors

In the 3-dimensional case the elasticity tensor takes the form of a constitutive 4-tensor and may be found from the linearized weak form of equilibrium. An example of such a calculation is found in Reese and Govindjee (1998).

In terms of the second Piola-Kirchoff stress tensor $\boldsymbol{S}$ we have

$$\dot{\boldsymbol{S}} = \mathbb{C} : \dot{\boldsymbol{E}}, \quad \dot{S}_{ij} = C_{ijkl}\dot{E}_{kl} \tag{2.32a}$$

$$\mathbb{C} = \frac{\partial \boldsymbol{S}}{\partial \boldsymbol{E}} = 2\frac{\partial \boldsymbol{S}}{\partial \boldsymbol{C}} = 4\frac{\partial^2 \tilde{U}(\boldsymbol{C}, \boldsymbol{X})}{\partial \boldsymbol{C} \partial \boldsymbol{C}}, \quad C_{ijkl} = 2\frac{\partial S_{ij}}{\partial C_{kl}} \tag{2.32b}$$

where $\mathbb{C}$ is the *material tangent modulus*.

The *spatial tangent modulus* $\mathbb{c}$ may be found by performing the push-forward operation (see Appendix C) on the material tangent $\mathbb{C}$ such that

$$J\mathbb{c} = \boldsymbol{F} \cdot \boldsymbol{F} \cdot \mathbb{C} \cdot \boldsymbol{F}^T \cdot \boldsymbol{F}^T. \tag{2.33}$$

The spatial tangent modulus $\mathbb{c}$ have the following relation with the Lie derivative, also known as the Truesdell rate, of the Kirchhoff stress

$$\boldsymbol{\pounds}_{\boldsymbol{v}}\boldsymbol{\tau} = \dot{\boldsymbol{\tau}} - \boldsymbol{l} \cdot \boldsymbol{\tau} - \boldsymbol{\tau} \cdot \boldsymbol{l}^T = J\mathbb{c} : \boldsymbol{d}. \tag{2.34}$$

In the ABAQUS/Standard-module the Jaumann-rate is used, defined as:

$$\boldsymbol{\tau}^{\Delta J} = \dot{\boldsymbol{\tau}} + \boldsymbol{\tau} \cdot \boldsymbol{w} - \boldsymbol{w} \cdot \boldsymbol{\tau} = \mathbb{C}^{\Delta J} : \boldsymbol{d}. \tag{2.35}$$

The Jaumann tangent modulus $\mathbb{C}^{\Delta J}$ can be found from the spatial tangent modulus $\mathbb{c}$ and the Kirchhoff stress tensor $\boldsymbol{\tau}$ by the following calculation

$$\mathbb{C}^{\Delta J} = J(\mathbb{c} + \tilde{\mathbb{C}}) \tag{2.36}$$

$$J\tilde{C}_{ijkl} = \frac{1}{2}(\delta_{ik}\tau_{jl} + \delta_{il}\tau_{jk} + \delta_{jk}\tau_{il} + \delta_{jl}\tau_{ik}). \tag{2.37}$$

Both rates are frame indifferent as shown in appendix C. The tangent modulus used in the ABAQUS/Standard UMAT-subroutine $\mathbb{C}^{ABA}$ is defined as $\frac{1}{J}\mathbb{C}^{\Delta J}$ in the ABAQUS documentation ABAQUS (2013, chap. 1).

2.3.2 Isotropy

A material is isotropic if its mechanical response are independent of the direction. In other words the internal force due to stretching in one directions should be the same even if the material is rotated and applied the same value of stretch. Some important mathematical properties of isotropic tensor functions such as for the Cauchy stress $\boldsymbol{\sigma} = \hat{\boldsymbol{\sigma}}(\boldsymbol{F})$ are (Gurtin, 1982, appendix)

1.

$$\hat{\boldsymbol{\sigma}}(\boldsymbol{F}) = \boldsymbol{R} \cdot \hat{\boldsymbol{\sigma}}(\boldsymbol{U}) \cdot \boldsymbol{R}^T = \hat{\boldsymbol{\sigma}}(\boldsymbol{R} \cdot \boldsymbol{U} \cdot \boldsymbol{R}^T) = \hat{\boldsymbol{\sigma}}(\boldsymbol{V}) = \hat{\boldsymbol{\sigma}}(\boldsymbol{b})$$

2.
$$\boldsymbol{\sigma} = \beta_1 \boldsymbol{I} + \beta_2 \boldsymbol{b} + \beta_3 \boldsymbol{b}^2, \quad \beta_k = f(I_1, I_2, I_3)$$

which shows another important property of isotropic materials in that the principal directions $\boldsymbol{n}_A$ of the Cauchy-stress $\boldsymbol{\sigma}$ and Kirchhoff stress $\boldsymbol{\tau}$ and the left Cauchy-Green strain tensor $\boldsymbol{b}$ are the same. The same property apply for the principal directions $\boldsymbol{N}_A$ of the second Piola-Kirchhoff stress tensor $\boldsymbol{S}$ and right Cauchy-green strain tensor $\boldsymbol{C}$.

2.3.3 Strain Energy Functions

Strain energy functions are fundamental to developing constitutive materials for materials during finite strains. Isotropic strain energy functions are scalar valued functions most commonly represented by the three invariants I_1, I_2 and $I_3 = J^2$, while for anisotropic materials like transversely isotropic materials it is common to define pseudo-invariants to model the material properties in the different directions (Prot et al., 2007). Only isotropic material models have been developed as part of this thesis.

Some common isotropic strain energy functions are:

1. Neo-Hookean material
$$U(I_1, J) = C_1\Big(I_1 - 3 - 2ln(J)\Big) + U(J)$$

2. Yeoh material
$$U(I_1, J) = \sum_{i=1}^{3} C_i(\bar{I}_1 - 3)^i + U(J)$$

3. Generalized Rivlin (polynomial) model
$$U(I_1, I_2, J) = \sum_{i,j=0}^{n} C_{ij}(I_1 - 3)^i(I_2 - 3)^j + U(J)$$

where $U(J)$ is the volumetric part of the strain energy function, with some variants such as

1.
$$U(J) = \tfrac{1}{D_1} ln(J)^2$$

2.
$$U(J) = \tfrac{1}{D_1}\Big((J-1)^2 + ln(J)^2\Big)$$

3.
$$U(J) = \sum_{k=1}^{3} \tfrac{1}{D_k}(J-1)^{2k}$$

where C_i and D_k are material constants related to the deviatoric and volumetric response of the material. For the Neo-Hookean material $2C_1$ and $\frac{2}{D_1}$ are associated with the initial shear modulus G and initial bulk modulus κ of linear elasticity. Another common feature is to decompose the deformation gradient into an *isochoric* and volumetric part. The isochoric formulation of the deformation gradient $\bar{\boldsymbol{F}}$ causes no volumetric change as shown by the definition

$$\bar{\boldsymbol{F}} = J^{-\frac{1}{3}}\boldsymbol{F}, \quad det(\bar{\boldsymbol{F}}) = det(J^{-\frac{1}{3}}\boldsymbol{F}) = J^{-1}J = 1 \tag{2.38}$$

thus the strain energy function U may be written as

$$U = U(I_1, I_2, J) = \tilde{U}(\bar{I}_1, \bar{I}_2) + \tilde{U}(J). \tag{2.39}$$

Strain energy functions with the isochoric-volumetric split $\tilde{U}$ will be characterized as *uncoupled* while the strain energy functions without this split will be characterized as *coupled*.

2.4 Finite Viscoelasticity

This section is a summary of the most important aspects from Reese and Govindjee (1998). While most viscoelastic theories are based on linear evolution laws (response assumed close to thermodynamic equilibrium) the theory described in the article is a non-linear evolution law suitable to describe response away from thermodynamic equilibrium for isotropic materials. To further discuss the concepts viscoelasticity the 1D case of a rheological model and some examples is described first.

2.4.1 Generalized Maxwell model - 1D linear viscoelasticity

In the case of small deformations and 1-dimensional behavior the concept of viscoelasticity may be described by a rheological model such as the generalized Maxwell model (sometimes referred to as the Wiechert Model, Tschoegl (2012, chap. 3)). The model consists of a long-term spring of stiffness K_∞ in parallel with an arbitrary number α of Maxwell elements which consists of a dash-pot of viscosity η_α in series with a spring of stiffness K_α. The deformation of each dash-pot x_α is the unknown variables of the system. Each of the viscous parallel elements force f_α can be expressed in terms of the spring or the rate of change of the internal viscous deformation $\dot{x}_\alpha$ as

$$f_\alpha = \eta_\alpha \dot{x}_\alpha \tag{2.40a}$$

$$f_\alpha = K_\alpha (x - x_\alpha). \tag{2.40b}$$

Equating equation (2.40a) and (2.40b) leads to a evolution equation for x_α

$$\dot{x}_\alpha = \frac{1}{\tau_\alpha}(x - x_\alpha) \tag{2.41}$$

where the *relaxation time* τ_α is introduced which is defined as

$$\tau_\alpha := \frac{\eta_\alpha}{K_\alpha}. \tag{2.42}$$

An illustration of the generalized Maxwell model is shown in figure 2.4.

Equation (2.41) is an ODE which may be solved in the time-domain. To illustrate, equation (2.41) is solved for a ramp function of x of the form

$$x(t) = \begin{cases} a\frac{t}{t_1} & t < t_1 \\ a & t \geq t_1 \end{cases} \tag{2.43}$$

the solution for equation (2.41) is then

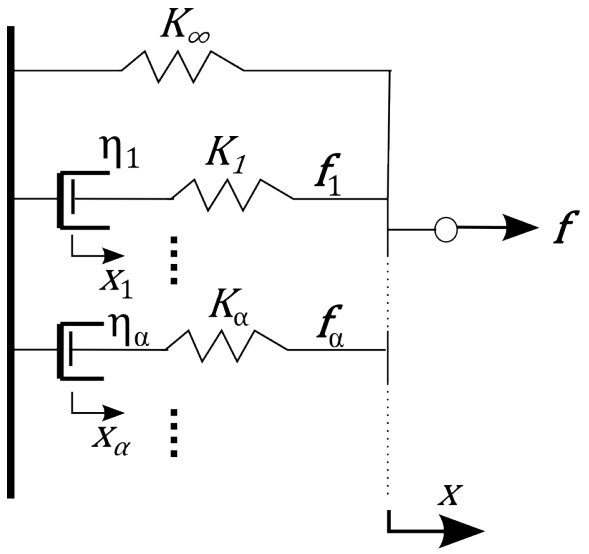

Figure 2.4: Sketch of the Generalized Maxwell model.

$$x_\alpha(t) = \begin{cases} \frac{a}{t_1}(t-\tau_\alpha) + a\frac{\tau_\alpha}{t_1}e^{-\frac{t}{\tau_\alpha}} & t < t_1 \\ \frac{a}{t_1} + a\frac{\tau_\alpha}{t_1}(e^{-\frac{t}{\tau_\alpha}} - e^{\frac{1-t}{\tau_\alpha}}) & t \geq t_1 \end{cases} \tag{2.44}$$

By setting $a = 1$ and $t_1 = 1$, x_α may be plotted for different values of τ_α as seen in figure 2.5. By setting $K_\infty = K_\alpha = 1$ the relaxation effect is apparent as seen in figure 2.6.

Given a ramp-function of the external force of the form

$$f(t) = f_\infty + f_1 = \begin{cases} P\frac{t}{t_1} & t < t_1 \\ P & t \geq t_1 \end{cases} \tag{2.45}$$

with f_1 as the force in a single Maxwell-element and f_∞ as the force in the spring element with stiffness K_∞. The total force in terms of the deformation x and x_1 is

$$f(t) = f_\infty + f_1 = K_\infty x + K_1(x - x_1). \tag{2.46}$$

Combining equation (2.46) with equation(2.41) leads to the following expression in terms of x_1

$$\tau_1(K_\infty + K_1)\dot{x}_1 + K_\infty x_1 - f(t) = 0 \tag{2.47}$$

with the solution in terms of x_1 as

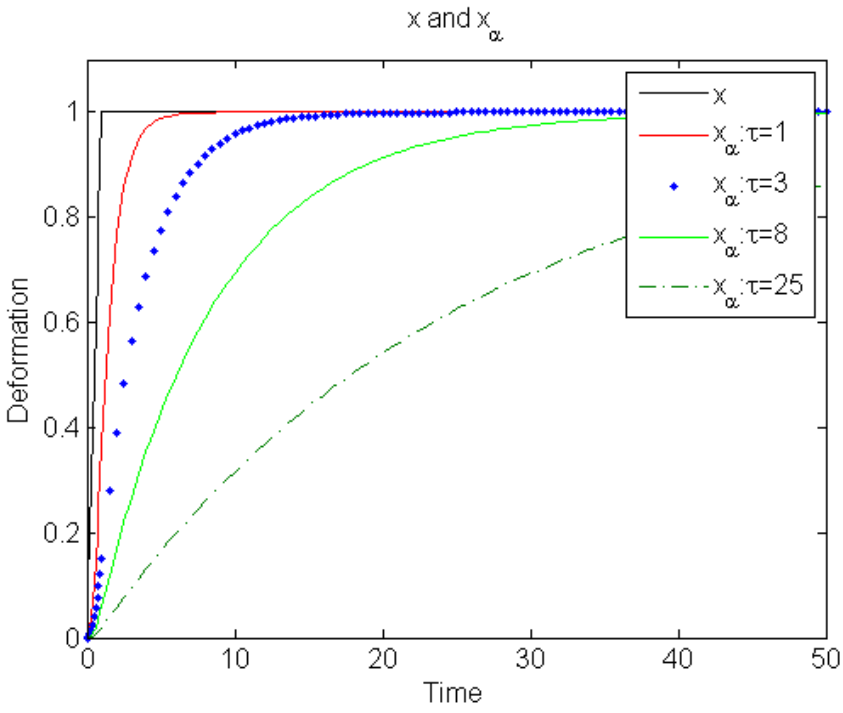

Figure 2.5: Total deformation x and the internal deformation x_α plotted with different values of τ_α.

$$x_1(t) = \begin{cases} \frac{P}{K_\infty}\left(\frac{t}{t_1} - \frac{K_\infty+K_1}{K_\infty}\frac{\tau_1}{t_1} + C_1 \exp\left(-\frac{K_\infty}{K_\infty+K_1}\frac{t}{\tau_1}\right)\right) & t < t_1 \\ \frac{P}{K_\infty}\left(1 + C_2 \exp -\frac{K_\infty}{K_\infty+K_1}\frac{t}{\tau_1}\right) & t \geq t_1 \end{cases} \tag{2.48}$$

As $x_1(t=0) = 0$ the first expression for $t < t_1$ collapse to

$$\frac{P}{K_\infty}\left(\frac{t}{t_1} + \frac{K_\infty + K_1}{K_\infty}\frac{\tau_1}{t_1}\left(\exp\left(-\frac{K_\infty}{K_\infty + K_1}\frac{t}{\tau_1}\right) - 1\right)\right).$$

As both expressions for x_1 must be equal at $t = t_1$, solving for C_2 leads to the final expression for x_1

$$x_1(t) = \begin{cases} \frac{P}{K_\infty}\left(\frac{t}{t_1} + \frac{K_\infty+K_1}{K_\infty}\frac{\tau_1}{t_1}\left(\exp\left(-\frac{K_\infty}{K_\infty+K_1}\frac{t}{\tau_1}\right) - 1\right)\right) & t < t_1 \\ \frac{P}{K_\infty}\left(1 + \frac{K_\infty+K_1}{K_\infty}\frac{\tau_1}{t_1}\left(1 - \exp\left(\frac{K_\infty}{K_\infty+K_1}\frac{t_1}{\tau_1}\right)\right)\exp\left(-\frac{K_\infty}{K_\infty+K_1}\frac{t}{\tau_1}\right)\right) & t \geq t_1 \end{cases} \tag{2.49}$$

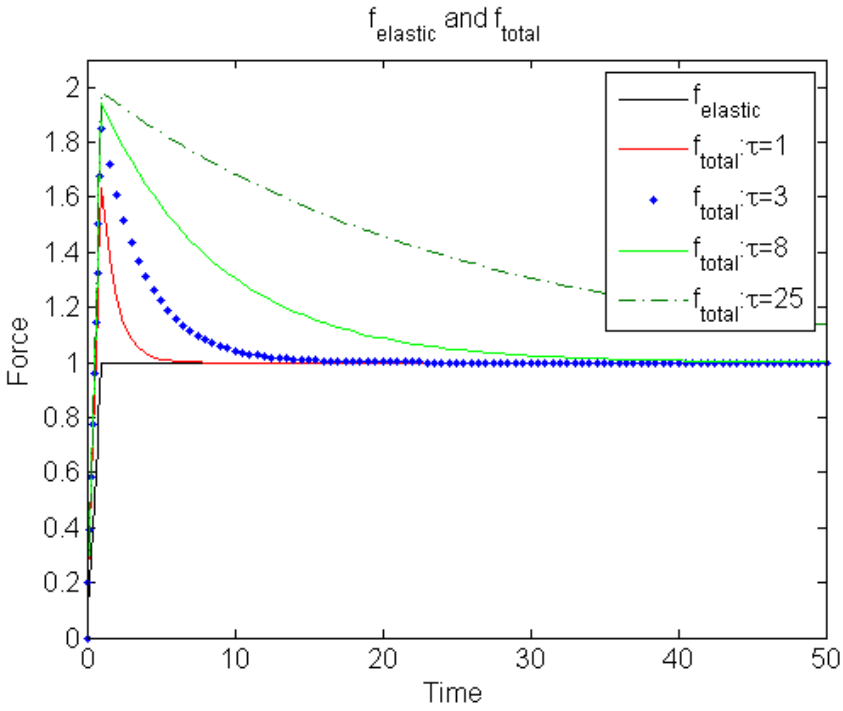

Figure 2.6: Total force f plotted for different values of τ_α.

With the total deformation x defined as

$$x(t) = \frac{K_1}{K_\infty + K_1} x_1(t) + \frac{f(t)}{K_\infty + K_1}$$

$$= \begin{cases} \frac{K_1}{K_\infty + K_1} x_1(t) + \frac{P \frac{t}{t_1}}{K_\infty + K_1} & t < t_1 \\ \frac{K_1}{K_\infty + K_1} x_1(t) + \frac{P}{K_\infty + K_1} & t \geq t_1 \end{cases} \tag{2.50}$$

It can be seen clearly in figure 2.7 that the system undergo creep deformations, the deformations continues beyond the time the peak load is reached, and that the time before equilibrium is reached is proportional with the time retardation parameter τ_1. The values of P, K_∞, K_1 and t_1 where all set to 1 in figure 2.7.

2.4.2 Derivation of the evolution equation

In Reese and Govindjee (1998) a *multiplicative decomposition* of the deformation gradient $\boldsymbol{F}$ is employed such that

$$\boldsymbol{F} = \boldsymbol{F}_e \cdot \boldsymbol{F}_i \tag{2.51}$$

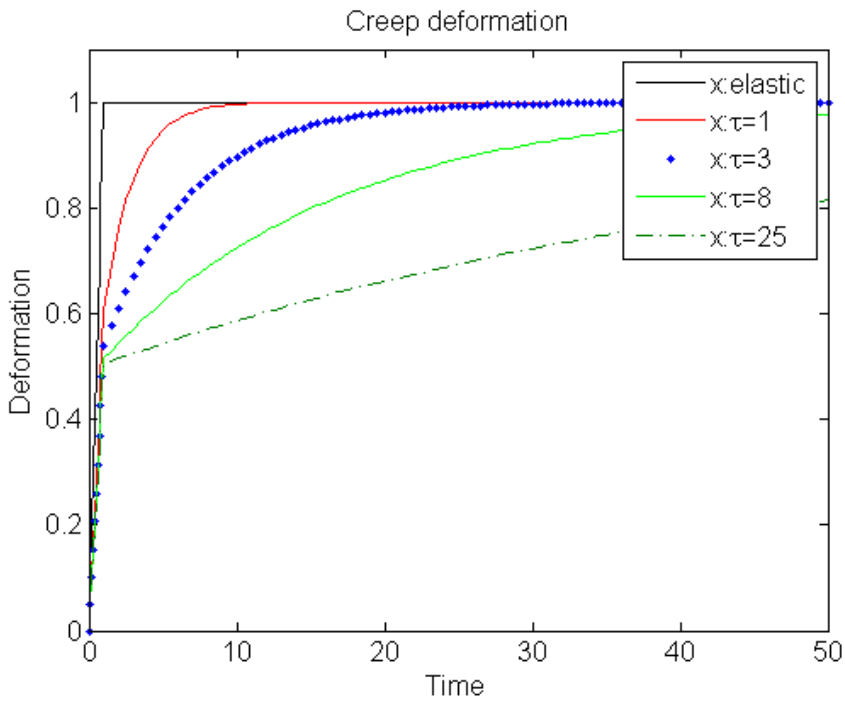

Figure 2.7: Deformation x plotted for different values of τ_α.

with $\boldsymbol{F}_e$ and $\boldsymbol{F}_i$ being the *elastic* and the *inelastic* part of the deformation gradient. To relate to the the generalized Maxwell model, $\boldsymbol{F}_e$ is analog to $x - x_\alpha$ while $\boldsymbol{F}_i$ is analog to x_α in the linear 1D case. In the general case an arbitrary number α of decompositions may be employed to increase the number of internal variables just like increasing the number of dash-pot elements in the generalized Maxwell model such that

$$\boldsymbol{F} = \boldsymbol{F}_e^1 \cdot \boldsymbol{F}_i^1 = \boldsymbol{F}_e^2 \cdot \boldsymbol{F}_i^2 = ... = \boldsymbol{F}_e^\alpha \cdot \boldsymbol{F}_i^\alpha$$

To develop the theory further some tensors have to be defined

$$\boldsymbol{C}_e := \boldsymbol{F}_e^T \cdot \boldsymbol{F}_e = (\boldsymbol{F}_i^{-T} \cdot \boldsymbol{F}^T) \cdot (\boldsymbol{F} \cdot \boldsymbol{F}_i^{-1}) = \boldsymbol{F}_i^{-T} \cdot \boldsymbol{C} \cdot \boldsymbol{F}_i^{-1} \tag{2.52a}$$

$$\boldsymbol{b}_e := \boldsymbol{F}_e \cdot \boldsymbol{F}_e^T = (\boldsymbol{F} \cdot \boldsymbol{F}_i^{-1}) \cdot (\boldsymbol{F}_i^{-T} \cdot \boldsymbol{F}^T) = \boldsymbol{F} \cdot \boldsymbol{C}_i^{-1} \cdot \boldsymbol{F}^T \tag{2.52b}$$

$$\boldsymbol{C}_i := \boldsymbol{F}_i^T \cdot \boldsymbol{F}_i \tag{2.52c}$$

where $\boldsymbol{b}_e$ is the *elastic left Cauchy-Green strain tensor* while $\boldsymbol{C}_e$ and $\boldsymbol{C}_i$ is the *elastic* and *inelastic right Cauchy-Green strain tensor*.

The strain energy function with α number of internal variables, in this case $\boldsymbol{C}_e$, may be defined in terms of the right Cauchy-Green strain tensor $\boldsymbol{C}$ such that

$$U := \tilde{U}(\boldsymbol{C}, \boldsymbol{H}_1, \boldsymbol{H}_2, ..., \boldsymbol{H}_\alpha) \tag{2.53}$$

where $\boldsymbol{H}_\alpha$ is the internal variables. Rewriting equation (2.27) point-wise leads to the *internal dissipation inequality*

$$\frac{1}{2}\boldsymbol{S} : \dot{\boldsymbol{C}} - \dot{U} \geq 0 \tag{2.54}$$

which may then be rewritten as

$$\big(\boldsymbol{S} - 2\frac{\partial U}{\partial \boldsymbol{C}}\big) : \frac{1}{2}\dot{\boldsymbol{C}} - \sum_{k=1}^{\alpha} \frac{\partial U}{\partial \boldsymbol{H}_k} : \dot{\boldsymbol{H}}_k \geq 0. \tag{2.55}$$

By splitting the free energy function into an equlibrium part U_{EQ} and a non-equilibrium (viscous) part U_{NEQ} and replacing $\boldsymbol{H}_k$ with the tensor $\boldsymbol{C}_e$ such that

$$U = \tilde{U}_{EQ}(\boldsymbol{C}) + \tilde{U}_{NEQ}(\boldsymbol{C}_e) = \tilde{U}_{EQ}(\boldsymbol{C}) + \hat{U}_{NEQ}(\boldsymbol{F}_i^{-T} \cdot \boldsymbol{C} \cdot \boldsymbol{F}_i^{-1}) = \tilde{U}(\boldsymbol{C}, \boldsymbol{F}_i) \tag{2.56}$$

the inequality (2.55) reduces to

$$\big(\boldsymbol{S} - 2\frac{\partial U_{EQ}}{\partial \boldsymbol{C}} - 2\boldsymbol{F}_i^{-T} \cdot \frac{\partial U_{NEQ}}{\partial \boldsymbol{C}_e} \cdot \boldsymbol{F}_i^{-1}\big) : \frac{1}{2}\dot{\boldsymbol{C}} - \frac{\partial U_{NEQ}}{\partial \boldsymbol{C}_e} : \frac{\partial \boldsymbol{C}_e}{\partial \boldsymbol{F}_i} : \dot{\boldsymbol{F}}_i \geq 0 \tag{2.57}$$

with the sum dropped to simplify further calculations. Identifying that the second Piola-Kirchhoff stress tensor $\boldsymbol{S}$ is defined as

$$\boldsymbol{S} = \boldsymbol{S}_{EQ} + \boldsymbol{S}_{NEQ} = 2\frac{\partial U}{\partial \boldsymbol{C}} = 2\frac{\partial U_{EQ}}{\partial \boldsymbol{C}} + 2\boldsymbol{F}_i^{-T} \cdot \frac{\partial U_{NEQ}}{\partial \boldsymbol{C}_e} \cdot \boldsymbol{F}_i^{-1} \tag{2.58}$$

reduces the inequality to

$$-\frac{\partial U_{NEQ}}{\partial \boldsymbol{C}_e} : \frac{\partial \boldsymbol{C}_e}{\partial \boldsymbol{F}_i} : \dot{\boldsymbol{F}}_i = -\frac{\partial U_{NEQ}}{\partial \boldsymbol{C}_e} : (\boldsymbol{l}_i^T \cdot \boldsymbol{C}_e + \boldsymbol{C}_e \cdot \boldsymbol{l}_i) \geq 0 \tag{2.59}$$

with $\boldsymbol{l}_i := \dot{\boldsymbol{F}}_i \cdot \boldsymbol{F}_i^{-1}$. By exploiting the symmetry of $\boldsymbol{C}_e$ and identifying that

$$\boldsymbol{\tau}_{NEQ} = \boldsymbol{F} \cdot \boldsymbol{S}_{NEQ} \cdot \boldsymbol{F}^T = 2\boldsymbol{F} \cdot \boldsymbol{F}_i^{-T} \cdot \frac{\partial U_{NEQ}}{\partial \boldsymbol{C}_e} \cdot \boldsymbol{F}_i^{-1} \cdot \boldsymbol{F}^T = 2\boldsymbol{F}_e \cdot \frac{\partial U_{NEQ}}{\partial \boldsymbol{C}_e} \cdot \boldsymbol{F}_e^T \tag{2.60}$$

leads to the following expression

$$-\boldsymbol{\tau}_{NEQ} \cdot \boldsymbol{b}_e^{-1} : (\boldsymbol{F}_e \cdot \boldsymbol{l}_i \cdot \boldsymbol{F}_e^T) \geq 0. \tag{2.61}$$

In Reese and Govindjee (1998) isotropy is assumed such that $\boldsymbol{b}_e$ and $\boldsymbol{\tau}_{NEQ}$ share the same principal directions. Another implication of assuming isotropy is that the NEQ Kirchhoff stress $\boldsymbol{\tau}_{NEQ}$ may be defined in terms of $\boldsymbol{b}_e$ so that $\boldsymbol{\tau}_{NEQ} = \tilde{\boldsymbol{\tau}}_{NEQ}(\boldsymbol{b}_e)$. With these considerations the inequality reduces to

$$-\boldsymbol{\tau}_{NEQ} : \frac{1}{2}\boldsymbol{\pounds}_{\boldsymbol{v}}\boldsymbol{b}_e \cdot \boldsymbol{b}_e^{-1} \geq 0. \tag{2.62}$$

To conclude the theory the isotropic 4-tensor $\mathbb{V}^{-1}$ is introduced defined as

$$\mathbb{V}^{-1} = \frac{1}{2\eta_D}\big(\mathbb{I}^{SYM} - \frac{1}{3}\boldsymbol{I}\otimes\boldsymbol{I}\big) + \frac{1}{9\eta_V}\boldsymbol{I}\otimes\boldsymbol{I} \tag{2.63a}$$

$$I_{ijkl}^{SYM} = \frac{1}{2}\big(\delta_{ik}\delta_{jl} + \delta_{il}\delta_{jk}\big) \tag{2.63b}$$

which satisfies the inequality condition (2.62) such that

$$-\frac{1}{2}\boldsymbol{\pounds}_{\boldsymbol{v}}\boldsymbol{b}_e \cdot \boldsymbol{b}_e^{-1} = \mathbb{V}^{-1} : \boldsymbol{\tau}_{NEQ}. \tag{2.64}$$

Finally the evolution equation is found as

$$-\frac{1}{2}\boldsymbol{\pounds}_{\boldsymbol{v}}\boldsymbol{b}_e \cdot \boldsymbol{b}_e^{-1} = \frac{1}{\eta_D} dev(\boldsymbol{\tau}_{NEQ}) + \frac{2}{3\eta_V} vol(\boldsymbol{\tau}_{NEQ})\boldsymbol{I} \tag{2.65}$$

with η_D and η_V defined as the *deviatoric* and *volumetric viscosity* and the deviatoric and volumetric parts of $\boldsymbol{\tau}_{NEQ}$, $dev(\boldsymbol{\tau}_{NEQ})$ and $vol(\boldsymbol{\tau}_{NEQ})$ defined as

$$vol(\boldsymbol{\tau}_{NEQ}) = \frac{1}{3}\boldsymbol{\tau}_{NEQ} : \boldsymbol{I} = \frac{1}{3} tr(\boldsymbol{\tau}_{NEQ}) \tag{2.66a}$$

$$dev(\boldsymbol{\tau}_{NEQ}) = \boldsymbol{\tau}_{NEQ} - vol(\boldsymbol{\tau}_{NEQ})\boldsymbol{I} \tag{2.66b}$$

2.4.3 Newton iteration of the evolution equation

To find the elastic left Cauchy-Green tensor $\boldsymbol{b_e}$ at each increment equation (2.65) have to be integrated. Because of its non-linearity a local Newton iteration have been proposed in Reese and Govindjee (1998).

The Lie-rate of the tensor $\boldsymbol{b_e}$ is defined as

$$\boldsymbol{\pounds}_{\boldsymbol{v}}\boldsymbol{b}_e = \dot{\boldsymbol{b_e}} - \boldsymbol{l}\cdot\boldsymbol{b_e} - \boldsymbol{b_e}\cdot\boldsymbol{l}^T \tag{2.67}$$

with the rate of change of $\boldsymbol{b}_e$ defined as

$$\begin{aligned}\dot{\boldsymbol{b_e}} &= \boldsymbol{F}\cdot\overline{(\dot{\boldsymbol{C}_i^{-1}})}\cdot\boldsymbol{F}^T + \dot{\boldsymbol{F}}\cdot\boldsymbol{C}_i^{-1}\cdot\boldsymbol{F}^T + \boldsymbol{F}\cdot\boldsymbol{C}_i^{-1}\cdot\dot{\boldsymbol{F}}^T \\ &= \boldsymbol{F}\cdot\overline{(\dot{\boldsymbol{C}_i^{-1}})}\cdot\boldsymbol{F}^T + (\dot{\boldsymbol{F}}\cdot\boldsymbol{F}^{-1})\cdot\boldsymbol{b_e} + \boldsymbol{b_e}\cdot(\boldsymbol{F}^{-T}\cdot\dot{\boldsymbol{F}}^T) \\ &= \boldsymbol{F}\cdot\overline{(\dot{\boldsymbol{C}_i^{-1}})}\cdot\boldsymbol{F}^T + \boldsymbol{l}\cdot\boldsymbol{b}_e + \boldsymbol{b}_e\cdot\boldsymbol{l}^T. \end{aligned} \tag{2.68}$$

Combining equation (2.67) and (2.68) leads to

$$\boldsymbol{\pounds}_v\boldsymbol{b}_e = \boldsymbol{F}\cdot\overline{(\dot{\boldsymbol{C}_i^{-1}})}\cdot\boldsymbol{F}^T \tag{2.69}$$

An operator split is set up such that $\dot{\boldsymbol{b_e}} = \boldsymbol{E} + \boldsymbol{I}$. With $\boldsymbol{E} = \boldsymbol{l}\cdot\boldsymbol{b}_e + \boldsymbol{b}_e\cdot\boldsymbol{l}^T$ as an elastic predictor and $\boldsymbol{I} = \boldsymbol{F}\cdot\overline{(\dot{\boldsymbol{C}_i^{-1}})}^{(n-1)}\cdot\boldsymbol{F}^T$ as an inelastic corrector.

For the elastic predictor-step the rate of change of $\boldsymbol{C}_i$ is assumed close to zero such that

$$\boldsymbol{b}_e^{tr} = \boldsymbol{F} \cdot (\boldsymbol{C}_i^{-1})^{(n-1)} \cdot \boldsymbol{F}^T \tag{2.70}$$

with n denoting the current global iteration.

For the inelastic corrector step the spatial velocity $\boldsymbol{l}$ is assumed close to zero. Which leads to

$$\dot{\boldsymbol{b}_e} \approx \boldsymbol{\pounds}_v \boldsymbol{b}_e = -2(\mathbb{V}^{-1} : \boldsymbol{\tau}_{NEQ}) \cdot \boldsymbol{b}_e \tag{2.71}$$

which may be solved by exponential mapping (see Appendix C) so that

$$\boldsymbol{b}_e = exp\Big(-2 \int_{t_{n-1}}^{t_n} (\mathbb{V}^{-1} : \boldsymbol{\tau}_{NEQ}) dt \Big) \cdot \boldsymbol{b}_e^{tr}$$

$$\begin{aligned} \boldsymbol{b}_e^{(n)} &\approx exp\bigg(-(t_n - t_{n-1}) \Big(\frac{1}{\eta_{_D}} dev[\boldsymbol{\tau_{NEQ}}] + \frac{2}{9\eta_{_V}} tr(\boldsymbol{\tau_{NEQ}}) \boldsymbol{I} \Big) \bigg) \cdot \boldsymbol{b}_e^{tr} \\ &= exp\bigg(-\Delta t \Big(\frac{1}{\eta_{_D}} dev(\boldsymbol{\tau}_{NEQ}) + \frac{2}{3\eta_{_V}} vol(\boldsymbol{\tau}_{NEQ}) \boldsymbol{I} \Big) \bigg) \cdot \boldsymbol{b}_e^{tr}. \end{aligned} \tag{2.72}$$

As isotropy is assumed equation (2.72) may be rewritten in terms of principal values of $\boldsymbol{b}_e$ and $\boldsymbol{b}_e^{tr}$ so that

$$\lambda_{Ae}^2 = exp\bigg(-\Delta t \frac{1}{\eta_{_D}} dev(\tau_{Ae}) + \frac{2}{3\eta_{_V}} vol(\boldsymbol{\tau}_{NEQ}) \bigg) (\lambda_{Ae}^2)^{tr} \tag{2.73}$$

and by introducing the logarithmic stretches $\epsilon_{Ae} = ln\big(\lambda_{Ae}\big)$ and $\epsilon_{Ae}^{tr} = ln\big((\lambda_{Ae}^2)^{tr}\big)$ leads to

$$\epsilon_{Ae} = -\Delta t \bigg(\frac{1}{2\eta_{_D}} dev(\tau_{Ae}) + \frac{1}{3\eta_{_V}} vol(\boldsymbol{\tau}_{NEQ}) \bigg) + \epsilon_{Ae}^{tr} \tag{2.74}$$

where τ_{Ae} is the principal values of $\boldsymbol{\tau}_{NEQ}$ while A have values (1,2,3). Note that due to isotropy the principal directions of $\boldsymbol{b}_e$ and $\boldsymbol{b}_e^{tr}$ is equal.

Rewriting equation (2.74) as a residual such that

$$r_A = \epsilon_{Ae} - \epsilon_{Ae}^{tr} + \Delta t \bigg(\frac{1}{2\eta_{_D}} dev(\tau_{Ae}) + \frac{1}{3\eta_{_V}} vol(\boldsymbol{\tau}_{NEQ}) \bigg) = 0 \tag{2.75}$$

and linearizing r_A around $\epsilon_{Ae} = \epsilon_{Ae}^{(k)}$, with k denoting the current local iteration, leads to

$$r_A \approx r_A \Big|_{\epsilon_{Ae}^{(k)}} + \sum_{B=1}^{3} \frac{\partial r_A}{\partial \epsilon_{Be}} \Big|_{\epsilon_{Ae}^{(k)}} \cdot \Delta \epsilon_{Be}^{(k)} = r_A^{(k)} + \sum_{B=1}^{3} K_{AB}^{(k)} \cdot \Delta \epsilon_{Be}^{(k)} = 0 \tag{2.76a}$$

$$\boldsymbol{r}^{(k)} + \boldsymbol{K}^{(k)} \cdot \boldsymbol{\Delta \epsilon}^{(k)} = \boldsymbol{0}, \quad \boldsymbol{\Delta \epsilon}^{(k)} = -(\boldsymbol{K}^{(k)})^{-1} \cdot \boldsymbol{r}^{(k)} \tag{2.76b}$$

with $\boldsymbol{\epsilon}^{(k+1)} = \boldsymbol{\epsilon}^{(k)} + \boldsymbol{\Delta\epsilon}^{(k)}$. Thus a Newton iteration is found using the vector $\boldsymbol{r}$ and the matrix $\boldsymbol{K}$ which have to be updated at each iteration.

This leads to the following iteration scheme:

At global iteration step n:

$$\boldsymbol{b}_e^{tr} = \boldsymbol{F}_k \cdot (\boldsymbol{C}_i^{-1})^{(n-1)} \cdot \boldsymbol{F}_k^T \longrightarrow (\lambda_{Ae}^{2(trial)}, \boldsymbol{n}_A)$$
$$(\lambda_{Ae}^2)^{(k=1)} = (\lambda_{Ae}^2)^{tr} \; and \; \epsilon = ln(\lambda)$$

At local iteration step k:

$$1: \quad r_A^{(k)} = \epsilon_{Ae}^{(k)} - \epsilon_{Ae}^{tr} + \Delta t \left(\frac{1}{2\eta_{_D}} dev(\tau_{Ae})^{(k)} + \frac{1}{3\eta_{_V}} vol(\boldsymbol{\tau}_{NEQ})^{(k)} \right)$$
$$2: \quad K_{AB}^{(k)} = \left. \frac{\partial r_A}{\partial \epsilon_{Be}} \right|_{\epsilon_{Ae}^{(k)}}$$
$$3: \quad \boldsymbol{\Delta\epsilon^{(k)}} = -(\boldsymbol{K}^{-1})^{(k)} \cdot \boldsymbol{r}^{(k)}$$
$$4: \quad \boldsymbol{\epsilon}^{(k+1)} = \boldsymbol{\epsilon}^{(k)} + \boldsymbol{\Delta\epsilon^{(k)}}$$
$$if \; norm(\Delta\epsilon^{(k)}) \leq tol, \; complete \; iteration$$
$$Update: \quad \boldsymbol{b}_e^{(n)} = \sum_{A=1}^{3} \lambda_{Ae}^2 (\boldsymbol{n}_A \otimes \boldsymbol{n}_A), \quad Store: \quad (\boldsymbol{C}_i^{-1})^{(n)} = \boldsymbol{F}^{-1} \cdot \boldsymbol{b}_e^{(n)} \cdot \boldsymbol{F}^{-T}$$

2.4.4 NEQ spatial tangent modulus

The derivation of the NEQ tangent modulus is explained in detail in Reese and Govindjee (1998) and only the most important aspects are covered in this section. The tangent modulus is an incremental tangent modulus in the sense that it is not exact but based on the following multiplicative decomposition of the deformation gradient

$$\boldsymbol{F} = \boldsymbol{F}_e^{tr} \cdot \boldsymbol{F}_i^{(n-1)} \tag{2.79}$$

found by re-writing equation (2.70) such that

$$\boldsymbol{b}_e^{tr} = \boldsymbol{F} \cdot (\boldsymbol{C}_i^{-1})^{(n-1)} \cdot \boldsymbol{F}^T = \boldsymbol{F} \cdot \left((\boldsymbol{F}_i^{-1})^{(n-1)} \cdot (\boldsymbol{F}_i^{-T})^{(n-1)} \right) \cdot \boldsymbol{F}^T$$
$$= \left(\boldsymbol{F} \cdot (\boldsymbol{F}_i^{-1})^{(n-1)} \right) \cdot \left(\boldsymbol{F} \cdot (\boldsymbol{F}_i^{-1})^{(n-1)} \right)^T = \boldsymbol{F}_e^{tr} \cdot (\boldsymbol{F}_e^{tr})^T. \tag{2.80}$$

with the advantage that $\boldsymbol{F}_i^{(n-1)}$ may be treated as constant when calculating the tangent modulus. First some tensors must be defined, the second Piola-Kirchhoff stress tensor $\boldsymbol{S}$ may be written in terms of the Kirchhoff stress tensor so that

$$\boldsymbol{S}_{NEQ} = \boldsymbol{F}^{-1} \cdot \boldsymbol{\tau}_{NEQ} \cdot \boldsymbol{F}^{-T}$$
$$= (\boldsymbol{F}_i^{-1})^{(n-1)} \cdot \left((\boldsymbol{F}_e^{-1})^{tr} \cdot \boldsymbol{\tau}_{NEQ} \cdot (\boldsymbol{F}_e^{-T})^{tr} \right) \cdot (\boldsymbol{F}_i^{-T})^{(n-1)}$$

$$= (\boldsymbol{F}_i^{-1})^{(n-1)} \cdot \tilde{\boldsymbol{S}}_{NEQ} \cdot (\boldsymbol{F}_i^{-T})^{(k-1)} \tag{2.81}$$

$$\tilde{\boldsymbol{S}}_{NEQ} = (\boldsymbol{F}_e^{-1})^{tr} \cdot \boldsymbol{\tau}_{NEQ} \cdot (\boldsymbol{F}_e^{-T})^{tr} \tag{2.82}$$

As $\boldsymbol{F}_i$ is treated as constant the material tangent modulus is

$$\mathbb{C}_{NEQ} = 2\frac{\partial \boldsymbol{S}_{NEQ}}{\partial \boldsymbol{C}}$$
$$= (\boldsymbol{F}_i^{-1})^{(n-1)} \cdot (\boldsymbol{F}_i^{-1})^{(n-1)} \cdot \tilde{\mathbb{C}}_{NEQ} \cdot (\boldsymbol{F}_i^{-T})^{(n-1)} \cdot (\boldsymbol{F}_i^{-T})^{(n-1)} \tag{2.83}$$

with the 4-tensor $\tilde{\mathbb{C}}_{NEQ}$ defined as

$$\tilde{\mathbb{C}}_{NEQ} = 2\frac{\partial \tilde{\boldsymbol{S}}_{NEQ}}{\partial \boldsymbol{C}_e^{tr}}. \tag{2.84}$$

As the spatial tangent modulus $\mathbb{c}_{NEQ}$ is found from the push-forward operation in equation (2.33) and considering that $\boldsymbol{F}_e^{tr} = \boldsymbol{F} \cdot (\boldsymbol{F}_i^{-1})^{(n-1)}$ leads to the following expression for $\mathbb{c}_{NEQ}$

$$J\mathbb{c}_{NEQ} = \boldsymbol{F}_e^{tr} \cdot \boldsymbol{F}_e^{tr} \cdot \tilde{\mathbb{C}}_{NEQ} \cdot (\boldsymbol{F}_e^{T})^{tr} \cdot (\boldsymbol{F}_e^{T})^{tr}. \tag{2.85}$$

The 4-tensor $\tilde{\mathbb{C}}_{NEQ}$ is given in Reese and Govindjee (1998) as

$$\tilde{\mathbb{C}}_{NEQ} = \sum_{A=1}^{3}\sum_{B=1}^{3} \frac{1}{(\lambda_{Ae})^2_{trial}(\lambda_{Be})^2_{trial}}(C_{AB}^{alg} - \tau_A 2\delta_{AB})\Big(\boldsymbol{N}_A \otimes \boldsymbol{N}_A \otimes \boldsymbol{N}_B \otimes \boldsymbol{N}_B\Big)$$
$$+\frac{1}{2}\sum_{A=1}^{3}\sum_{B=1}^{3} 2\frac{S_B^* - S_A^*}{(\lambda_{Be})^2_{trial} - (\lambda_{Ae})^2_{trial}}\Big(\boldsymbol{N}_A \otimes \boldsymbol{N}_B \otimes \boldsymbol{N}_A \otimes \boldsymbol{N}_B$$
$$+\boldsymbol{N}_A \otimes \boldsymbol{N}_B \otimes \boldsymbol{N}_B \otimes \boldsymbol{N}_A\Big)$$
$$= \sum_{A=1}^{3}\sum_{B=1}^{3}\sum_{C=1}^{3}\sum_{D=1}^{3}(\tilde{C}_{NEQ})_{ABCD}\boldsymbol{N}_A \otimes \boldsymbol{N}_B \otimes \boldsymbol{N}_C \otimes \boldsymbol{N}_D \tag{2.86}$$

with $(\tilde{C}_{NEQ})_{ABCD}$ consisting of a total of 21 components with values

$$(\tilde{C}_{NEQ})_{AAAA} = \frac{C_{AA}^{ALG} - 2\tau_A}{(\lambda_{Ae}^4)^{tr}} \tag{2.87a}$$

$$(\tilde{C}_{NEQ})_{AABB} = \frac{C_{AB}^{ALG}}{(\lambda_{Ae}^2)^{tr}(\lambda_{Be}^2)^{tr}}, \quad A \neq B \tag{2.87b}$$

$$(\tilde{C}_{NEQ})_{ABAB} = (\tilde{C}_{NEQ})_{ABBA} = \frac{S_B - S_A}{(\lambda_{Be}^2)^{tr} - (\lambda_{Ae}^2)^{tr}}, \quad A \neq B \tag{2.87c}$$

where $\boldsymbol{C}^{ALG}$ is the algorithmic tangent modulus and S_A is the principal values of the NEQ part of the second Piola-Kirchhoff stress tensor $\boldsymbol{S}_{NEQ}$. Recalling that the vectors $\boldsymbol{N}_A$ and $\boldsymbol{N}_B$ are orthogonal ($A \neq B$) it can be shown that

$$\Big(\sum_{B=1}^{3}\lambda_B \boldsymbol{n}_B\otimes\boldsymbol{N}_B\Big)\cdot\Big(\sum_{A=1}^{3}\boldsymbol{N}_A\otimes\boldsymbol{N}_A\Big)\cdot\Big(\sum_{C=1}^{3}\lambda_C(\boldsymbol{n}_C\otimes\boldsymbol{N}_C)^T\Big)$$
$$=\sum_{B=1}^{3}\sum_{C=1}^{3}\lambda_B\lambda_C\delta_{BC}\boldsymbol{n}_B\otimes\boldsymbol{n}_C=\sum_{B=1}^{3}\lambda_B^2\boldsymbol{n}_B\otimes\boldsymbol{n}_B$$
$$=\sum_{A=1}^{3}\lambda_A^2\boldsymbol{n}_A\otimes\boldsymbol{n}_A. \tag{2.88}$$

With this in mind the push-forward operation for the spatial tangent modulus $\mathbb{c}_{NEQ}$ in equation (2.85) leads to

$$J\mathbb{c}_{NEQ}=\sum_{A=1}^{3}\sum_{B=1}^{3}\sum_{C=1}^{3}\sum_{D=1}^{3}J(c_{NEQ})_{ABCD}\boldsymbol{n}_A\otimes\boldsymbol{n}_B\otimes\boldsymbol{n}_C\otimes\boldsymbol{n}_D \tag{2.89}$$

$$=\sum_{A=1}^{3}\sum_{B=1}^{3}\sum_{C=1}^{3}\sum_{D=1}^{3}(\tilde{C}_{NEQ})_{ABCD}\lambda_{Ae}^{tr}\lambda_{Be}^{tr}\lambda_{Ce}^{tr}\lambda_{De}^{tr}\boldsymbol{n}_A\otimes\boldsymbol{n}_B\otimes\boldsymbol{n}_C\otimes\boldsymbol{n}_D \tag{2.90}$$

with the 21 components of $J(c_{NEQ})_{ABCD}$ found as

$$J(c_{NEQ})_{AAAA}=C_{AA}^{ALG}-2\tau_{Ae} \tag{2.91a}$$
$$J(c_{NEQ})_{AABB}=C_{AB}^{ALG},\quad A\neq B \tag{2.91b}$$
$$J(c_{NEQ})_{ABAB}=(c_{NEQ})_{ABBA}=\frac{\tau_{Be}(\lambda_{Ae}^2)^{tr}-\tau_{Ae}(\lambda_{Be}^2)^{tr}}{(\lambda_{Be}^2)^{tr}-(\lambda_{Ae}^2)^{tr}},\quad A\neq B \tag{2.91c}$$

As the NEQ Kirchhoff stress $\boldsymbol{\tau}_{NEQ}$ and the trial stretches λ_{Ae}^{tr} are known and found during the local Newton iteration it leaves to define the algorithmic tangent modulus $\boldsymbol{C}^{ALG}$.

The algorithmic tangent modulus is defined as

$$C_{AB}^{ALG}=\frac{\partial\tau_{Ae}}{\partial\epsilon_{Be}^{tr}},\quad \Delta\tau_{Ae}=\sum_{B=1}^{3}C_{AB}^{ALG}\Delta\epsilon_{Be}^{tr}. \tag{2.92}$$

Taking into consideration that ϵ_{Be}^{tr} is not constant between the *global* increments, equation (2.76a) may be modified as

$$\Delta r_A=\sum_{B=1}^{3}K_{AB}\Delta\epsilon_{Be}-\Delta\epsilon_{Ae}^{tr}=0 \tag{2.93}$$

with Δ denoting the perturbations in the global iteration. With this $\boldsymbol{C}^{ALG}$ may be found as

$$\Delta\tau_{Ae}=\sum_{B=1}^{3}\frac{\partial\tau_{Ae}}{\partial\epsilon_{Be}}\Delta\epsilon_{Be}=\sum_{C=1}^{3}\sum_{B=1}^{3}\frac{\partial\tau_{Ae}}{\partial\epsilon_{Be}}K_{BC}^{-1}\Delta\epsilon_{Ce}^{tr}$$

$$= \sum_{C=1}^{3} C_{AC}^{ALG} \Delta\epsilon_{Ce}^{tr} \tag{2.94a}$$

$$C_{AC}^{ALG} = \sum_{B=1}^{3} \frac{\partial \tau_{Ae}}{\partial \epsilon_{Be}} K_{BC}^{-1} \tag{2.94b}$$

with the matrix $\boldsymbol{K}$ defined in equation (2.76a).

Remark (Symmetry of $\boldsymbol{C}^{ALG}$)**.** *Reese and Govindjee (1998) provides a proof of the symmetric properties of $\boldsymbol{C}^{ALG}$. Upon further inspection of the implemented material models the calculated $\boldsymbol{C}^{ALG}$ have shown to be unsymmetric, because of that a unsymmetric solver have been used in some of the calculations in this thesis. The Neo-Hookean and Yeoh-material models have been tested and performs well with a symmetric solver, while the hydrogel material model have been tested with only a unsymmetric solver.*

2.4.5 Summary of Finite Viscoelasticity

To summarize the theory the NEQ-part of the strain energy function U_{NEQ} and the material tangent modulus for the NEQ-part implemented in the UMAT subroutine $\mathbb{C}_{NEQ}^{ABA}$ must be defined. The strain energy function of the NEQ-part is defined as in Bonet (2001) as

$$U_{NEQ}(\boldsymbol{C}_e) = \beta U_{EQ}(\boldsymbol{C})\Big|_{\boldsymbol{C}=\boldsymbol{C}_e} \tag{2.95}$$

with the material scaling parameter β added to make a linear relation between the EQ material constants and the NEQ material constants (f. ex. $C_{1e} = \beta C_1$), alternatively the NEQ material constants may be chosen to be independent of the EQ material constants, but this is likely to increase the calculation effort needed to fit the material models to experimental data. The NEQ material tangent modulus $\mathbb{C}_{NEQ}^{ABA}$ is then found from equation (2.36) as

$$\mathbb{C}_{NEQ}^{ABA} = \frac{1}{J}\mathbb{C}_{NEQ}^{\Delta J} = (\mathbb{c}_{NEQ} + \tilde{\mathbb{C}}_{NEQ}) \tag{2.96}$$

$$J(\tilde{C}_{NEQ})_{ijkl} = \frac{1}{2}\Big(\delta_{ik}(\tau_{NEQ})_{jl} + \delta_{il}(\tau_{NEQ})_{jk} + \delta_{jk}(\tau_{NEQ})_{il} + \delta_{jl}(\tau_{NEQ})_{ik}\Big). \tag{2.97}$$

The iteration process is shown in figure 2.8. Note that for all material models, except the hydrogel material model presented in the next chapter, $\boldsymbol{F} = \boldsymbol{F}^{TOT}$.

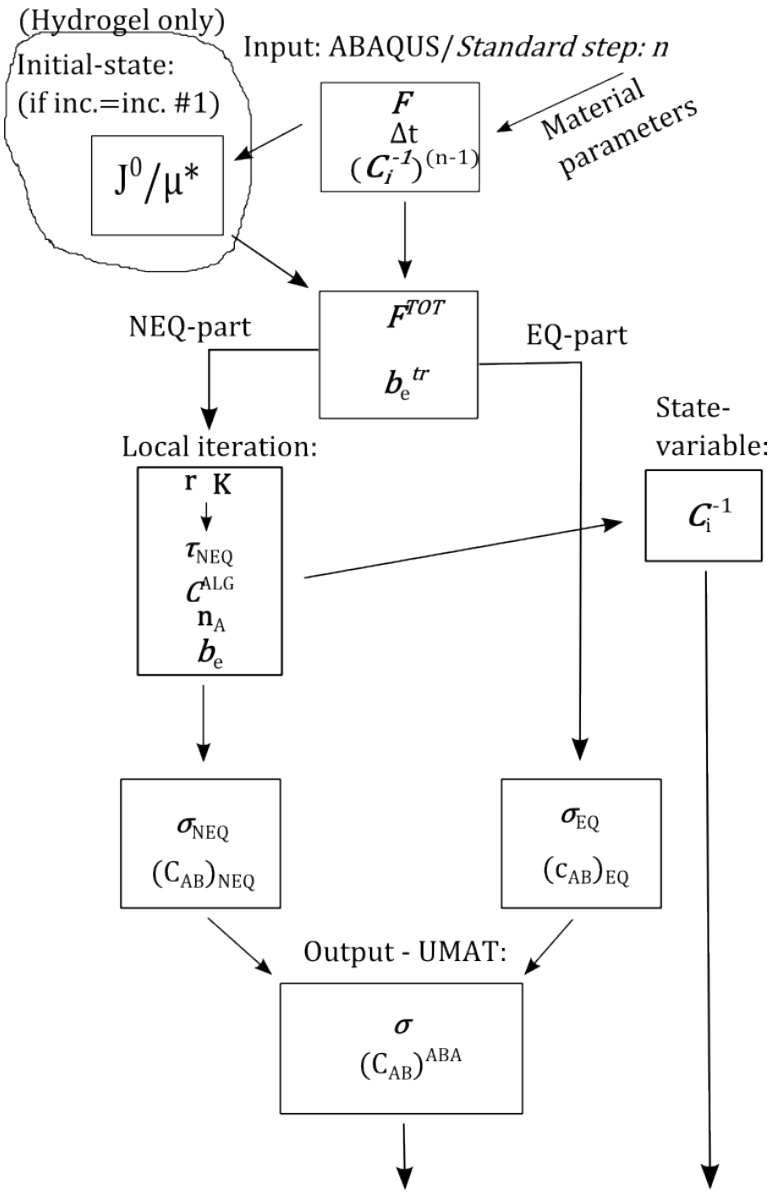

Figure 2.8: Float-chart of the iteration process at each integration point during the ABAQUS/*Standard* Finite Element analysis.

2.5 Variational approach to determine the material tangent modulus

Chapter 4 of the ABAQUS documentation (ABAQUS, 2013) provides a practical method to determine the Jaumann rate of the Kirchhoff stress $\boldsymbol{\tau}$ by calculation of the variations of the isochoric left Cauchy-Green tensor $\bar{\boldsymbol{b}}$ and its two first invariants $\bar{I}_1$ and $\bar{I}_2$, and the variation of the determinant J of the deformation gradient. The variation of the second invariant is left out as the constitutive models evaluated in this thesis are independent of it. The variations are given as

$$\delta\bar{\boldsymbol{b}} = \mathbb{H} : \delta\boldsymbol{e} + \delta\boldsymbol{w}\cdot\bar{\boldsymbol{b}} - \bar{\boldsymbol{b}}\cdot\delta\boldsymbol{w} \tag{2.98a}$$

$$\delta\bar{I}_1 = 2\bar{\boldsymbol{b}} : \delta\boldsymbol{e} \tag{2.98b}$$

$$\delta J = J\delta\epsilon^{vol} \tag{2.98c}$$

with the 4-tensor $\mathbb{H}$, 2-tensor $\delta\boldsymbol{e}$ and scalar $\delta\epsilon^{vol}$ given as

$$H_{ijkl} := \frac{1}{2}(\delta_{ik}\bar{b}_{jl} + \bar{b}_{ik}\delta_{jl} + \delta_{il}\bar{b}_{jk} + \bar{b}_{il}\delta_{jk}) \tag{2.99a}$$

$$\delta\epsilon^{vol} := \boldsymbol{I} : \delta\boldsymbol{D} \tag{2.99b}$$

$$\delta\boldsymbol{e} := \delta\boldsymbol{d} - \frac{1}{3}\delta\epsilon^{vol}\boldsymbol{I}. \tag{2.99c}$$

Given a tensor function of the Kirchhoff stress such that $\boldsymbol{\tau} = \hat{\boldsymbol{\tau}}(\bar{\boldsymbol{b}}, \bar{I}_1, J)$ the variation of the Kirchhoff stress is then given as

$$\delta\boldsymbol{\tau} = \frac{\partial\hat{\boldsymbol{\tau}}}{\partial\bar{\boldsymbol{b}}} : \delta\bar{\boldsymbol{b}} + \frac{\partial\hat{\boldsymbol{\tau}}}{\partial\bar{I}_1}\delta\bar{I}_1 + \frac{\partial\hat{\boldsymbol{\tau}}}{\partial J}\delta J. \tag{2.100}$$

The goal is then to rewrite equation (2.100) on the following form

$$\delta\boldsymbol{\tau} = \mathbb{A} : \delta\boldsymbol{d} + \delta\boldsymbol{w}\cdot\boldsymbol{\tau} - \boldsymbol{\tau}\cdot\delta\boldsymbol{w} = \mathbb{C}^{\Delta J} : \delta\boldsymbol{d} + \delta\boldsymbol{w}\cdot\boldsymbol{\tau} - \boldsymbol{\tau}\cdot\delta\boldsymbol{w}. \tag{2.101}$$

where $\mathbb{C}^{\Delta J}$ is the Jaumann tangent modulus, $\boldsymbol{w}$ is the spin tensor and $\boldsymbol{d}$ is the rate of deformation tensor.

Finally the tangent modulus implemented in the UMAT-subroutine is given as

$$\mathbb{C}^{ABA}_{NEQ} = \frac{1}{J}\mathbb{C}^{\Delta J} \tag{2.102}$$

Chapter 3

Constitutive models

The main objective of this master thesis was to obtain a stable viscoelastic constitutive model for hydrogel materials, based on the constitutive model developed by Kang and Huang (2010), coded in a UMAT-subroutine. As experimental data from a spherical Ugelstad polymeric particle was available, a viscoelastic Neo-Hookean constitutive model was initially implemented in a UMAT-subroutine in order to model the viscoelastic response of the polymer particle and to test the stability of the finite viscoelasticity model with finite element models. As the experimental compression data showed a "s"-shaped force-deflection curve, some different variants of the Neo-Hookean constitutive model and the Yeoh constitutive model was also implemented in UMAT-subroutines. The derivations of the different constitutive models implemented are shown in this chapter.

3.1 Yeoh hyperelastic model

The Yeoh hyperelastic model is a polynomial model proposed by Yeoh (1993). The material model have been implemented in the UMAT-file *YEOH3visco.for*. The strain energy function has the following form

$$U_{EQ} = U(\bar{I}_1, J) = \sum_{i=1}^{3} C_i(\bar{I}_1 - 3)^i + \sum_{k=1}^{3} \frac{1}{D_k}(J-1)^{2k} \tag{3.1}$$

where C_i and D_i are material constants related to the shear modulus G and the bulk modulus κ.

By applying the assumptions from section 2.4.5, U_{NEQ} may be defined as

$$U_{NEQ} = U(\bar{I_{1e}}, J_e) = \beta \sum_{i=1}^{3} C_i(\bar{I}_{1e} - 3)^i + \beta \sum_{k=1}^{3} \frac{1}{D_k}(J_e - 1)^{2k} \tag{3.2}$$

with $\bar{I}_{1e}$ defined as ${J_e}^{-\frac{2}{3}} I_1(\boldsymbol{C_e}) = {J_e}^{-\frac{2}{3}} I_1(\boldsymbol{b_e})$ and J_e defined as $\sqrt{I_3(\boldsymbol{C_e})}$.

The second Piola-Kirchoff stress tensor $\boldsymbol{S}$ is then found as

$$\boldsymbol{S} = \boldsymbol{S}_{EQ} + \boldsymbol{S}_{NEQ} \tag{3.3a}$$

$$\boldsymbol{S}_{EQ} = b_1 \frac{\partial \bar{I}_1}{\partial \boldsymbol{C}} + 2p_e \frac{\partial J}{\partial \boldsymbol{C}} = b_1 J^{-\frac{2}{3}} (\boldsymbol{I} - \frac{1}{3} I_1 \boldsymbol{C}^{-1}) + pJ\boldsymbol{C}^{-1} \tag{3.3b}$$

$$\begin{aligned} \boldsymbol{S}_{NEQ} &= \boldsymbol{F}_i^{-1} \cdot (\beta b_{1e} \frac{\partial \bar{I}_{1e}}{\partial \boldsymbol{C}_e} + 2\beta p_e \frac{\partial J_e}{\partial \boldsymbol{C}_e}) \cdot \boldsymbol{F}_i^{-T} \\ &= \beta b_{1e} {J_e}^{-\frac{2}{3}} (\boldsymbol{C}_i^{-1} - \frac{1}{3} I_{1e} \boldsymbol{C}^{-1}) + \beta p_e J_e \boldsymbol{C}^{-1} \end{aligned} \tag{3.3c}$$

with the variables b_1, b_{1e}, p and p_e defined as

$$b_1 := 2\frac{\partial}{\partial \bar{I}_1} \left(\sum_{i=1}^{3} C_i (\bar{I}_1 - 3)^i \right) = 2C_1 + 4C_2(\bar{I}_1 - 3) + 6C_3(\bar{I}_1 - 3)^2 \tag{3.4a}$$

$$b_{1e} := 2\frac{\partial}{\partial \bar{I}_{1e}} \left(\sum_{i=1}^{3} C_i (\bar{I}_{1e} - 3)^i \right) = 2C_1 + 4C_2(\bar{I}_{1e} - 3) + 6C_3(\bar{I}_{1e} - 3)^2 \tag{3.4b}$$

$$p := \frac{\partial}{\partial J} \left(\sum_{k=1}^{3} \frac{1}{D_k} (J-1)^{2k} \right) = \frac{2}{D_1}(J-1) + \frac{4}{D_2}(J-1)^3 + \frac{6}{D_2}(J-1)^5 \tag{3.4c}$$

$$p_e := \frac{\partial}{\partial J_e} \left(\sum_{k=1}^{3} \frac{1}{D_k} (J_e-1)^{2k} \right) = \frac{2}{D_1}(J_e-1) + \frac{4}{D_2}(J_e-1)^3 + \frac{6}{D_2}(J_e-1)^5. \tag{3.4d}$$

The Kirchhoff stress tensor $\boldsymbol{\tau}$ and Cauchy stress tensor $\boldsymbol{\sigma}$ may then be found by the push-forward operation of the second Piola-Kirchoff stress tensor $\boldsymbol{S}$ (equation (3.3a)) such that

$$\boldsymbol{\tau} = J\boldsymbol{\sigma} = \boldsymbol{F} \cdot \boldsymbol{S} \cdot \boldsymbol{F}^T = \boldsymbol{\tau}_{EQ} + \boldsymbol{\tau}_{NEQ} \tag{3.5a}$$

$$\boldsymbol{\tau}_{EQ} = b_1 (\bar{\boldsymbol{b}} - \frac{1}{3} \bar{I}_1 \boldsymbol{I}) + pJ\boldsymbol{I} \tag{3.5b}$$

$$\boldsymbol{\tau}_{NEQ} = \beta b_{1e} (\bar{\boldsymbol{b}}_e - \frac{1}{3} \bar{I}_{1e} \boldsymbol{I}) + \beta p_e J_e \boldsymbol{I} \tag{3.5c}$$

with $\bar{\boldsymbol{b}}_e$ defined as ${J_e}^{-\frac{2}{3}} \boldsymbol{b}_e$.

The tangent modulus of the EQ-part $\mathbb{C}_{EQ}^{ABA}$ calculated in the UMAT-subroutine is defined as

$$\mathbb{C}_{EQ}^{ABA} = a_1 \mathbb{H} - a_2 (\boldsymbol{I} \otimes \bar{\boldsymbol{b}} + \bar{\boldsymbol{b}} \otimes \boldsymbol{I}) + a_3 \bar{\boldsymbol{b}} \otimes \bar{\boldsymbol{b}} + a_4 \boldsymbol{I} \otimes \boldsymbol{I} + dp \boldsymbol{I} \otimes \boldsymbol{I} \tag{3.6}$$

with the variables a_1, a_2, a_3, a_4 and dp defined as

$$a_1 := \frac{b_1}{J} \tag{3.7a}$$

$$a_2 := \frac{1}{J}\Big(\frac{\bar{I}_1}{3}b_2 + \frac{2}{3}b_1\Big) \tag{3.7b}$$

$$a_3 := \frac{b_2}{J} \tag{3.7c}$$

$$a_4 := \frac{1}{J}\Big((\frac{\bar{I}_1}{3})^2 b_2 + \frac{2}{3}\frac{\bar{I}_1}{3}b_1\Big) \tag{3.7d}$$

$$dp := \frac{\partial(pJ)}{\partial J} =$$

$$\frac{2}{D_1}(2J-1) + \frac{4}{D_2}\Big((J-1)^3 + 3J(J-1)^2\Big) + \frac{6}{D_2}\Big((J-1)^5 + 5J(J-1)^4\Big) \tag{3.7e}$$

$$b_2 := 2\frac{\partial b_1}{\partial \bar{I}_1} = 8C_2 + 24C_3(\bar{I}_1 - 3) \tag{3.7f}$$

and the 4-tensor $\mathbb{H}$ defined as

$$H_{ijkl} := \frac{1}{2}(\delta_{ik}\bar{b}_{jl} + \bar{b}_{ik}\delta_{jl} + \delta_{il}\bar{b}_{jk} + \bar{b}_{il}\delta_{jk}). \tag{3.8}$$

The tangent modulus of the NEQ-part (viscous part) $\mathbb{C}^{ABA}_{NEQ}$ is calculated as described in section 2.4.4 and 2.4.5. The calculation steps for the tangent modulus of the EQ-part $\mathbb{C}^{ABA}_{EQ}$ is shown below.

3.1.1 Calculation of the EQ-part tangent modulus

The EQ-part of the tangent modulus have been calculated by using variations as described in section 2.5. Recalling that

$$\delta\epsilon^{vol} := \boldsymbol{I} : \delta\boldsymbol{D} \tag{3.9a}$$

$$\delta\boldsymbol{e} := \delta\boldsymbol{d} - \frac{1}{3}\delta\epsilon^{vol}\boldsymbol{I} \tag{3.9b}$$

$$\delta\bar{\boldsymbol{b}} = \mathbb{H} : \delta\boldsymbol{e} + \delta\boldsymbol{w}\cdot\bar{\boldsymbol{b}} - \bar{\boldsymbol{b}}\cdot\delta\boldsymbol{w} \tag{3.9c}$$

$$\delta\bar{I}_1 = 2\bar{\boldsymbol{b}} : \delta\boldsymbol{e} \tag{3.9d}$$

$$\delta J = J\delta\epsilon^{vol} \tag{3.9e}$$

and taking note of the following useful properties

$$\mathbb{H} : \boldsymbol{I} = 2\bar{\boldsymbol{b}} \tag{3.10a}$$

$$\delta\boldsymbol{w}\cdot\boldsymbol{I} - \boldsymbol{I}\cdot\delta\boldsymbol{w} = \boldsymbol{0} \tag{3.10b}$$

the variation of the Kirchhoff stress $\boldsymbol{\tau}$ may be found as

$$\delta(\tau_{EQ})_{ij} = \frac{\partial b_1}{\partial \bar{I}_1}(\bar{b}_{ij} - \frac{1}{3}\bar{I}_1\delta_{ij})\delta\bar{I}_1 + b_1(\delta\bar{b}_{ij} - \frac{1}{3}\delta\bar{I}_1\delta_{ij}) + \frac{\partial(pJ)}{J}\delta_{ij}\delta J$$

$$= \frac{1}{2}b_2(\bar{b}_{ij} - \frac{1}{3}\bar{I}_1\delta_{ij})\delta\bar{I}_1 + b_1(\delta\bar{b}_{ij} - \frac{1}{3}\delta\bar{I}_1\delta_{ij}) + dp\delta_{ij}\delta J$$

$$= b_2(\bar{b}_{ij}\bar{b}_{kl} - \frac{2}{3}\bar{I}_1\delta_{ij}\bar{b}_{kl})\delta e_{kl}$$

$$+b_1(H_{ijkl} - \frac{2}{3}\delta_{ij}\bar{b}_{kl})\delta e_{kl} + b_1(\delta w_{ik}\bar{b}_{kj} - \bar{b}_{ik}\delta w_{kj})$$

$$+dp\delta_{ij}J\delta\epsilon^{vol}.$$

Exploiting equation (3.10b) it may be shown that

$$b1(\delta\boldsymbol{w}\cdot\bar{\boldsymbol{b}} - \bar{\boldsymbol{b}}\cdot\delta\boldsymbol{w}) = b1(\delta\boldsymbol{w}\cdot(\bar{\boldsymbol{b}} - \frac{1}{3}\bar{I}_1\boldsymbol{I}) - (\bar{\boldsymbol{b}} - \frac{1}{3}\bar{I}_1\boldsymbol{I})\cdot\delta\boldsymbol{w})$$

$$= -(\boldsymbol{\tau}_{EQ}\cdot\delta\boldsymbol{w} - \delta\boldsymbol{w}\cdot\boldsymbol{\tau}_{EQ}).$$

This leads to the Jaumann-rate such that

$$\delta\boldsymbol{\tau}_{EQ} + \boldsymbol{\tau}_{EQ}\cdot\delta\boldsymbol{w} - \delta\boldsymbol{w}\cdot\boldsymbol{\tau}_{EQ} = \mathbb{C}^{\Delta J} : \delta\boldsymbol{d}$$

$$= b_2(\bar{\boldsymbol{b}}\otimes\bar{\boldsymbol{b}} - \frac{2}{3}\bar{I}_1\boldsymbol{I}\otimes\bar{\boldsymbol{b}}) : \delta\boldsymbol{e}$$

$$+b_1(\mathbb{H} - \frac{2}{3}\boldsymbol{I}\otimes\bar{\boldsymbol{b}}) : \delta\boldsymbol{e} + Jdp\boldsymbol{I}\delta\epsilon^{vol}$$

$$= \Big(b_2(\bar{\boldsymbol{b}}\otimes\bar{\boldsymbol{b}} - \frac{2}{3}\bar{I}_1\boldsymbol{I}\otimes\bar{\boldsymbol{b}}) + b_1(\mathbb{H} - \frac{2}{3}\boldsymbol{I}\otimes\bar{\boldsymbol{b}})\Big) : \delta\boldsymbol{d}$$

$$-\frac{1}{3}\Big(b_2(\bar{\boldsymbol{b}}\otimes\bar{\boldsymbol{b}} - \frac{2}{3}\bar{I}_1\boldsymbol{I}\otimes\bar{\boldsymbol{b}}) + b_1(\mathbb{H} - \frac{2}{3}\boldsymbol{I}\otimes\bar{\boldsymbol{b}})\Big) : \boldsymbol{I}\delta\epsilon^{vol} + Jdp\boldsymbol{I}\delta\epsilon^{vol}.$$

As $\bar{\boldsymbol{b}}\otimes\bar{\boldsymbol{b}} : \boldsymbol{I} = \bar{I}_1\bar{\boldsymbol{b}}$, $\mathbb{H} : \boldsymbol{I} = 2\bar{\boldsymbol{b}}$ and $\delta\epsilon^{vol} := \boldsymbol{I} : \delta\boldsymbol{D}$ this leads to

$$\mathbb{C}^{\Delta J} : \delta\boldsymbol{d} = \Big(\delta\boldsymbol{d} = b_1\mathbb{H} - (\frac{\bar{I}_1}{3}b_2 + \frac{2}{3}b_1)(\boldsymbol{I}\otimes\bar{\boldsymbol{b}} + \bar{\boldsymbol{b}}\otimes\boldsymbol{I})$$

$$+b_2\bar{\boldsymbol{b}}\otimes\bar{\boldsymbol{b}} + \big((\frac{\bar{I}_1}{3})^2b_2 + \frac{2}{3}\frac{\bar{I}_1}{3}b_1\big)\boldsymbol{I}\otimes\boldsymbol{I} + Jdp\boldsymbol{I}\otimes\boldsymbol{I}\Big) : \delta\boldsymbol{d}.$$

The material tangent is then found as

$$\mathbb{C}^{ABA}_{EQ} = \frac{1}{J}\mathbb{C}^{\Delta J} = a_1\mathbb{H} - a_2(\boldsymbol{I}\otimes\bar{\boldsymbol{b}} + \bar{\boldsymbol{b}}\otimes\boldsymbol{I}) + a_3\bar{\boldsymbol{b}}\otimes\bar{\boldsymbol{b}} + a_4\boldsymbol{I}\otimes\boldsymbol{I} + dp\boldsymbol{I}\otimes\boldsymbol{I}. \quad (3.15)$$

3.1.2 Viscoelastic iteration variables

At each increment the internal variables $\boldsymbol{C}_i^{-1}$ must be found as described in section 2.4.3. For the YEOH-material the deviatoric and volumetric parts of $\boldsymbol{\tau}_{NEQ}$ is given as

$$dev(\boldsymbol{\tau}_{NEQ}) = \boldsymbol{\tau}_{NEQ} - \frac{1}{3}tr(\boldsymbol{\tau}_{NEQ})\boldsymbol{I} = \beta b_{1e}(\bar{\boldsymbol{b}}_e - \frac{1}{3}\bar{I}_{1e}\boldsymbol{I}) \tag{3.16a}$$

$$vol(\boldsymbol{\tau}_{NEQ}) = \frac{1}{3}tr(\boldsymbol{\tau}_{NEQ}) = \frac{1}{3}tr(\boldsymbol{\tau}_{NEQ}) = \beta p_e J_e \tag{3.16b}$$

Equation 2.75 then collapse to

$$r_A = \epsilon_{Ae} - \epsilon_{Ae}^{tr} + v_1 b_{1e} dev(\bar{b}_{Ae}) + v_2 p_e J_e \tag{3.17}$$

$$dev(\bar{b}_{Ae}) = \frac{2}{3}\bar{\lambda}_{Ae}^2 - \frac{1}{3}\bar{\lambda}_{Be}^2 - \frac{1}{3}\bar{\lambda}_{Ce}^2 \quad (A \neq B \neq C),\ (A,B,C)\epsilon(1,3)$$

$$\bar{\lambda}_{Ae}^2 = J_e^{-\frac{2}{3}}\lambda_{Ae}^2, \quad v_1 = \frac{\Delta t\beta}{2\eta_D}, \quad v_2 = \frac{\Delta t\beta}{3\eta_V}. \tag{3.18}$$

The next step is to determine the matrix $\boldsymbol{K}$. By applying the following derivatives

$$\frac{\partial J_e}{\partial \epsilon_{Be}} = J_e, \quad \frac{\partial \lambda_{Ae}}{\partial \epsilon_{Be}} = \lambda_{Ae}\delta_{AB} \tag{3.19a}$$

$$\frac{\partial \bar{\lambda}_{Ae}^2}{\partial \epsilon_{Be}} = -\frac{2}{3}J_e^{-\frac{5}{3}}\lambda_{Ae}^2\frac{\partial J_e}{\partial \epsilon_{Be}} + J_e^{-\frac{2}{3}}2\lambda_{Ae}\frac{\partial \lambda_{Ae}}{\partial \epsilon_{Be}}$$

$$= (2\delta_{AB} - \frac{2}{3})\bar{\lambda}_{Ae}^2 \tag{3.19b}$$

$$\frac{\partial \bar{I}_{1e}}{\partial \epsilon_{Be}} = \frac{4}{3}\bar{\lambda}_{Be}^2 - \frac{2}{3}(\bar{\lambda}_{Ae}^2 + \bar{\lambda}_{Ce}^2)$$

$$= 2\big(\frac{2}{3}\bar{\lambda}_{Be}^2 - \frac{1}{3}(\bar{\lambda}_{Ae}^2 + \bar{\lambda}_{Ce}^2)\big) = 2dev(\bar{b}_{Be}) \tag{3.19c}$$

$$\frac{\partial dev(\bar{b}_{Ae})}{\partial \epsilon_{Be}} = \tag{3.19d}$$

$$= \frac{2}{3}\big(\frac{4}{3}\bar{\lambda}_{Ae}^2 + \frac{1}{3}\bar{\lambda}_{Be}^2 + \frac{1}{3}\bar{\lambda}_{Ce}^2\big) \quad A = B$$

$$= \frac{2}{3}\big(-\frac{2}{3}\bar{\lambda}_{Ae}^2 - \frac{2}{3}\bar{\lambda}_{Be}^2 + \frac{1}{3}\bar{\lambda}_{Ce}^2\big) \quad A \neq B \tag{3.19e}$$

the matrix $\boldsymbol{K}$ is defined as

$$K_{AB} = \frac{\partial r_A}{\partial \epsilon_{Be}} = \delta_{AB} + v_1\Big(\frac{\partial b_{1e}}{\partial \bar{I}_{1e}}dev(\bar{b}_{Ae})\frac{\partial \bar{I}_{1e}}{\partial \epsilon_{Be}}$$

$$+b_{1e}\frac{\partial dev(\bar{b}_{Ae})}{\partial \epsilon_{Be}}\Big) + v_2\frac{\partial(p_e J_e)}{\partial J_e}\frac{\partial J_e}{\partial \epsilon_{Be}}$$

$$= v_1\left(b_{2e}dev(\bar{b}_{Ae})dev(\bar{b}_{Be}) + b_{1e}\frac{\partial dev(\bar{b}_{Ae})}{\partial \epsilon_{Be}}\right) + \delta_{AB} + v_2(dp)_e J_e. \tag{3.20}$$

With the variables b_{1e}, b_{2e} and $(dp)_e$ defined as

$$(dp)_e := \frac{2}{D_1}(2J_e - 1) + \frac{4}{D_2}\Big((J_e - 1)^3 + 3J_e(J_e - 1)^2\Big) + \frac{6}{D_2}\Big((J_e - 1)^5 + 5J_e(J_e - 1)^4\Big) \tag{3.21a}$$

$$b_{1e} := 2C_1 + 4C_2(\bar{I}_{1e} - 3) + 6C_3(\bar{I}_{1e} - 3)^2 \tag{3.21b}$$

$$b_{2e} := 2\frac{\partial b_{1e}}{\partial \bar{I}_1} = 8C_2 + 24C_3(\bar{I}_{1e} - 3). \tag{3.21c}$$

The algorithmic tangent modulus $\boldsymbol{C}^{alg}$ is defined as

$$C^{alg}_{AC} = \frac{\partial \tau_A}{\partial \epsilon_{Be}} K^{-1}_{BC} \tag{3.22}$$

with

$$\frac{\partial \tau_A}{\partial \epsilon_{Be}} = \beta b_{2e} dev(\bar{b}_{Ae}) dev(\bar{b}_{Be}) + \beta b_{1e} \frac{\partial dev(\bar{b}_{Ae})}{\partial \epsilon_{Be}} + \beta (dp)_e J_e. \tag{3.23}$$

3.2 Neo-Hookean hyperelastic model - uncoupled variant

The Neo-Hookean hyperelastic model is one of the simplest polynomial hyperelastic models. Three variants of the Neo-Hookean model have been implemented for calculations with ABAQUS/Standard as UMAT-subroutines. Two uncoupled UMAT subroutines *NeoHookeVisco.for* and *NeoHookeViscoV2.for* and one coupled model *NeoHookeViscoCoupled.for*. The first two models is based on a split of the strain energy function into an *isochoric* (volumetric) and a deviatoric part. The model implemented into the UMAT *NeoHookeVisco.for* is defined in terms of the following strain energy function

$$U_{EQ} = U(\bar{I}_1, J) = C_1(\bar{I}_1 - 3) + \frac{1}{D_1}(J - 1)^2 \tag{3.24}$$

with the NEQ-part defined as

$$U_{NEQ} = U(\bar{I}_{1e}, J_e) = C_1(\bar{I}_{1e} - 3) + \frac{1}{D_1}(J_e - 1). \tag{3.25}$$

From this it can concluded that this Neo-Hookean model may be viewed as a special simplified case of the Yeoh-model with $i, k = 1$. The variables defined in section 3.1 collapse to

$$b_1 = b_{1e} = 2C_1, \quad b_2 = b_{2e} = 0 \tag{3.26a}$$

$$p = \frac{2}{D_1}(J - 1), \quad p_e = \frac{2}{D_1}(J_e - 1) \tag{3.26b}$$

$$a_1 = \frac{b_1}{J}, \quad a_2 = \frac{2}{3}\frac{b_1}{J} = \frac{2}{3}a_1 \tag{3.26c}$$

$$a_3 = 0, \quad a_4 = \frac{1}{J}\frac{2\bar{I}_1}{9}b_1 = \frac{2\bar{I}_1}{9}a_1 \tag{3.26d}$$

$$dp = \frac{2}{D_1}(2J-1), \quad (dp)_e = \frac{2}{D_1}(2J_e-1) \tag{3.26e}$$

This leads to the following expressions for the Kirchoff stress tensors $\boldsymbol{\tau}_{EQ}$ and $\boldsymbol{\tau}_{NEQ}$ and the EQ material tangent $\mathbb{C}_{EQ}^{ABA}$

$$\boldsymbol{\tau}_{EQ} = b_1(\bar{\boldsymbol{b}} - \frac{1}{3}\bar{I}_1\boldsymbol{I}) + pJ\boldsymbol{I} \tag{3.27a}$$

$$\boldsymbol{\tau}_{NEQ} = \beta b_{1e}(\bar{\boldsymbol{b}}_e - \frac{1}{3}\bar{I}_{1e}\boldsymbol{I}) + \beta p_e J_e \boldsymbol{I} \tag{3.27b}$$

$$\mathbb{C}_{EQ}^{ABA} = a_1\Big(\mathbb{H} - \frac{2}{3}(\boldsymbol{I}\otimes\bar{\boldsymbol{b}} + \bar{\boldsymbol{b}}\otimes\boldsymbol{I}) + \frac{2}{3}\frac{\bar{I}_1}{3}\boldsymbol{I}\otimes\boldsymbol{I}\Big) + dp\boldsymbol{I}\otimes\boldsymbol{I} \tag{3.27c}$$

3.2.1 Viscoelastic iteration variables

The Neo-Hookean model gives a simpler expression to solve for the viscoelastic variables as b_{1e} is constant. The necessary viscoelastic iteration variables $\boldsymbol{R}$, $\boldsymbol{K}$ and $\boldsymbol{C}^{ALG}$ is then

$$r_A = \epsilon_{Ae} - \epsilon_{Ae}^{tr} + v_1 b_{1e} dev(\bar{b}_{Ae}) + v_2 p_e J_e \tag{3.28}$$

$$K_{AB} = \delta_{AB} + v_1 b_{1e}\Big((2\delta_{AB} - \frac{2}{3})\bar{\lambda}_{Be}^2 - \frac{2}{3}dev(\bar{b}_{Ae})\Big) + v_2 (dp)_e J_e \tag{3.29}$$

$$C_{AC}^{alg} = \frac{\partial\tau_A}{\partial\epsilon_{Be}}K_{BC}^{-1}, \quad \frac{\partial\tau_A}{\partial\epsilon_{Be}} = \beta b_{1e}\Big((2\delta_{AB} - \frac{2}{3})\bar{\lambda}_{Be}^2 - \frac{2}{3}dev(\bar{b}_{Ae})\Big) + \beta(dp)_e J_e \tag{3.30}$$

with b_{1e} and $(dp)_e$ defined by equation (3.26e) and (3.26a) and v_1 and v_2 defined by equation (3.18).

3.2.2 Interchanging the volumetric part of the strain energy function

A UMAT with the volumetric part of the strain energy function $U(J) = \frac{1}{D_1}(J-1)^2$ interchanged with $U(J) = \frac{1}{D_1}\Big((J-1)^2 + ln(J)^2\Big)$. This only results in a change of the variables p, p_e, dp and $(dp)_e$ which is then defined as

$$p = \frac{2}{D_1}\Big((J-1) + \frac{ln(J)}{J}\Big), \quad p_e = \frac{2}{D_1}\Big((J_e-1) + \frac{ln(J_e)}{J_e}\Big) \tag{3.31a}$$

$$dp = \frac{2}{D_1}\Big((2J-1) + \frac{1}{J}\Big), \quad (dp)_e = \frac{2}{D_1}\Big((2J_e-1) + \frac{1}{J_e}\Big). \tag{3.31b}$$

This material model is implemented in the UMAT-file *NeoHookeViscoV2.for*.

Linearizing $\frac{ln(J)}{J}$ around $J = 1$ gives the following expression for p

$$p \approx \frac{4}{D_1}(J-1) \tag{3.32}$$

which shows that the initial bulk modulus κ^0 is equal to $\frac{4}{D_1}$ for this kind of strain energy function.

3.3 Neo-Hookean hyperelastic model - coupled variant

Another Neo-Hookean model have been implemented into a UMAT-subroutine to possibly improve the modeling of compressible materials. The model is implemented in the UMAT-file *NeoHookeViscoCoupled.for* modeled with the following strain energy function

$$U_{EQ} = U(I_1, J) = C_1(I_1 - 3 - 2ln(J)) + \frac{1}{D_1}(ln(J))^2 \tag{3.33}$$

where the first part is identical to the elastic part of the strain energy function shown in Kang and Huang (2010) based on statistical mechanics as shown in Flory et al. (1976) with $\frac{1}{2}Nk_BT = C_1$. The NEQ-part is then defined as

$$U_{NEQ} = U(I_{1e}, J_e) = \beta C_1\big(I_{1e} - 3 - 2ln(J_e)\big) + \beta\frac{1}{D_1}ln(J_e)^2. \tag{3.34}$$

The second Piola-Kirchhoff stress tensor $\boldsymbol{S}$ is then found as

$$\boldsymbol{S} = \boldsymbol{S}_{EQ} + \boldsymbol{S}_{NEQ} \tag{3.35a}$$

$$\boldsymbol{S}_{EQ} = 2C_1(\boldsymbol{I} - \boldsymbol{C}^{-1}) + \frac{2}{D_1}ln(J)\boldsymbol{C}^{-1} \tag{3.35b}$$

$$\begin{aligned}\boldsymbol{S}_{NEQ} &= \boldsymbol{F}_i^{-1} \cdot \big(\beta 2C_1(\boldsymbol{I} - \boldsymbol{C}_e^{-1}) + \beta\frac{2}{D_1}ln(J_e)\boldsymbol{C}_e^{-1}\big) \cdot \boldsymbol{F}_i^{-T} \\ &= \beta 2C_1(\boldsymbol{C}_i^{-1} - \boldsymbol{C}^{-1}) + \beta\frac{2}{D_1}ln(J_e)\boldsymbol{C}^{-1}.\end{aligned} \tag{3.35c}$$

The Kirchhoff stress $\boldsymbol{\tau}$ is then found from the push-forward operation as

$$\boldsymbol{\tau} = J\boldsymbol{\sigma} = \boldsymbol{F} \cdot \boldsymbol{S} \cdot \boldsymbol{F}^T = \boldsymbol{\tau}_{EQ} + \boldsymbol{\tau}_{NEQ} \tag{3.36a}$$

$$\boldsymbol{\tau}_{EQ} = 2C_1(\boldsymbol{b} - \boldsymbol{I}) + \frac{2}{D_1}ln(J)\boldsymbol{I} \tag{3.36b}$$

$$\boldsymbol{\tau}_{NEQ} = \beta 2C_1(\boldsymbol{b}_e - \boldsymbol{I}) + \beta\frac{2}{D_1}ln(J_e)\boldsymbol{I}. \tag{3.36c}$$

The tangent modulus of the EQ-part $\mathbb{C}_{EQ}^{ABA}$ calculated in the UMAT-subroutine is defined as

$$\mathbb{C}_{EQ}^{ABA} = \frac{2C_1}{J}J^{\frac{2}{3}}\mathbb{H} + \frac{2}{D_1}\frac{1}{J}\boldsymbol{I} \otimes \boldsymbol{I}. \tag{3.37}$$

The calculation of the tangent modulus is shown below.

3.3.1 Calculation of the EQ-part tangent modulus

Rewriting the EQ-Kirchhoff stress $\boldsymbol{\tau}_{EQ}$ in terms of $\bar{\boldsymbol{b}}$ and J leads to the following expression

$$\boldsymbol{\tau}_{EQ} = 2C_1(J^{\frac{2}{3}}\bar{\boldsymbol{b}} - \boldsymbol{I}) + \frac{2}{D_1}ln(J)\boldsymbol{I}. \tag{3.38}$$

The variation of $\boldsymbol{\tau}_{EQ}$ is then

$$\delta\boldsymbol{\tau}_{EQ} = 2C_1\big(\frac{2}{3}J^{-\frac{1}{3}}\bar{\boldsymbol{b}}\delta J + J^{\frac{2}{3}}\delta\bar{\boldsymbol{b}}\big) + \frac{2}{D_1}\frac{1}{J}\boldsymbol{I}\delta J$$

$$= 2C_1J^{\frac{2}{3}}\Big((\frac{2}{3}\bar{\boldsymbol{b}}\otimes\boldsymbol{I}) : \delta\boldsymbol{d} + \mathbb{H} : \delta\boldsymbol{e} + (\delta\boldsymbol{w}\cdot\bar{\boldsymbol{b}} - \bar{\boldsymbol{b}}\cdot\delta\boldsymbol{w})\Big)$$

$$+\big(\frac{2}{D_1}\boldsymbol{I}\otimes\boldsymbol{I}\big) : \delta\boldsymbol{d}.$$

Recalling the properties of equation (3.10b) it may then be shown that

$$\delta\boldsymbol{\tau}_{EQ} + \boldsymbol{\tau}_{EQ}\cdot\delta\boldsymbol{w} - \delta\boldsymbol{w}\cdot\boldsymbol{\tau}_{EQ} = \mathbb{C}^{\Delta J} : \delta\boldsymbol{d}$$

$$= 2C_1J^{\frac{2}{3}}\Big((\frac{2}{3}\bar{\boldsymbol{b}}\otimes\boldsymbol{I}) : \delta\boldsymbol{d} + \mathbb{H} : \delta\boldsymbol{e}\Big)$$

$$+\big(\frac{2}{D_1}\boldsymbol{I}\otimes\boldsymbol{I}\big) : \delta\boldsymbol{d}$$

$$= 2C_1J^{\frac{2}{3}}\Big((\frac{2}{3}\bar{\boldsymbol{b}}\otimes\boldsymbol{I}) : \delta\boldsymbol{d} + \mathbb{H} : \delta\boldsymbol{d} - (\frac{2}{3}\bar{\boldsymbol{b}}\otimes\boldsymbol{I}) : \delta\boldsymbol{d}\Big)$$

$$+\big(\frac{2}{D_1}\boldsymbol{I}\otimes\boldsymbol{I}\big) : \delta\boldsymbol{d}$$

$$= \Big(2C_1J^{\frac{2}{3}}\mathbb{H} + \frac{2}{D_1}\boldsymbol{I}\otimes\boldsymbol{I}\Big) : \delta\boldsymbol{d}. \tag{3.41}$$

The tangent modulus of the EQ-part $\mathbb{C}_{EQ}^{ABA}$ is then defined as

$$\mathbb{C}_{EQ}^{ABA} = \frac{2C_1}{J}J^{\frac{2}{3}}\mathbb{H} + \frac{2}{D_1}\frac{1}{J}\boldsymbol{I}\otimes\boldsymbol{I} \tag{3.42}$$

with $\mathbb{H}$ defined by equation (3.8).

3.3.2 Viscoelastic iteration variables

By splitting the viscous Kirchhoff stress $\boldsymbol{\tau}_{NEQ}$ into a deviatoric and volumetric part

$$dev(\boldsymbol{\tau}_{NEQ}) = \boldsymbol{\tau}_{NEQ} - \frac{1}{3}tr(\boldsymbol{\tau}_{NEQ})\boldsymbol{I} = \beta 2C_1(\boldsymbol{b}_e - \frac{I_{1e}}{3}\boldsymbol{I}) = \beta 2C_1 dev(\boldsymbol{b}_e) \tag{3.43a}$$

$$vol(\boldsymbol{\tau}_{NEQ}) = \frac{1}{3}tr(\boldsymbol{\tau}_{NEQ}) = \beta 2C_1(\frac{I_{1e}}{3} - 1)\boldsymbol{I} + \beta\frac{2}{D_1}ln(J_e) \tag{3.43b}$$

the vector $\boldsymbol{r}$ and matrix $\boldsymbol{K}$ is then defined as

$$r_A = \epsilon_{Ae} - \epsilon^{tr}_{Ae} + v_1 2C_1 dev(b_{Ae}) + v_2\Big(2C_1(\frac{I_{1e}}{3} - 1) + \frac{2}{D_1} ln(J_e)\Big) \tag{3.44}$$

$$\begin{aligned} K_{AB} &= \delta_{AB} + v_1 2C_1 \frac{\partial dev(b_{Ae})}{\partial \epsilon_{Be}} + v_2\Big(2C_1 \frac{\partial I_{1e}}{\partial \epsilon_{Be}} \frac{1}{3} + \frac{2}{D_1} \frac{1}{J_e} \frac{\partial J_e}{\partial \epsilon_{Be}}\Big) \\ &= \delta_{AB} + v_1 2C_1 \big(2\delta_{AB} - \frac{2}{3}\big)\lambda^2_{Be} + v_2\Big(2C_1 \frac{2}{9}\lambda^2_{Be} + \frac{2}{D_1}\Big) \end{aligned} \tag{3.45}$$

with the variables v_1 and v_2 defined by equation (3.18). The algorithmic tangent modulus is then defined as

$$C^{alg}_{AC} = \frac{\partial \tau_A}{\partial \epsilon_{Be}} K^{-1}_{BC} \tag{3.46}$$

with

$$\frac{\partial \tau_A}{\partial \epsilon_{Be}} = \beta 2C_1 \frac{\partial \lambda^2_{Ae}}{\partial \epsilon_{Be}} + \frac{2}{D_1} \frac{1}{J_e} \frac{\partial J_e}{\partial \epsilon_{Be}} = \beta\Big(4C_1 \lambda^2_{Ae} \delta_{AB} + \frac{2}{D_1}\Big). \tag{3.47}$$

3.4 Hydrogel Constitutive model

The viscoelastic hydrogel model implemented is a combined model consisting of the elastic hydrogel model developed by Kang and Huang (2010) and finite viscoelasticity developed by Reese and Govindjee (1998). The polymer chain network is assumed to be incompressible while the mix of solvent with the polymer particles is assumed to cause the volumetric deformations of the material. This material behavior is modeled by part 1 and part 2 respectively of the strain energy function as shown below. A good example of this behavior is the dissipation of water observed from hydrogels during compression.

The strain energy function from Kang and Huang (2010) is

$$\begin{aligned} U_{EQ} &= \frac{1}{2} N k_B T (I_1 - 3 - 2\ln(J)) \\ &+ \frac{k_B T}{\nu}[(J-1)\ln(\frac{J-1}{J}) + \chi \frac{J-1}{J}] - \frac{\mu}{\nu}(J-1) \end{aligned} \tag{3.48}$$

with the new parameters defined as

N	=	Number of polymer chains per unit volume
k_B	=	Boltzmanns constant
T	=	Absolute temperature
ν	=	Volume per solvent molecule
μ	=	Chemical potential of the hydrogel
χ	=	Energy parameter

in this case Nk_BT is the initial shear modulus during small strains.
The NEQ strain energy function is then found as

$$U_{NEQ} = \frac{1}{2}\beta N k_B T[I_{1e} - 3 - 2\ln(J_e)]$$
$$+ \beta\frac{k_B T}{\nu}[(J_e - 1)\ln(\frac{J_e - 1}{J_e}) + \chi\frac{J_e - 1}{J_e}] - \beta\frac{\mu}{\nu}(J_e - 1). \tag{3.49}$$

To further develop the theory, the second Piola Kirchhoff stress tensor is then found as

$$\boldsymbol{S} = \boldsymbol{S}_{EQ} + \boldsymbol{S}_{NEQ} \tag{3.50a}$$
$$\boldsymbol{S}_{EQ} = 2\frac{\partial U_{EQ}}{\partial \boldsymbol{C}} = Nk_BT\big(\boldsymbol{I} + f(J)\boldsymbol{C}^{-1}\big) \tag{3.50b}$$
$$\boldsymbol{S}_{NEQ} = \boldsymbol{F}_i^{-1} \cdot 2\frac{\partial U_{NEQ}}{\partial \boldsymbol{C}_e} \cdot \boldsymbol{F}_i^{-T}$$
$$= \beta Nk_BT\big(\boldsymbol{C}_i^{-1} + f(J_e)\boldsymbol{C}^{-1}\big) \tag{3.50c}$$

The Kirchhoff stress tensor is then found from the push-forward operation as

$$\boldsymbol{\tau} = J\boldsymbol{\sigma} = \boldsymbol{F}\cdot\boldsymbol{S}\cdot\boldsymbol{F}^T = \boldsymbol{\tau}_{EQ} + \boldsymbol{\tau}_{NEQ} \tag{3.51a}$$
$$\boldsymbol{\tau}_{EQ} = Nk_BT\big(\boldsymbol{b} + f(J)\boldsymbol{I}\big) \tag{3.51b}$$
$$\boldsymbol{\tau}_{NEQ} = \beta Nk_BT\big(\boldsymbol{b}_e + f(J_e)\boldsymbol{I}\big) \tag{3.51c}$$

with the function $f(y)$ defined as

$$f(y) = \frac{\partial}{\partial y}\left(\frac{1}{N\nu}\Big((y-1)\ln(\frac{y-1}{y}) + \chi\frac{y-1}{y} - \frac{\mu}{k_BT}\Big)\right)\cdot y - 1$$
$$= \frac{1}{N\nu}\Big(\ln(\frac{y-1}{y})y + 1 - N\nu + \frac{\chi}{y} - \frac{\mu}{k_BT}y\Big). \tag{3.52}$$

3.4.1 Initial state-variable

The function $f(y)$ approach $-\infty$ as y approach 1 which leads to the chemical potential μ approaching a value of $-\infty$ if the initial state should be stress-free. This is solved by Kang and Huang (2010) by introducing an initial swelling deformation $\boldsymbol{F}^0$ such that the initial state is stress free. The total deformation of the hydro gel is then defined as $\boldsymbol{F}^{TOT} = \boldsymbol{F}\cdot\boldsymbol{F}^0$.

The initial deformation gradient $\boldsymbol{F}^0$ with a given chemical potential μ may then be found be solving

$$(\tau_{EQ}^{(0)})_A = Nk_BT\left((\lambda^{(0)})^2 + \frac{1}{N\nu}\Big(\ln(\frac{J^{(0)}-1}{J^{(0)}})J^{(0)} + 1 - N\nu + \frac{\chi}{J^{(0)}} - \frac{\mu}{k_BT}J^{(0)}\Big)\right) = 0 \tag{3.53}$$

for the case of isotropic swelling with $J^{(0)} = \lambda^{(0)}\lambda^{(0)}\lambda^{(0)}$. For the case of constraints causing anisotropic swelling ($\lambda_1^{(0)}$, $\lambda_2^{(0)}$ and/or $\lambda_3^{(0)} \neq 0$) the initial stress may be found by some modifications as shown in Kang and Huang (2010). Alternatively the chemical potential μ may be found by equation (3.53) if the initial deformations are known or prescribed.

The initial state of the elastic part of the decomposed deformation gradient $\boldsymbol{F}_e^0$ is identical to the initial deformation gradient $\boldsymbol{F}^0$ as

$$(\tau_{NEQ}^{(0)})_A = Nk_BT\left((\lambda_e^{(0)})^2 + \frac{1}{N\nu}\left(\ln(\frac{J_e^{(0)}-1}{J_e^{(0)}})J_e^{(0)} + 1 - N\nu + \frac{\chi}{J_e^{(0)}} - \frac{\mu}{k_BT}J_e^{(0)}\right)\right) = 0 \tag{3.54}$$

which leads to $J^{(0)} = J_e^{(0)}$ and $\lambda_A^{(0)} = \lambda_{Ae}^{(0)}$.

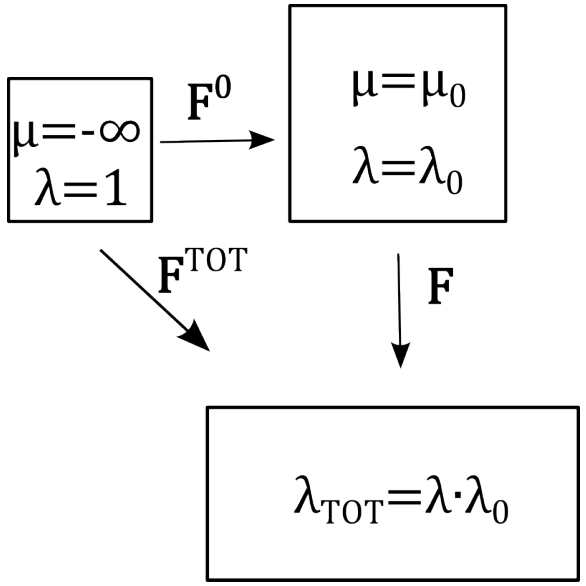

Figure 3.1: Sketch of the decomposition of the deformation gradient

3.4.2 The EQ-part tangent modulus

The tangent modulus of the EQ-part $\mathbb{C}_{EQ}^{ABA}$ is found by the variation of the Kirchhoff stress as performed in the previous sections. The calculation are shown in detail in Kang and Huang (2010) leading to

$$\mathbb{C}_{EQ}^{ABA} = Nk_BT\left(J^{-\frac{1}{3}}\mathbb{H} + \frac{g(J)}{J}\boldsymbol{I}\otimes\boldsymbol{I}\right) \tag{3.55}$$

which have some similarities to equation (3.37). The function $g(y)$ is defined as

$$g(y) = \frac{\partial f(y)}{\partial y} \cdot y = \frac{1}{N\nu}\Big(\ln(\frac{y-1}{y})y + \frac{y}{y-1} - \frac{\chi}{y} - \frac{\mu}{k_B T} y\Big). \tag{3.56}$$

3.4.3 Viscoelastic iteration variables

The viscoelastic variables $\boldsymbol{r}$, $\boldsymbol{K}$ and $\boldsymbol{C}^{ALG}$ must be found to complete the hydrogel viscoelastic model and to find the internal variables $\boldsymbol{C}_i$ and the NEQ constitutive tangent $\mathbb{C}^{ABA}_{NEQ}$. The deviatoric and volumetric parts of $\boldsymbol{\tau_{NEQ}}$ is given as

$$dev(\boldsymbol{\tau}_{NEQ}) = \boldsymbol{\tau}_{NEQ} - \frac{1}{3} tr(\boldsymbol{\tau}_{NEQ})\boldsymbol{I} = \beta N k_B T(\boldsymbol{b}_e - \frac{I_{1e}}{3}\boldsymbol{I}) = \beta N k_B T dev(\boldsymbol{b}_e) \tag{3.57a}$$

$$vol(\boldsymbol{\tau}_{NEQ}) = \frac{1}{3} tr(\boldsymbol{\tau}_{NEQ}) = \beta N k_B T\Big(\frac{I_{1e}}{3} + f(J_e)\Big) \tag{3.57b}$$

The vector $\boldsymbol{r}$ is given as

$$\begin{aligned} r_A &= \epsilon_{Ae} + \Delta t\Big(\frac{1}{2\eta_D} dev(\tau_A) + \frac{1}{3\eta_V} vol(\boldsymbol{\tau}_{NEQ})\Big) - (\epsilon_{Ae})_{trial} \\ &= \epsilon_{Ae} - (\epsilon_{Ae})_{trial} + N k_B T\Big(v_1 dev(b_{Ae}) + v_2\Big(\frac{I_{1e}}{3} + f(J_e)\Big)\Big) \end{aligned} \tag{3.58}$$

with the variables v_1 and v_2 defined by equation (3.18). The matrix K is then found as

$$\begin{aligned} K_{AB} &= \delta_{AB} + N k_B T\Big(v_1 \frac{\partial dev(b_{Ae})}{\partial \epsilon_{Be}} + v_2\Big(\frac{\partial I_{1e}}{\partial \epsilon_{Be}}\frac{1}{3} + \frac{\partial f(J_e)}{\partial J_e}\frac{\partial J_e}{\partial \epsilon_{Be}}\Big)\Big) \\ &= \delta_{AB} + N k_B T\Big(v_1\big(2\delta_{AB} - \frac{2}{3}\big)\lambda^2_{Be} + v_2\Big(\frac{2}{9}\lambda^2_{Be} + g(J_e)\Big)\Big) \end{aligned} \tag{3.59}$$

with the function $g(J_e)$ defined by equation (3.56).
Finally the incremental tangent modulus $\boldsymbol{C}^{ALG}$ is found as

$$C^{alg}_{AC} = \frac{\partial \tau_A}{\partial \epsilon_{Be}} K^{-1}_{BC} \tag{3.60}$$

with

$$\frac{\partial \tau_A}{\partial \epsilon_{Be}} = \beta N k_B T\Big(\frac{\partial \lambda^2_{Ae}}{\partial \epsilon_{Be}} + \frac{\partial f(J_e)}{\partial J_e}\frac{\partial J_e}{\partial \epsilon_{Be}}\Big) = \beta N k_B T\Big(2\lambda^2_{Ae}\delta_{AB} + g(J_e)\Big). \tag{3.61}$$

The viscoelastic hydrogel material model have been implemented in the UMAT-file *KANGViscous.for*.

Chapter 4

Numerical tests

To test the material models numerically a creep test and a relaxation test under large deformations have been performed with *ABAQUS/Standard*. The element tested is a single 20-node quadratic reduced integration brick element (C3D20R) with all sides length equal to 1mm.

The material models where tested with the following values for the Neo-Hookean material models:

Name	2C1	2/D1	η_{DEV}	η_{VOL}	β	UMAT-file
NH1	3	120	15	600	1	*KANGViscous.for*
NH2	3	120	15	600	1	*KANGViscousV2.for*
NHC	3	120	15	600	1	*KANGViscousCoupled.for*
NH1:2-el	3	120	15/240	600/1200	1/1	*KANGViscous2EL.for*

Table 4.1: Values of the Neo-Hookean material constants during the FEM tests.

where NH1 is the first variant of the uncoupled Neo-Hookean material model described in section 3.2 and NH2 is the second variant of the uncoupled Neo-Hookean material. NHC is the coupled Neo-Hookean material described in section 3.3 while NH1:2-el is the first material model with 2 viscous (internal) elements. The Yeoh-material (YEOHV) and the hydrogel material model (KANG) was tested with the following values:

Name	2C1	2C2	2C3	2/D1	2/D1	2/D1
			η_{DEV}	η_{VOL}	β	UMAT-file
YEOHV	3	-0.01	0.0016	120	12	1
			15	600	1	*YEOH3Visco.for*

Name	Nk_BT	$N\nu$	χ	η_{DEV}	η_{VOL}	β	UMAT-file
KANG	1.5	0.0375	0.48	15	600	1	*KANGViscous.for*

Table 4.2: Values of the Yeoh and hydrogel material constants during the FEM tests.

The material constants have the following units:

$$
\begin{array}{lcl}
[C1] & = & [MPa] \\
[C2] & = & [MPa] \\
[C3] & = & [MPa] \\
[D1] & = & [(MPa)^{-1}] \\
[D2] & = & [(MPa)^{-1}] \\
[D3] & = & [(MPa)^{-1}] \\
[Nk_BT] & = & [MPa] \\
[\eta_{DEV}] & = & [MPa \cdot s] \\
[\eta_{VOL}] & = & [MPa \cdot s] \\
[\beta] & = & [\ ] \\
[N\nu] & = & [\ ] \\
[\chi] & = & [\ ]
\end{array}
$$

Table 4.3: Units of the material constants.

while the force shown in the figures have units of MPa.

4.1 Creep test

The solid element described is prescribed a a traction force of 10 newton on one edge normal to the 2-direction ($t_2^0 = 20$) as a ramp force over a time period of 1 second and then held constant in the succeeding step for 35 seconds. The deformations at the initial step and at the end of step 1 and step 2 are shown in figure 4.1.

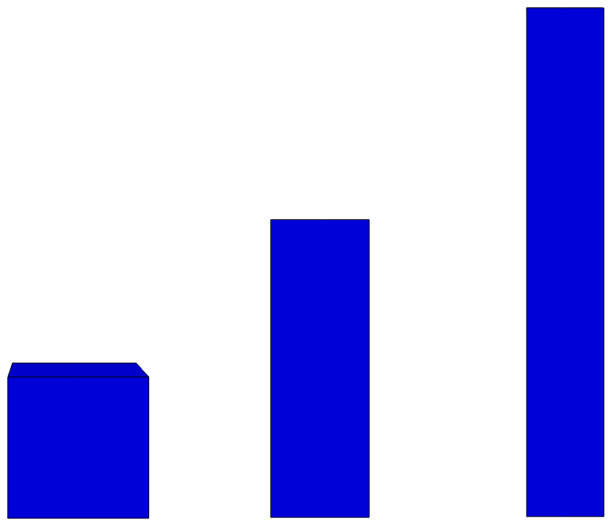

Figure 4.1: Deformation of the solid element at $t = 0, 1, 36$.

As seen in figure 4.2 the initial tangent of the material models at small deformations are close, while the stiffness of the YEOH material increases more non-linearly with the strain. The Neo-Hookean model with an extra viscous element is stiffer during the loading phase as expected.

The resulting stretch values shown in figure 4.3 shows that the behavior is as predicted by the linear results (figure 2.7). It is also clear that a time-period of 35 seconds of the second step is insufficient for the second viscous variable $\boldsymbol{b}_e^{(2)}$ to reach thermodynamic equilibrium $\boldsymbol{b}_e^{(2)} \approx 0$ due to the high viscosity values prescribed to the second viscous element. Recalling from the generalized Maxwell model that the relaxation time τ in the linear case is given as $\tau = \frac{\eta}{K}$ the deviatoric and volumetric relaxation times may be approximated from the shear-module G and the bulk modulus κ as

$$\tau_{DEV} \approx \frac{\eta_{DEV}}{G} \approx \frac{\eta_{DEV}}{2C1} = \begin{cases} 5 & \text{First viscous element} \\ 80 & \text{Second viscous element} \end{cases} \tag{4.1a}$$

$$\tau_{VOL} \approx \frac{\eta_{VOL}}{\kappa} \approx \frac{\eta_{DEV}}{2/D1} = \begin{cases} 5 & \text{First viscous element} \\ 10 & \text{Second viscous element} \end{cases} \tag{4.1b}$$

which indicates that the second element needs a much greater time-period to reach thermodynamic equilibrium. Figure 4.4 shows this effect.

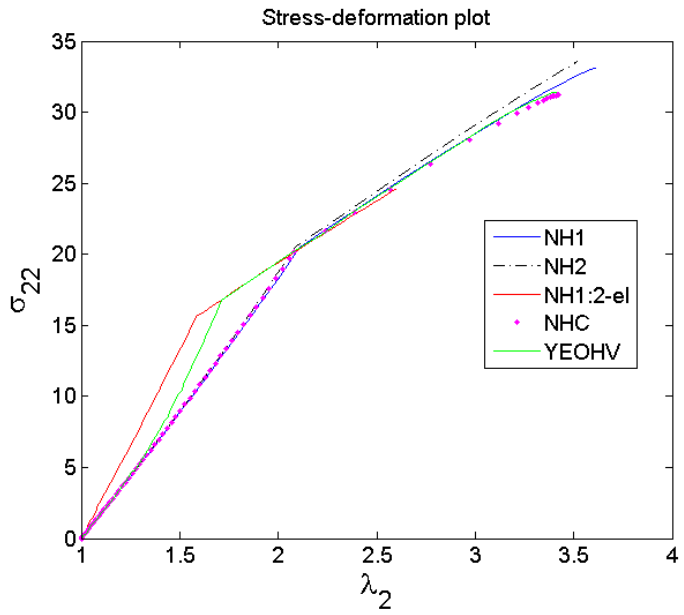

Figure 4.2: Stress-stretch results of the Neo-Hookean and Yeoh material models.

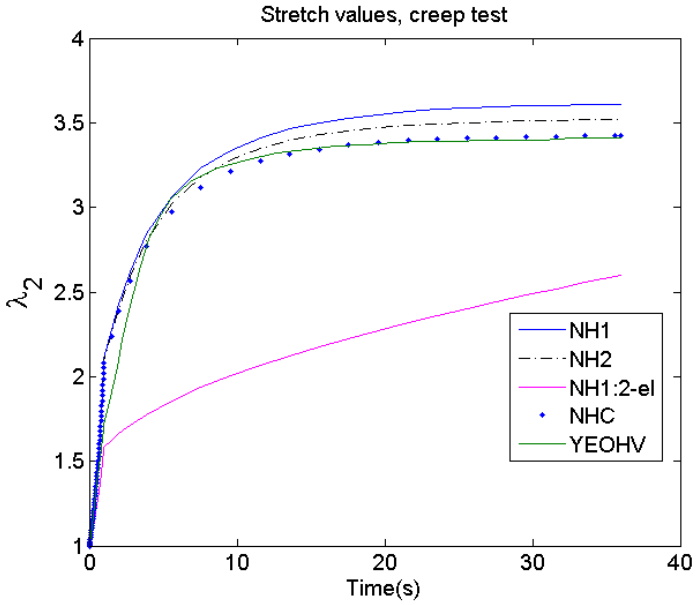

Figure 4.3: Stretch results of the Neo-Hookean and Yeoh material models.

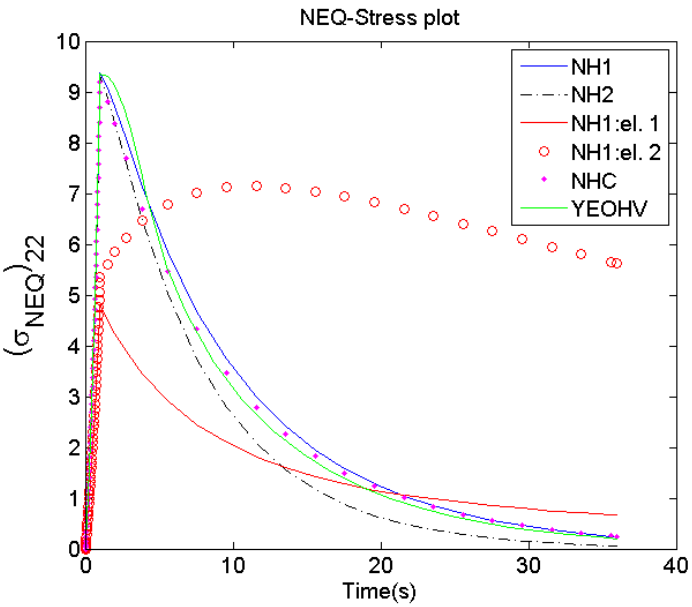

Figure 4.4: NEQ-Stress results of the Neo-Hookean and Yeoh material models.

The hydrogel viscoelastic models response depends greatly on the initial chemical potential μ and the corresponding initial swelling stretches $\lambda^{(0)}$ as shown in figure 4.5. The *normalized chemical potential* from Kang and Huang (2010) is defined as

$$\mu^* = \frac{\mu}{k_B T} \tag{4.2}$$

with the following values and corresponding swelling stretches tested:

μ^*	$\lambda^{(0)}$
0	1.490
-0.04	1.302
-0.4	1.093

Table 4.4: Values of μ^* and the corresponding value of $\lambda^{(0)}$ used in the FEM test.

The compressibility of the hydrogel material also varies greatly with the normalized chemical potential as shown in figure 4.6, which shows Poisson's ratio for the different values of μ^* where values close to 0.5 shows nearly incompressible behavior.

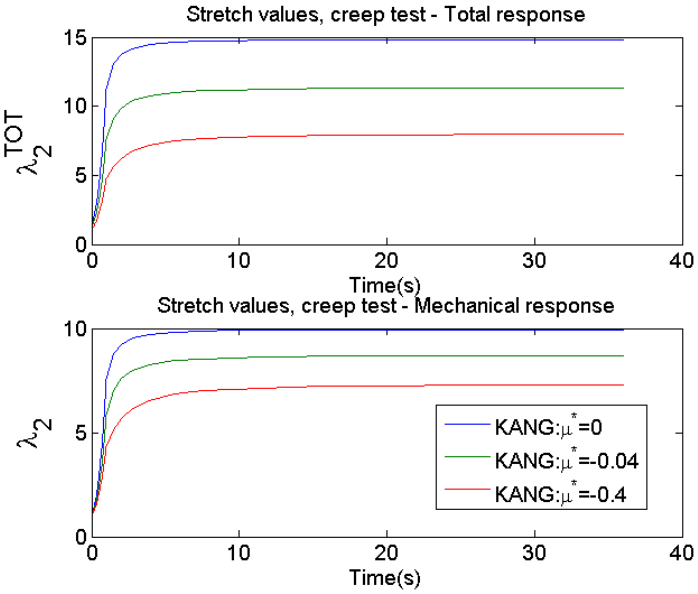

Figure 4.5: Stretch values of the hydrogel material model at different values of normalized chemical potential μ^*.

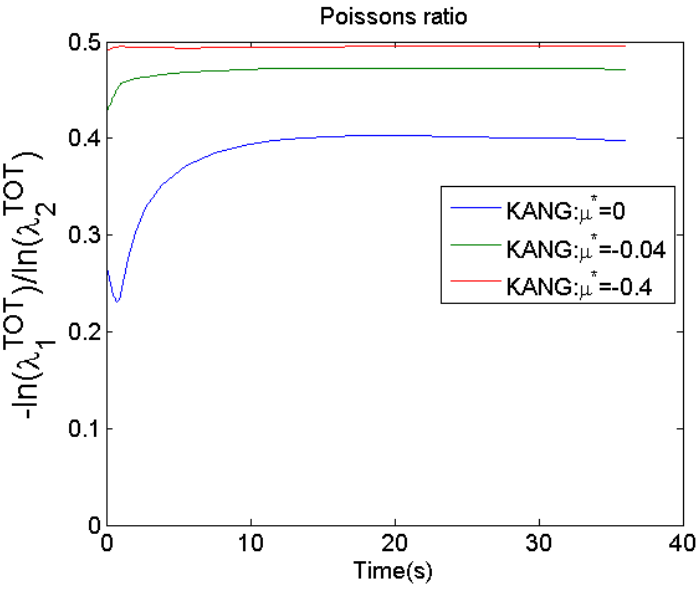

Figure 4.6: Poisson's ratio of the hydrogel material model at different values of normalized chemical potential μ^*.

4.2 Relaxation test

A relaxation test was done with the same properties and setup as for the creep test. The solid element is deformed such that $\lambda_2 = 3.5$ over a time-period of 1 second and held in the following step for 35 seconds. Figure 4.7 and 4.8 shows the total stress and NEQ-stresses in the 2-direction and it is clear that the viscoelastic behavior is as predicted in the linear case (figure 2.6).

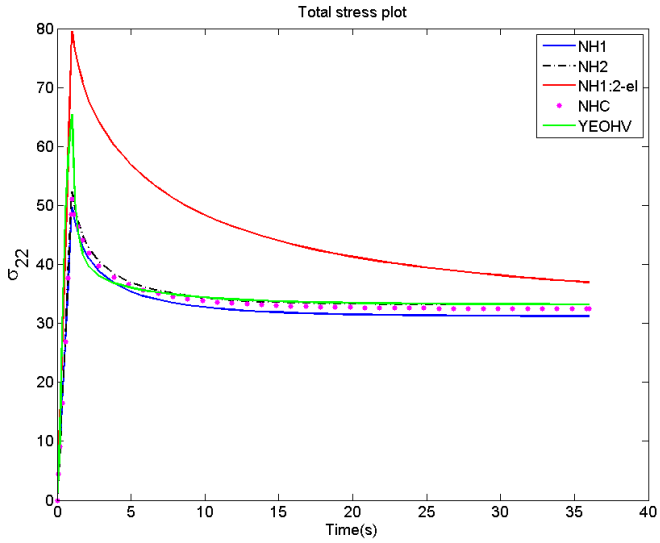

Figure 4.7: Total stress results of the Neo-Hookean and Yeoh material models.

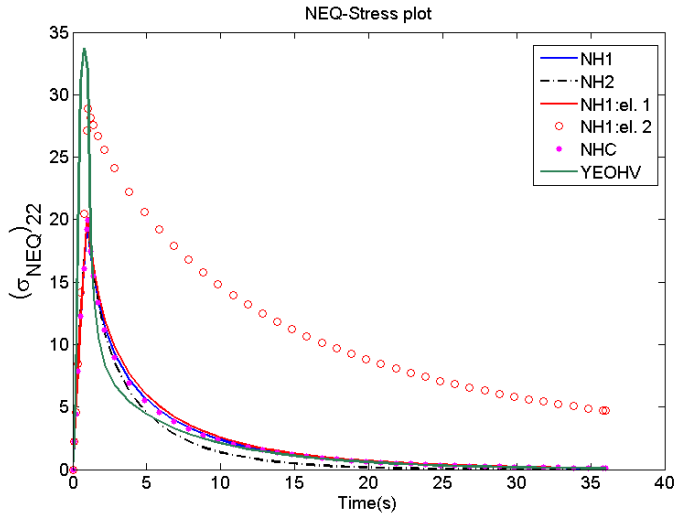

Figure 4.8: NEQ-stress results of the Neo-Hookean and Yeoh material models.

The hydrogel material behavior in terms of compressibility is almost the same as in the creep-test case as shown in figure 4.9.

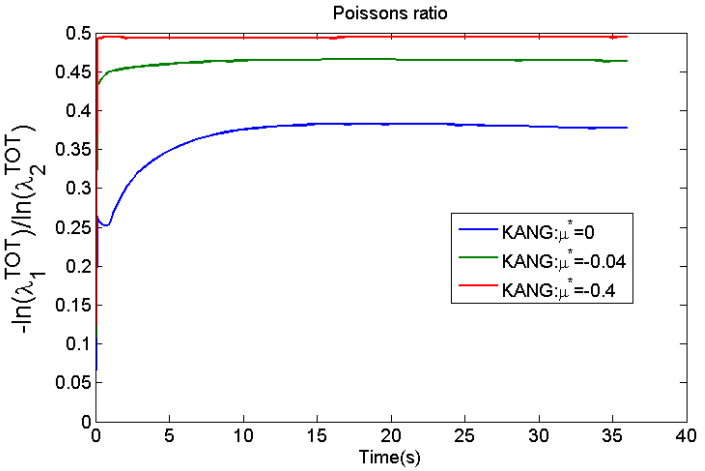

Figure 4.9: Poisson's ratio of the hydrogel material model at different values of normalized chemical potential μ^*.

4.3 Hydrogel swelling

To illustrate the large swelling due to change in the chemical potential in the hydrogel material model, a FEM-model with 8-node axisymmetric coupled temperature-displacement elements (CAX8RT) was subject to a change of normalized chemical potential from $\mu^* = -0.5$ to $\mu^* = 0$ over a time-step of 1 second, then held for 10 seconds. The model is a half-sphere with a radius of $60\mu m$ restrained from movement on the flat surface.

The following material properties where used:

$$\begin{array}{lcl} [Nk_BT] & = & 3 \\ [N\nu] & = & 0.075 \\ [\chi] & = & 0.48 \\ [\eta_{DEV}] & = & 30 \\ [\eta_{VOL}] & = & 600 \\ [\beta] & = & 1 \end{array}$$

Table 4.5: Material constants used in the swelling test.

The resulting swelling is shown in figure 4.10 while the displacement at the top of the

half-sphere is shown in figure 4.11, which shows that the swelling continues after the first step.

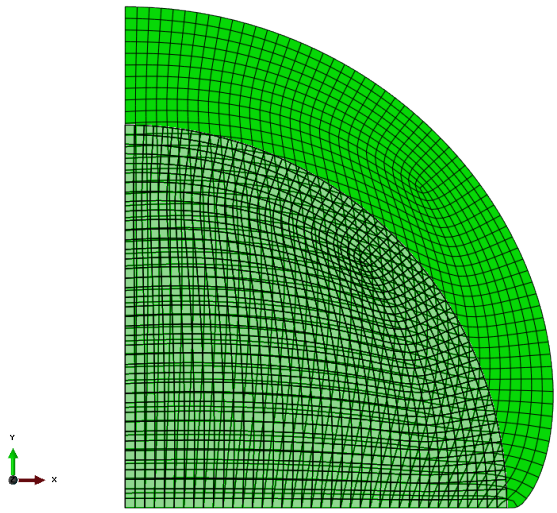

Figure 4.10: Chemical potential variation induced swelling of a half-sphere axisymmetric FEM-model.

The swelling in the 2-direction equals $\lambda_2 = 1.39$ at the center of the halfsphere while unrestrained isotropic swelling from $\mu^* = -0.5$ to $\mu^* = 0$ would make $\lambda_2 = 1.41$ where the small difference in the stretch values is due to the constraint in the 1- and 3-direction. Due to the rapid swelling rate when μ^* approaches zero, very small time-steps ($\Delta t = 0.015$) where necessary for the FEM-solution to converge.

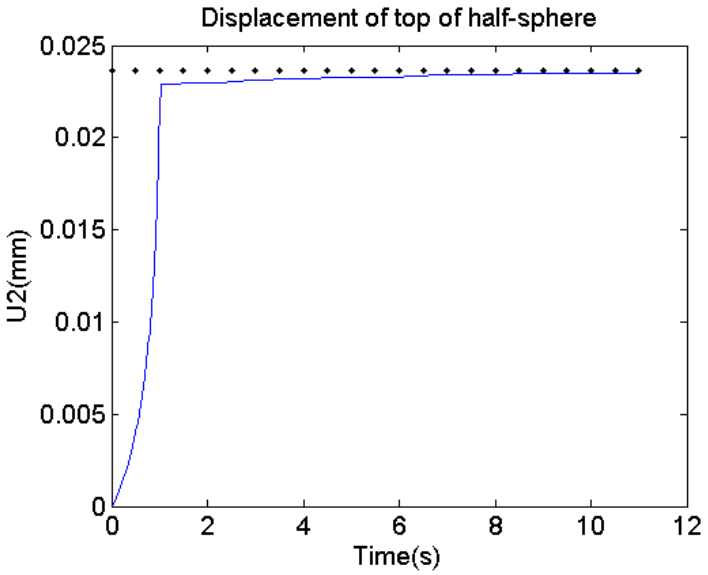

Figure 4.11: Displacement of the top of the half-sphere due to chemical potential variation-induced swelling.

4.4 The impact of the material scaling parameter on the viscous variables

In Reese and Govindjee (1998) equation (2.64) is linearized around $\boldsymbol{b}_e = \boldsymbol{I}$ which leads to

$$\dot{\boldsymbol{C}}_i = \frac{1}{\tau}(\boldsymbol{C} - \boldsymbol{C}_i), \quad \tau = \frac{\eta_{DEV}}{G} = \frac{\eta_{VOL}}{\kappa} \tag{4.3}$$

where τ is the relaxation time close to thermodynamic equilibrium while G and κ is mechanical properties of the NEQ stress close to thermodynamic equilibrium. As the material scaling parameter β is added to the NEQ part of the strain energy equation τ is given as

$$\tau = \frac{\eta_{DEV}}{\beta G} = \frac{\eta_{VOL}}{\beta \kappa} \tag{4.4}$$

which means that the parameter β decrease the relaxation times for $\beta > 1$ and increase the relaxation time for $\beta < 1$ as seen in figure 4.12. As seen in figure 4.13 the relaxation time may be held close to constant by multiplying the initial viscosity η_0 with β, while the increase in the NEQ stress is proportional to β.

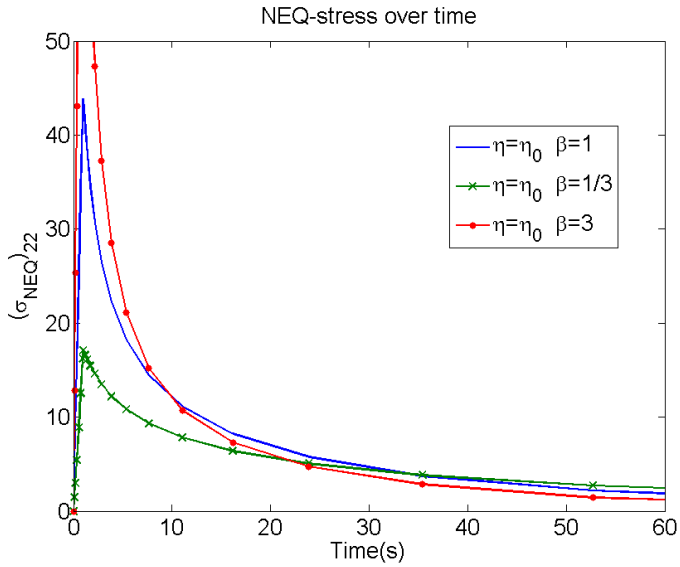

Figure 4.12: NEQ-stress over time with the same values of viscosity and changing β.

4.5 Summary

The material models show satisfactory stability and behavior undergoing large strains in uniaxial tension. The normalized chemical potentials impact of the hydrogel materials volumetric behavior have also been identified as an important initial parameter of the materials mechanical response. The hydrogel material model is also shown to be sensitive to changes in normalized chemical potential μ^* when μ^* is close to zero.

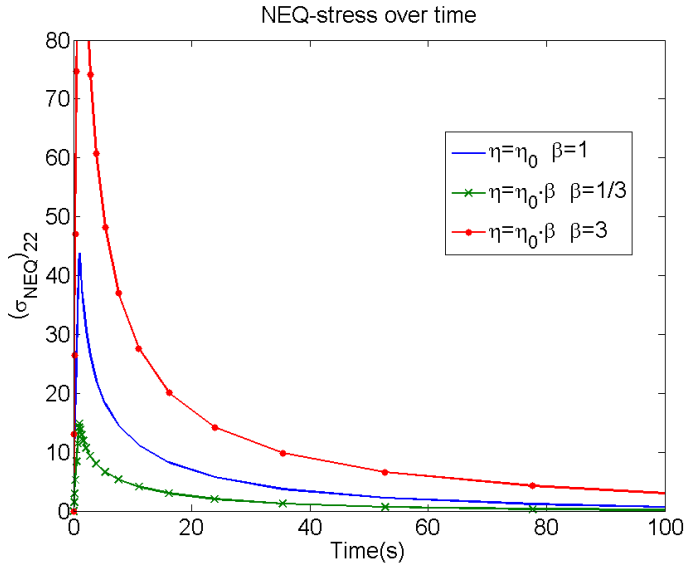

Figure 4.13: NEQ-stress over time with the values of viscosity scaled to the values of β.

Chapter 5

Material testing and material parameter estimation

The material models described in chapter 4 have been used to fit material parameters to two sets of experimental indentation experiments. The viscoelastic hydrogel material model have been matched with indentation experiments of a hydrogel material while the viscoelastic Neo-Hookean and Yeoh material models have been matched with a nanoindentation experiment of an acrylic Ugelstad sphere.

5.1 Material parameter estimation of a hydrogel material

A series of indentation experiments of a hydrogel material have been performed at the Division of Biophysics and Medical Technology, NTNU. The gels have thickness of 1.25mm and contains 10% acrylamide and 3% bis-acrylamide with a 10mM acetate buffer with pH5 and 0.15M NaCl covering the gel.

All experiments are relaxation experiments performed by pressing a spherical or flat indenter 130μm into the gel over a step-time of approximately 2.6 seconds and then held in position while the reaction force is monitored. The diameter of the flat indenter is 4.5mm while the cross-sectional diameter of the conical indenter is 4.5mm.

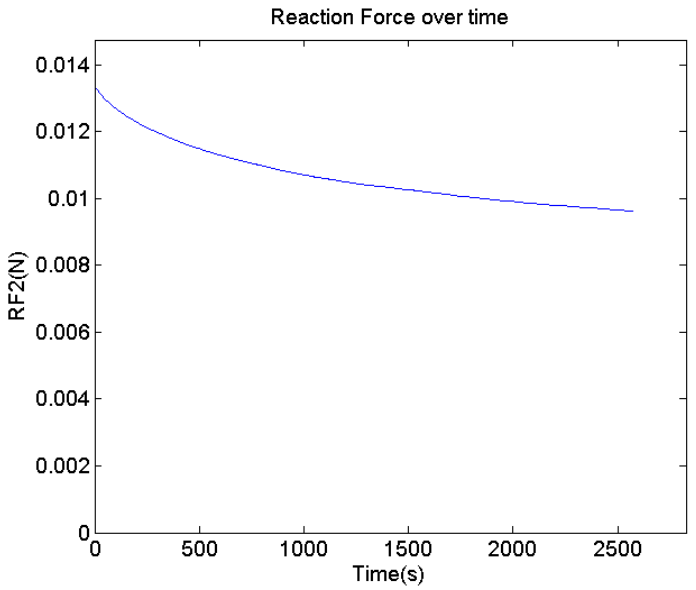

Figure 5.1: Reaction force in units of Newton from an experiment with a conical indenter.

The experimental data shows long relaxation times which may indicate high viscosity values as seen in figure 5.1.

5.1.1 The finite element model

Two axisymmetric finite element models (FEM) have been constructed for use with *ABAQUS/Standard*. The gel is modeled with a radius of 15mm and thickness of 1.25mm on a rigid surface while the indenter is modeled as an analytic surface in both cases.

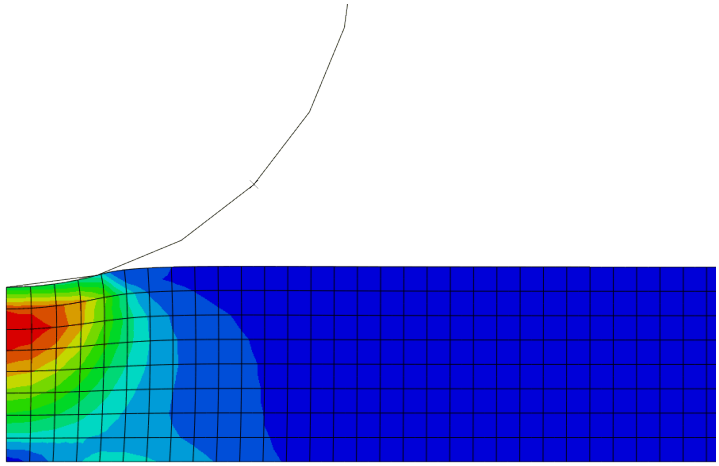

Figure 5.2: FEM model with a spherical indenter.

The gel consists of 8-node bi-quadratic reduced integration elements (CAX8R) with an element size of roughly 0.15mm by 0.15mm with a total of 800 elements. In the model with the flat indenter the edge of the analytic surface was curved slightly to avoid issues with high stress concentrations near the edge of the indenter as seen in figure 5.4. All forces are in units of Newton while all lengths are in units of mm.

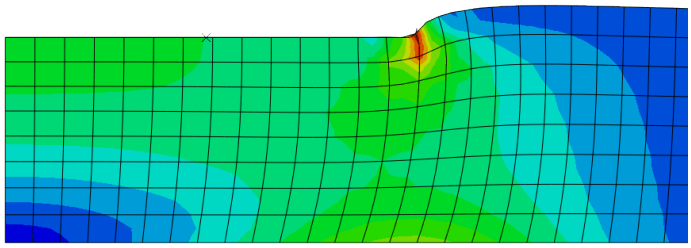

Figure 5.3: FEM model with a flat indenter.

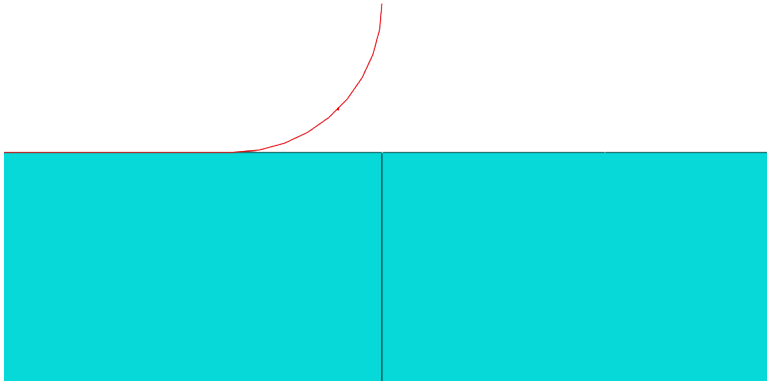

Figure 5.4: The curved edge of the flat indenter.

5.1.2 The inverse FEM-procedure

An inverse FEM-procedure have been set up using the *MATLAB* function *lsqnonlin* and *ABAQUS* Python scripts. The non-linear least square method used is the Trust-region-reflective algorithm which minimizes the error of the experimental and FEM results through a series of iteration. The input values are the material parameters while the resulting vector function $\boldsymbol{f}$ being minimized is defined as

$$f_i = \frac{(RF_2^{FEM})_i - (RF_2^{EXP})_i}{(RF_2^{EXP})_i} \tag{5.1}$$

where RF_2^{FEM} and RF_2^{EXP} is reaction force in the vertical direction calculated with the FEM-model and the measured force from the experimental data. Given a set of material parameters $\boldsymbol{x}$ the function $\boldsymbol{f}$ is minimized in terms of $\boldsymbol{x}$ such that

$$\min_{\boldsymbol{x}} ||\boldsymbol{f}||^2 = \min_{\boldsymbol{x}} \sum_{i=1}^{n} f_i^2(\boldsymbol{x}) \tag{5.2}$$

which is done by the *MATLAB* function as explained in the documentation (MATLAB, 2013).

To determine the number of viscous elements α necessary, the inverse FEM material parameter fitting procedure was performed on the data-set *Fil9Aam* with $\alpha = 1, 2, 3$ with the material scaling parameter $\beta_\alpha = 1$. The preliminary material fit shown in figure 5.5 indicates that $\alpha = 3$ provides a reasonable accuracy in describing the viscoelastic properties of the material, provided $\beta_\alpha = 1$, which amounts to six viscoelastic material parameters to be found $(\eta^1_{DEV}, \eta^1_{VOL}, \eta^2_{DEV}, \eta^2_{VOL}, \eta^3_{DEV}, \eta^3_{VOL})$. For the case of the material parameter $\beta \neq 1$, $\alpha = 1$ provides a good fit of the reaction force reducing the amount of viscoelastic material parameters to three $(\eta_{DEV}, \eta_{VOL}, \beta)$ in this case, but due to time-constraints this option was not investigated further.

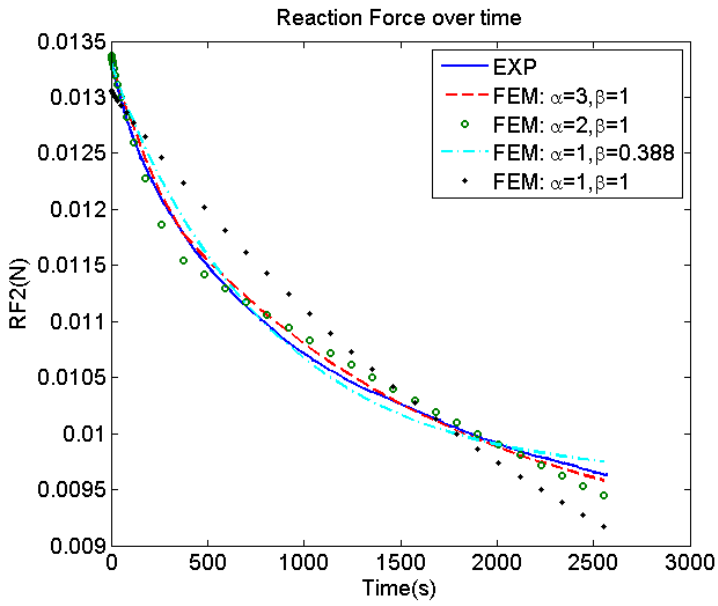

Figure 5.5: Resulting reaction force for different values of α after the inverse-FEM procedure.

5.1.3 Experimental data

Four gel samples from the same main gel material have been tested with a total of ten data files analyzed with the inverse FEM-procedure shown in table 5.1.

Gel sample	Spherical Indenter Data files	Flat Indenter Data files
1	Fil9Aam, Fil10Aam	
2	Fil1Aam2, Fil2Aam2	Flat1Aam2
3	Fil3Aam3	Flat2Aam3, Flat3Aam3, Flat4Aam3
4		Flat2Aam4

Table 5.1: Hydrogel samples and their associated experimental data.

Figure 5.6 and 5.7 shows the normalized experimental data with the reaction force, RF2, shown as the change of weight from the point the indenter is pushed into the gel in units of Newton. The standard gravity g is assumed to equal $9.81\frac{m}{s^2}$.

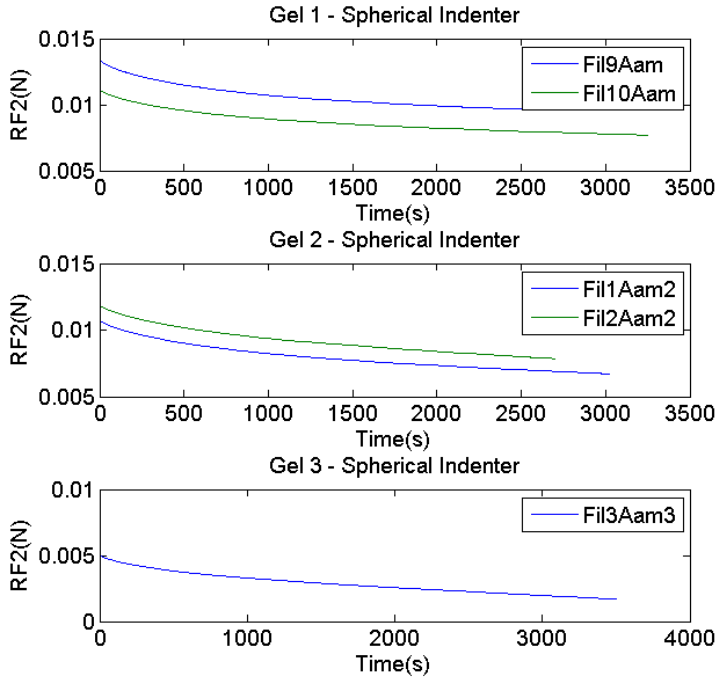

Figure 5.6: Reaction force (RF2) from experiment with spherical indenter.

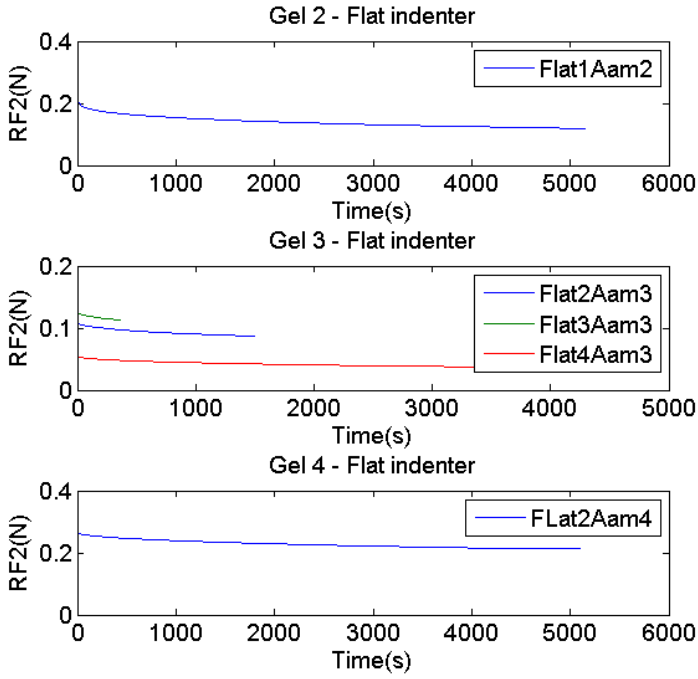

Figure 5.7: Reaction force (RF2) from experiment with flat indenter.

It is clear that there is a significant variation in the material response for the different samples and no conclusion for the material parameters of the material may be made with this set of experimental data. It was reported issues with having the gel stick properly to the glass which may have caused the gels to float in the buffer solution. Some inhomogeneities in the gel-samples was also observed. The inverse FEM-procedure have still been applied to the data to further test the material model and to possibly identify preliminary relaxation times for the viscous elements.

5.1.4 Results

The hydrogel experimental data have been analyzed with the inverse FEM-procedure with the assumptions that $\beta_\alpha = 1$, $\frac{k_B T}{\nu} = 40\ [MPa]$, $\chi = 0.48$ and the normalized chemical potential μ^* is equal to -0.04 using three viscous elements. Table 5.2 and 5.3 shows the resulting material parameters from the inverse FEM-procedure and the squared vector norm of the vector function $\boldsymbol{f}$ defined as $||\boldsymbol{f}||^2 = \sum_{i=1}^{N} f_i^2$.

Data file	Fil1Aam2	Fil2Aam2	Fil3Aam3	Fil9Aam	Fil10Aam
Nk_BT	$5.14 \cdot 10^{-3}$	$5.65 \cdot 10^{-3}$	$2.42 \cdot 10^{-3}$	$5.91 \cdot 10^{-3}$	$5.33 \cdot 10^{-3}$
$N\nu$	$1.29 \cdot 10^{-4}$	$1.41 \cdot 10^{-4}$	$0.61 \cdot 10^{-4}$	$1.48 \cdot 10^{-4}$	$1.33 \cdot 10^{-4}$
χ	0.48	0.48	0.48	0.48	0.48
η^1_{DEV}	130.13	148.46	8.0	687.14	673.99
η^1_{VOL}	1191.2	1606.96	718.0	716.23	446.00
β^1	1	1	1	1	1
η^2_{DEV}	2.88	5.93	0.6	4.28	2.80
η^2_{VOL}	2966.4	3729.84	3480	3679.32	3465.01
β^2	1	1	1	1	1
η^3_{DEV}	10.34	11.03	8.0	13.24	13.34
η^3_{VOL}	74.05	354.52	70.0	70.32	71.73
β^3	1	1	1	1	1
$\|\|\boldsymbol{f}\|\|^2$	$0.59 \cdot 10^{-3}$	$1.09 \cdot 10^{-3}$	$12.6 \cdot 10^{-3}$	$1.05 \cdot 10^{-3}$	$0.41 \cdot 10^{-3}$

Table 5.2: Material parameters identified with the inverse FEM-procedure for the spherical indenter experiment.

Data file	Flat1Aam2	Flat2Aam3	Flat2Aam4	Flat3Aam3	Flat4Aam3
Nk_BT	$5.0 \cdot 10^{-3}$	$2.26 \cdot 10^{-3}$	$5.10 \cdot 10^{-3}$	$2.39 \cdot 10^{-3}$	N/A
$N\nu$	$1.25 \cdot 10^{-4}$	$0.57 \cdot 10^{-4}$	$1.28 \cdot 10^{-4}$	$0.60 \cdot 10^{-4}$	N/A
χ	0.48	0.48	0.48	0.48	0.48
η^1_{DEV}	213.0	14.23	250.0	8.31	N/A
η^1_{VOL}	788.0	737.01	1230.0	717.88	N/A
β^1	1	1	1	1	1
η^2_{DEV}	0.001	0.64	0.6	4.30	N/A
η^2_{VOL}	1993	3995.2	3080	3675.55	N/A
β^2	1	1	1	1	1
η^3_{DEV}	11.5	16.67	120	13.12	N/A
η^3_{VOL}	119	70.43	75	70.30	N/A
β^3	1	1	1	1	1
$\|\|\boldsymbol{f}\|\|^2$	$62.5 \cdot 10^{-3}$	$133.8 \cdot 10^{-3}$	$1.72 \cdot 10^{-3}$	$1.72 \cdot 10^{-3}$	N/A

Table 5.3: Material parameters identified with the inverse FEM-procedure for the flat indenter experiment.

5.1.5 Discussion

The tested gel was observed to not stick properly to the surface during testing which is most likely the reason to the large variations in the experimental data, as well as some inhomogeneities in the gel material. The finite element model with the flat indenter also had some issues with large stress concentrations and distorted elements near the edge of the indenter which caused the finite element iteration to diverge. As a result no material parameters where found with the inverse FEM-procedure from the experimental data

Flat4Aam3. As the experimental data shows, the small reaction force and corresponding low stiffness is likely to cause the elements near the outer edge of the flat indenter to distort excessively.

The initial assumptions that the parameters $\frac{k_B T}{\nu} = 40\ [MPa]$, $\chi = 0.48$ and $\mu^* = -0.04$ should also be investigated and may not be the case for this gel. The initial bulk modulus κ is proportional to $\frac{k_B T}{\nu}$ as seen from equation 3.51b and with the initial shear modulus G approximately equal to Nk_BT which is in the range of $10^{-3}-10^{-2}\ [MPa]$ the material is close to incompressible. Pritchard et al. (2013) reports an initial Poisson ratio of 0.5 which relaxes to 0.26 for a gel with 30% acrylamide immersed in water, in the finite element model the Poisson ratio stays close to 0.5 for the full time-series which is likely due to a constant chemical potential and small initial swelling during the analysis. With this in mind it is clear that initial assumptions regarding the mentioned material parameters may need to be modified.

The initial swelling $\lambda^{(0)}$ which is equal to 1.3 and its impact on the resulting stress in the gel may make it necessary to scale the reaction force and/or the depth of indentation, but this have not been done in the analysis.

To compare the resulting material parameters the following parameters are introduced.

$$G^0 = \beta N k_B T \tag{5.3a}$$

$$\kappa^0 = \beta \frac{k_B T}{\nu} \tag{5.3b}$$

$$(\tau_{DEV})_i = \frac{G^0}{\eta^i_{DEV}}, \quad i = 1, 2, 3 \tag{5.3c}$$

$$(\tau_{VOL})_i = \frac{\kappa^0}{\eta^i_{VOL}}, \quad i = 1, 2, 3 \tag{5.3d}$$

where G^0 and κ^0 is related to the initial shear modulus and bulk modulus while $(\tau_{DEV})_i$ and $(\tau_{VOL})_i$ is approximate time relaxation parameters for the deviatoric and volumetric part. κ^0 is given as $40\ [MPa]$ while the other parameters are shown in table 5.4 and 5.5.

Data file	Fil1Aam2	Fil2Aam2	Fil3Aam3	Fil9Aam	Fil10Aam
G^0	$5.14 \cdot 10^{-3}$	$5.65 \cdot 10^{-3}$	$2.42 \cdot 10^{-3}$	$5.91 \cdot 10^{-3}$	$5.33 \cdot 10^{-3}$
$(\tau_{DEV})_1$	$25.3 \cdot 10^3$	$26.3 \cdot 10^3$	$3.3 \cdot 10^3$	$116.3 \cdot 10^3$	$126.5 \cdot 10^3$
$(\tau_{VOL})_1$	29.8	40.2	20.0	17.9	11.2
$(\tau_{DEV})_2$	$0.6 \cdot 10^3$	$1.1 \cdot 10^3$	$0.2 \cdot 10^3$	$0.7 \cdot 10^3$	$0.5 \cdot 10^3$
$(\tau_{VOL})_2$	74.2	93.2	87.0	92.0	86.6
$(\tau_{DEV})_3$	$2.0 \cdot 10^3$	$2.0 \cdot 10^3$	$3.3 \cdot 10^3$	$2.2 \cdot 10^3$	$2.5 \cdot 10^3$
$(\tau_{VOL})_3$	1.9	8.9	1.8	1.8	1.8

Table 5.4: Initial shear modulus and approximate relaxation times found with the inverse FEM-procedure for the spherical indenter experiment.

Data file	Flat1Aam2	Flat2Aam3	Flat2Aam4	Flat3Aam3	Flat4Aam3
G^0	$5.0 \cdot 10^{-3}$	$2.3 \cdot 10^{-3}$	$5.1 \cdot 10^{-3}$	$2.4 \cdot 10^{-3}$	N/A
$(\tau_{DEV})_1$	$42.6 \cdot 10^3$	$6.3 \cdot 10^3$	$49.0 \cdot 10^3$	$3.5 \cdot 10^3$	N/A
$(\tau_{VOL})_1$	19.7	18.4	30.8	17.9	N/A
$(\tau_{DEV})_2$	$0.01 \cdot 10^3$	$0.3 \cdot 10^3$	$0.1 \cdot 10^3$	$1.8 \cdot 10^3$	N/A
$(\tau_{VOL})_2$	49.8	99.9	77.0	91.9	N/A
$(\tau_{DEV})_3$	$2.3 \cdot 10^3$	$7.4 \cdot 10^3$	$23.5 \cdot 10^3$	$5.5 \cdot 10^3$	N/A
$(\tau_{VOL})_3$	3.0	1.8	1.9	1.8	N/A

Table 5.5: Initial shear modulus and approximate relaxation times found with the inverse FEM-procedure for the flat indenter experiment.

The hydrogel material was tested as four samples, shown in table 5.1. It is clear that sample 3 deviates the most with values of the initial shear modulus G^0 between 2.3 and 2.4 kPa, while analyzing sample 1, 2 and 4 give initial shear modulus values between 5.0 and 5.9 kPa.

While there is problems regarding highly variable experimental data and uncertainty in the values of $\frac{k_B T}{\nu}$, χ and μ^* the material parameters found will hopefully provide some good start values for further analysis. It is also clear that allowing the material scaling parameter β to have other values than 1 would most likely improve the curve fit with less viscous elements.

5.2 Material parameter estimation of a PMMA particle

A series of nanoindentation experiments performed on acrylic Ugelstad particles with diameter $3\mu m$ have been performed at the *NTNU Nanomechanical Lab*, He et al. (2009). The experiments have been performed with a flat indenter compressing the particles. As the particles have been shown to exhibit viscoelastic behavior, the experimental data have been analyzed with the inverse FEM-procedure with the material models NH1, NH2, NHC and YEOHV (see chapter 4 for abbreviations).

5.2.1 The finite element model

The spherical particle have been idealized as an axisymmetric half-sphere due to symmetry, as seen in figure 5.8, where the deflection of the indenter in the FE-model is half of the total deflection of the indenter from experimental data. The mesh of the half-sphere consists of 216 8-node bi-quadratic reduced integration elements (CAX8R) with an element size of about 0.1 by 0.1 μm which is constrained from movement in the 2-direction.

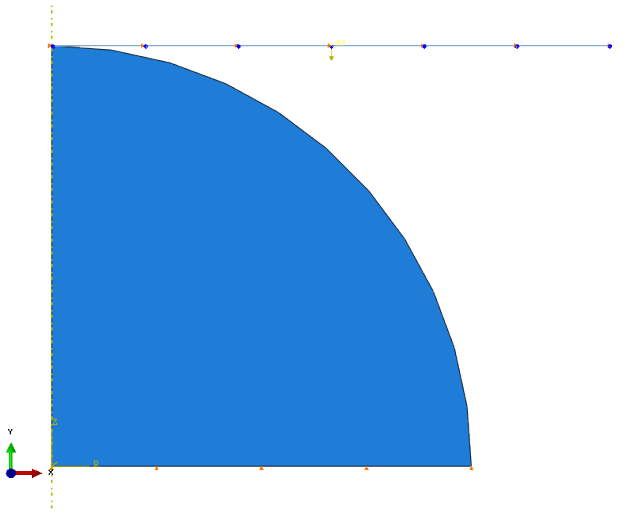

Figure 5.8: Finite element model of the Ugelstad particle.

5.2.2 Experimental data

The experimental data consists of a set of time-series with different load-times t_R, holding times t_H and peak loads $P2$. As seen from the Force-Deflection curve in figure 5.9 the material is highly non-linear and load-rate dependent.

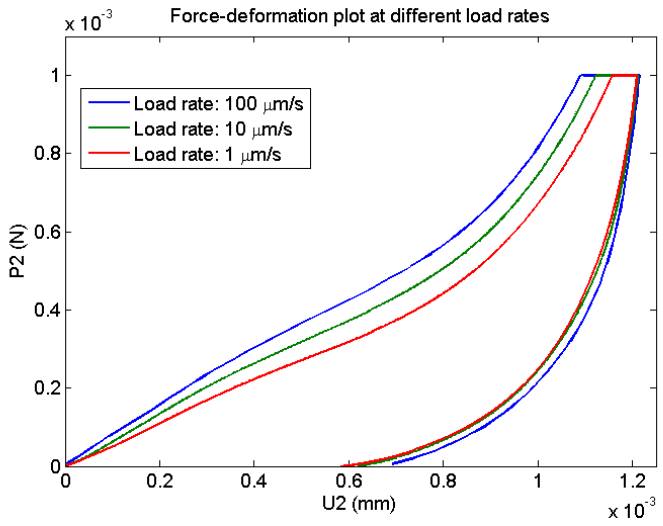

Figure 5.9: Force-deflection curve of the experimental data at different load rates.

5.2.3 Results

The time-series with peak load $P2 = 1mN$, load-time $t_R = 10s$ and holding time $t_H = 100s$ have been analyzed with the inverse FEM-procedure described in section 5.1.2 with the residual function defined as

$$f_i = \frac{(U2_2^{FEM})_i - (U2_2^{EXP})_i}{(U2_2^{EXP})_i} \tag{5.4}$$

where $(U2_2^{FEM})_i$ and $(U2_2^{EXP})_i$ is the deflection of the indenter and the first data point is taken at $t = 3s$ to avoid dividing by values close to zero. The results using 1 viscous element with β set to one is shown in table 5.6.

The results in figure 5.10 and 5.11 shows that the fit of the deflection curve after the peak load is good for the Yeoh material model, but the material models used in the analysis can not capture the non-linear force-deflection curve found by the experimental data during loading with the initial assumptions.

Material model	NH1	NH2	NHC	YEOHV
$C1$	909.9	2110.8	442.7	508.8
$D1$	$20.4 \cdot 10^{-3}$	$99.9 \cdot 10^{-3}$	$19.4 \cdot 10^{-3}$	$10.7 \cdot 10^{-3}$
η^1_{DEV}	2507.0	6052.6	2636.7	977.6
η^1_{VOL}	2848.0	2423.6	1003.1	160.3
β^1	1	1	1	1
$C2$				-146.8
$C3$				4.8
$D2$				15.8
$D3$				$17.9 \cdot 10^{-3}$
$\|\|\boldsymbol{f}\|\|^2$	$24.0 \cdot 10^{-2}$	$9.2 \cdot 10^{-2}$	$14.9 \cdot 10^{-2}$	$9.1 \cdot 10^{-2}$

Table 5.6: Material parameters identified from experimental data with load $P2 = 1000\mu N$, ramp-time $t_R = 10s$ and hold time $t_H = 100s$ with 1 viscous element and $\beta = 1$.

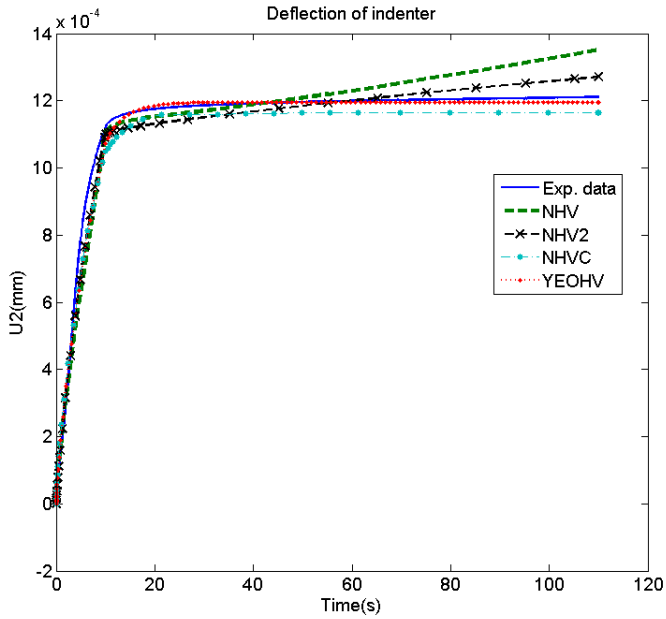

Figure 5.10: Deflection at the indenter with the different material models with material parameters from table 5.6.

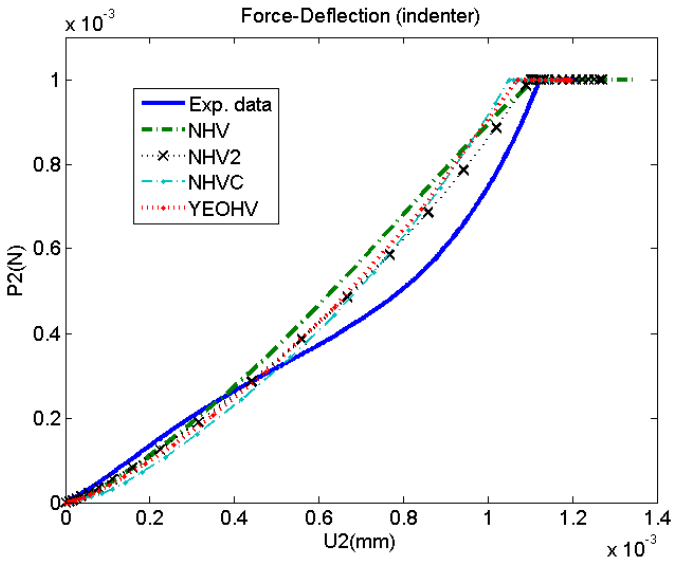

Figure 5.11: Force-deflection plot with the different material models with material parameters from table 5.6.

Another analysis allowing the material scaling factor β to vary was performed for the materials NH2 and NHC with two viscous elements. The material NH1 was analyzed with only one viscous element due to an error in the analysis, but will be used to compare with the other results. The resulting material parameters are shown in table 5.7 while the resulting force-deflection plot is shown in figure 5.12.

Material model	NH1	NH2	NHC
$C1$	101.9	94.2	96.7
$D1$	$0.98 \cdot 10^{-3}$	$0.69 \cdot 10^{-3}$	$0.51 \cdot 10^{-3}$
η^1_{DEV}/β^1	64.7	215.7	199.2
η^1_{VOL}/β^1	5391.9	6768.4	2089.3
β^1	4.75	0.03	0.01
η^2_{DEV}/β^2		8.2	9.0
η^2_{VOL}/β^2		466.2	232.7
β^2		27.0	25.4
$\|\|\boldsymbol{f}\|\|^2$	$5.37 \cdot 10^{-2}$	$4.07 \cdot 10^{-2}$	$4.12 \cdot 10^{-2}$

Table 5.7: Material parameters identified from experimental data with load $P2 = 1000\mu N$, ramp-time $t_R = 10s$ and hold time $t_H = 100s$ with two viscous element and variable β values.

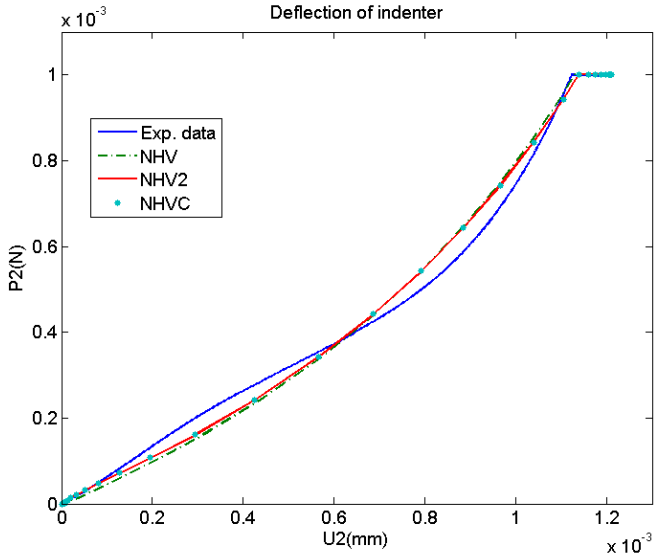

Figure 5.12: Force-deflection plot with the different material models with material parameters from table 5.7.

5.2.4 Discussion

As seen in figure 5.11, the material models used in the fitting procedure was not successful in accurately predicting the force-deflection curve from the experimental data with one viscous element and with the material scaling $\beta = 1$. The impact on the resulting time-deflection curve is shown in figure 5.13 for the Yeoh-material model for different peak loads and a constant load rate of $0.1\frac{mN}{s}$. The fit is good for the values of $P2$ where the Yeoh-materials force-deflection curve is close to the experimental curve but not at the points where it deviates from the curve.

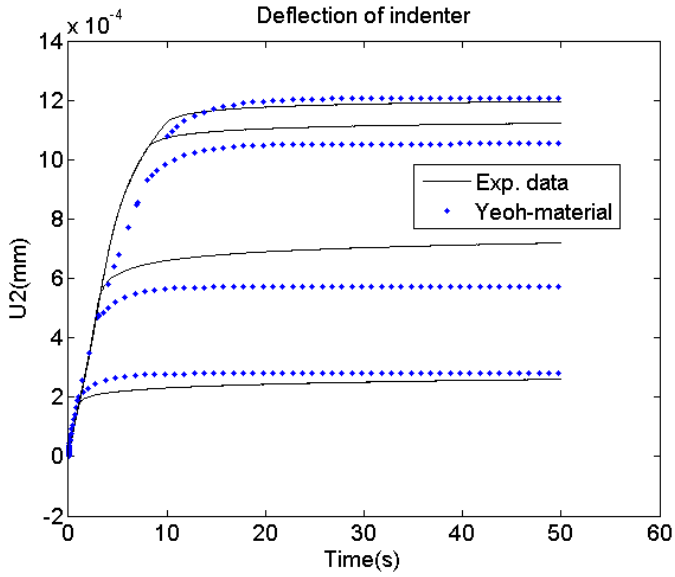

Figure 5.13: Time-deflection plot of the Yeoh-material at peak loads $P2 = 100, 300, 800, 1000\mu N$ with material parameters from table 5.6.

Looking at the values of D_1 and C_1 for the Neo-Hookean material models and recalling that the initial shear-modulus $G = 2C_1$ and the initial bulk modulus $\kappa = \frac{2}{D_1}$ ($\kappa = \frac{4}{D_1}$ for NH2), it is clear that the inverse FEM-procedure predicts very low values of κ compared to G as seen in table 5.8. From linear elasticity the relationship between Poisson's ratio ν, the bulk modulus and the shear modulus is given as Slaughter (2002, chap. 5)

$$\frac{\kappa}{G} = \frac{2(1+\nu)}{3(1-2\nu)}. \tag{5.5}$$

It may then be seen from table 5.8 that the results leads to negative values of Poisson's ratio. While this is found to be the case for some rare materials Evans (1991) it is very unlikely to be the case for the polymer particle tested. The material properties found in table 5.6 must then be discarded as unphysical and a new analysis with stricter lower bounds on the initial bulk modulus or $2/D_1$ is performed.

Material model	NH1	NH2	NHC	YEOHV
$(\frac{\kappa}{G})^{(0)}$	0.11	0.02	0.23	0.37
ν^0	-0.63	-0.91	-0.39	-0.21

Table 5.8: Approximate ratio between the bulk modulus and the shear modulus and initial Poisson's ratio for the tested material models with material parameters from table 5.6.

Since the initial fit was bad with one viscous element and a material scaling parameter $\beta = 1$, a new analysis with two viscous elements and a varying material scaling parameter was performed for the material models NH2 and NHC, while the inverse FEM-procedure was performed with one viscous element and varying β for the NH1 material model. The Yeoh material model was not analyzed due to time constraints.

The results proved to both better fit the force-deflection curve and give physically plausible initial values of Poisson's ratio ν^0 for the material models, as shown in figure 5.12 and table 5.9. While the material models still struggle to match the "s"-shaped force-deflection curve, adding more viscous elements or changing the initial material values for the inverse FEM-procedure might help increase the fit to the experimental data.

The curve-fit for the NH1 material model with only one viscous element is almost as good as for the other material models with two viscous elements. This may indicate that a more advanced hyperelastic material model is necessary in order to model the material or that the initial material parameter values are close to a local minimum of the residual function $\boldsymbol{f}(\boldsymbol{x})$.

Material model	NH1	NH2	NHC
$(\frac{\kappa}{G})^{(0)}$	10.1	30.9	20.2
ν^0	0.45	0.48	0.47

Table 5.9: Approximate ratio between the bulk modulus and the shear modulus and initial Poisson's ratio for the tested material models with material parameters from table 5.7.

Figure 5.14 shows the time-deflection plots at a load rate of $0.1\frac{mN}{s}$ using the NH2 material model with two viscous elements. While the curve fit is decent for some of the high peak loads ($P2 = 800, 100\mu N$) the response deviates by up to 25 % for the peak load of 100 μN. The creep seems also to continue at a lower rate than the experimental data indicates after the peak load is reached, which may be modeled better with an extra viscous element with higher relaxation times.

The nanoindentation device is reported to have an accuracy of 100 nN and 1 nm He et al. (2009) which gives high accuracy compared to the experimental data which have peak loads between 100-1000 mN and peak deflections between 0.27-1.2 μm so the error from the experimental data is most likely small.

The finite element model and the initial simplification of symmetry by modeling only half the sphere may lead to some modeling errors, but an initial test of the axisymmetric model with the whole sphere yielded the expected result; twice the deflection of the half-sphere. The contact properties chosen was 'hard' normal behavior and frictionless tangential behavior, these choices may have some impact on the end result.

As discussed in Reese and Govindjee (1998), viscoelastic models based on linear evolution equations is not suitable for systems undergoing large creep deformations, in this case the materials creep deformations seems to be relatively small and a model based on finite linear viscoelasticity may give a successful result with less computational effort. Also introducing NEQ material parameters independent of the EQ material parameters may give better results, but the disadvantage with this approach is that more parameters need to be fit to experimental data.

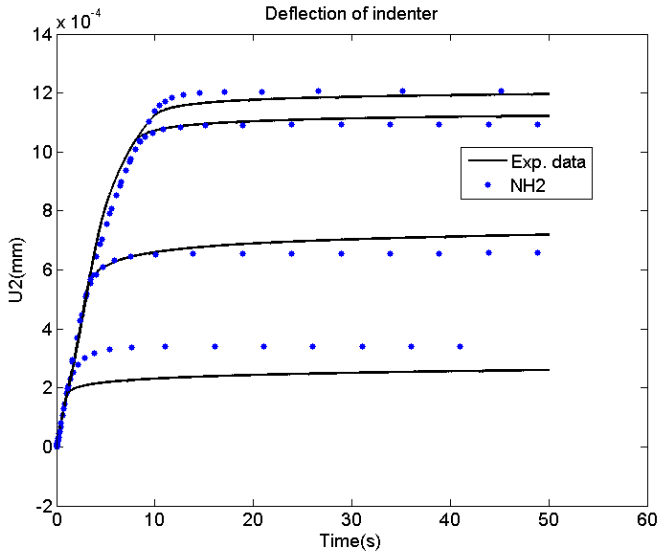

Figure 5.14: Time-deflection plot of the NH2-material at peak loads $P2 = 100, 300, 800, 1000\mu N$ with material parameters from table 5.7.

In Ogden et al. (2004) the problems concerning fitting of hyperelastic material parameters to experimental data and the issue with non-unique sets of optimal material parameters which may occur during this process is discussed. In the article they show how a set of optimal parameters found from one experimental test results in bad values for an experiment with different boundary conditions. In this case the material parameters are only analyzed by solving one boundary-value problem which may cause the material parameters to be incompatible with solving other boundary-value problems.

Chapter 6

Conclusion

As discussed in chapter 4, the implemented UMAT-subroutines behave well numerically during large deformation and shows the expected viscoelastic response when it comes to force-relaxation and creep during finite element analysis. The hydrogel models sensibility to change in normalized chemical potential μ^* is also discussed. Due to the high rate of swelling close to $\mu^* = 0$ small time-steps are necessary for the solution to converge. The relation between the material scaling parameter β, the material parameters and the viscosity η have also been shown for the linearized case with the resulting relaxation time. With this in mind, interpreting further results in terms of relaxation times instead of viscosities, might give a more intuitive understanding of the physical property of the material.

Even though there was some issues with the experimental hydrogel data, the viscoelastic material model have been able to match the data from the relaxation experiment with a spherical indenter to a high degree of accuracy. From a finite element modeling point of view, the experiment with a flat indenter causes issues with distorted elements and may not be recommended for the purpose of extracting material parameters with the inverse FEM-procedure.

The variations of the Neo-Hookean material model were not successful in mimicking the response of the acrylic particle accurately. The Yeoh material model may provide better results, but based on the results from the first analysis with the material scaling parameter set to 1, a model better suited for non-linear behavior in compression is most likely necessary to properly model the particles mechanical response.

Chapter 7

Further work

Hydrogel materials have a large variety of possible applications. The developed viscoelastic hydrogel material model will hopefully provide a good tool for the modeling of hydrogel materials in the future.

Acknowledgment

I would like to thank Assoc. Prof. Victorien Prot for helpful guidance on this master thesis. I am also grateful to Prof. Bjrn Skallerud for initiating this project and Division of Biophysics and Medical Technology, NTNU and NTNU Nanomechanical lab for providing the experimental data for this master thesis.

Bibliography

ABAQUS, 2013. Version 6.13. Dassault Systèmes.

Armero, F., 2014. Lecture notes: Structural mechanics, lecture notes from the course CE232: Structural Mechanics at the Department of Civil and Environmental Engineering, UC Berkeley Spring 2014.

Bonet, J., 2001. Large strain viscoelastic constitutive models. International Journal of Solids and Structures 38 (17), 2953–2968.

Evans, K. E., 1991. Auxetic polymers: a new range of materials. Endeavour 15 (4), 170–174.

Flory, P., Gordon, M., McCrum, N., 1976. Statistical thermodynamics of random networks [and discussion]. Proceedings of the Royal Society of London. Series A, Mathematical and Physical Sciences, 351–380.

Galaev, I. Y., Mattiasson, B., 1999. smartpolymers and what they could do in biotechnology and medicine. Trends in biotechnology 17 (8), 335–340.

Gentile, G., Greco, F., Larobina, D., 2013. Stress-relaxation behavior of a physical gel: Evidence of co-occurrence of structural relaxation and water diffusion in ionic alginate gels. European Polymer Journal 49 (12), 3929–3936.

Gurtin, M. E., 1982. An introduction to continuum mechanics. Academic press.

He, J., Zhang, Z., Kristiansen, H., 2009. Compression properties of individual micron-sized acrylic particles. Materials Letters 63 (20), 1696–1698.

Hong, W., Zhao, X., Zhou, J., Suo, Z., 2008. A theory of coupled diffusion and large deformation in polymeric gels. Journal of the Mechanics and Physics of Solids 56 (5), 1779–1793.

Kang, M. K., Huang, R., 2010. A variational approach and finite element implementation for swelling of polymeric hydrogels under geometric constraints. Journal of Applied Mechanics 77 (6), 061004.

Lubliner, J., 1985. A model of rubber viscoelasticity. Mechanics Research Communications 12 (2), 93–99.

Marsden, J. E., Hughes, T. J., 1994. Mathematical foundations of elasticity. Courier Corporation.

MATLAB, 2013. version 8.10.0 (R2013a). The MathWorks Inc., Natick, Massachusetts.

McGinty, B., published date unknown. `http://www.continuummechanics.org/cm/index.html`, [Online; accessed 1-May-2015].

Ogden, R., Saccomandi, G., Sgura, I., 2004. Fitting hyperelastic models to experimental data. Computational Mechanics 34 (6), 484–502.

Ogden, R. W., 1997. Non-linear elastic deformations. Courier Corporation.

Pritchard, R. H., Lava, P., Debruyne, D., Terentjev, E. M., 2013. Precise determination of the poisson ratio in soft materials with 2d digital image correlation. Soft Matter 9 (26), 6037–6045.

Prot, V., Skallerud, B., Holzapfel, G., 2007. Transversely isotropic membrane shells with application to mitral valve mechanics. constitutive modelling and finite element implementation. International journal for numerical methods in engineering 71 (8), 987–1008.

Reese, S., Govindjee, S., 1998. A theory of finite viscoelasticity and numerical aspects. International Journal of Solids and Structures 35 (26), 3455–3482.

Slaughter, W. S., 2002. The linearized theory of elasticity. Springer.

Tschoegl, N. W., 2012. The phenomenological theory of linear viscoelastic behavior: An introduction. Springer Science & Business Media.

Urayama, K., Takigawa, T., 2012. Volume of polymer gels coupled to deformation. Soft Matter 8 (31), 8017–8029.

Yeoh, O., 1993. Some forms of the strain energy function for rubber. Rubber Chemistry and technology 66 (5), 754–771.

Appendix A

Five UMAT-subroutines coded in *.for* files have been made as part of this Master Thesis. The material properties (PROPS) for input from ABAQUS are numbered as follows

PROPS	NH1	NH2	NHC	YEOHV	KANGViscous
1	$C1$	$C1$	$C1$	$C1$	Nk_BT
2	$D1$	$D1$	$D1$	$C2$	$N\nu$
3	η_{DEV}	η_{DEV}	η_{DEV}	$C3$	χ
4	η_{VOL}	η_{VOL}	η_{VOL}	$D1$	η_{DEV}
5	β	β	β	$D2$	η_{VOL}
6				$D3$	β
7				η_{DEV}	
8				η_{VOL}	
9				β	

where the material models NH1, NH2, NH3 and YEOHV (for abbreviation see chapter 4) are coded in the FORTRAN files *NeoHookeVisco.for*, *NeoHookeViscoV2.for*, *NeoHookeCoupled.for* and *YEOH3visco.for*. The hydrogel material model, KANGViscous, is coded in the FORTRAN file *KANGViscous.for*. Additionally the FORTRAN files with *2EL* or *3EL* at the end of the file name are coded with 2 and 3 viscous elements. The state-variables (STATEV) are numbered as follows

STATEV	NH1	NH2	NHC	YEOHV	KANGViscous
1	C_{11}^{-1}	C_{11}^{-1}	C_{11}^{-1}	C_{11}^{-1}	$\lambda_1^{(0)}$
2	C_{22}^{-1}	C_{22}^{-1}	C_{22}^{-1}	C_{22}^{-1}	$\lambda_2^{(0)}$
3	C_{33}^{-1}	C_{33}^{-1}	C_{33}^{-1}	C_{33}^{-1}	$\lambda_3^{(0)}$
4	C_{12}^{-1}	C_{12}^{-1}	C_{12}^{-1}	C_{12}^{-1}	C_{11}^{-1}
5	C_{13}^{-1}	C_{13}^{-1}	C_{13}^{-1}	C_{13}^{-1}	C_{22}^{-1}
6	C_{23}^{-1}	C_{23}^{-1}	C_{23}^{-1}	C_{23}^{-1}	C_{33}^{-1}
7					C_{12}^{-1}
8					C_{13}^{-1}
9					C_{23}^{-1}

The 2-element and 3-element subroutines requires a minimum of 12 and 18 (15 and 21 for the hydrogel material) state-variables with the numbering continuing in the same pattern as shown in the table.

For the viscoelastic models NH1, NH2, NHC and YEOHV, the comments in the FORTRAN files and chapter 3 should be sufficient for understanding the code. As the FORTRAN file *KANGViscous.for* contain some extra subroutines and may need to be modified, parts of the code will be covered.

KANGViscous

```
C    MATERIAL PROPERTIES
C
C     DNKT = N*K*T  DvN = v*N   DkTV = K*T/v    BmukT = mu/K*T
C     K := BOLTZMANNS CONSTANT  N := # POLYMER CHAINS / UNIT VOLUME
C     T := ABSOLUTE TEMPERATURE v := VOLUME PER SOLVENT MOLECULE
C     mu := CHEMICAL POTENTIAL   chi := DIMENSIONLESS ENERGY PARAMETER
C     NKT := INITIAL SHEAR MODULUS  BETA := SCALING CONSTANT OF NEQ-STRESS
C     VISCdev := DEVIATORIC VISCOSITY
C     VISCVOL := VOLUMETRIC VISCOSITY
C -----------------------------------------------------------------
C
      DNKT=PROPS(1)
      DvN=PROPS(2)
      DkTV=DNKT/DvN
      chi=PROPS(3)
      VISCdev=PROPS(4)
      VISCvol=PROPS(5)
      BETA=PROPS(6)
C
C     For use in coupled temp-disp analysis
c      BmukT=Bmukt0+TEMP
C
      BmukT=-0.04D0
C
C     CALCULATE INITIAL SWELLING
C
      if (KSTEP.EQ.1 .AND. KINC.EQ.1) then
        CALL DJ0calc (DvN, chi, BmukT, DJ0c)
        STATEV(1)=DJ0c**(ONE/THREE)
        STATEV(2)=DJ0c**(ONE/THREE)
        STATEV(3)=DJ0c**(ONE/THREE)
      END IF
      Dl01=STATEV(1)
      Dl02=STATEV(2)
      Dl03=STATEV(3)
C
```

At the start of the FORTRAN script the material properties are defined, six in total and another three for each extra viscous element. The variable named *BmukT* is the normalized chemical potential $\mu^* = \frac{\mu}{k_B T}$ and must be modified for use in a coupled temperature-displacement analysis. The subroutine *DJOcalc* calculates the initial swelling values $\lambda^{(0)}$ as discussed in section 3.4.1 with a Newton-iteration of equation (3.53). If a prescribed initial swelling is used, this part of the code may be commented out and *STATEV(1)*, *STATEV(2)* and *STATEV(3)* can be prescribed directly. The initial value of μ^* (*BmukT*) may then be calculated from equation (3.53).

```
      SUBROUTINE DJ0calc (vN, chi, DmukT, DJ0)

      IMPLICIT NONE

      DOUBLE PRECISION, INTENT(IN) :: vN
      DOUBLE PRECISION, INTENT(IN) :: chi
      DOUBLE PRECISION, INTENT(IN) :: DmukT

      DOUBLE PRECISION, PARAMETER :: VARTEST = 1.0D-8
      DOUBLE PRECISION, INTENT(OUT) :: DJ0
      DOUBLE PRECISION :: VAR0
      DOUBLE PRECISION :: VAR1
      DOUBLE PRECISION :: F
      DOUBLE PRECISION :: DF
      integer :: K1
```

```
      VAR0=1.5D0
      do K1=1,25,1
        F=vN*VAR0**(-1.D0/3.D0)
     1   + (log(1.D0-1.D0/VAR0)+(1.D0-vN)/VAR0+chi/(VAR0**2.D0)-DmukT)
        DF=-(vN/3.D0)*VAR0**(-4.D0/3.D0)-(1.D0-vN)/(VAR0**2.D0)
     1   - 2.D0*chi/(VAR0**3.D0)+1.D0/(VAR0**2.D0-VAR0)

      VAR1=VAR0-F/DF

        IF (ABS(VAR1-VAR0) .LE. VARTEST) THEN
            DJ0 = VAR1
            RETURN
        END IF
       VAR0=VAR1

      END DO

      RETURN

      END SUBROUTINE DJ0calc
```

The variables *fvisc* and *gvisc* are defined in equation (3.52) and (3.56), so if only the volumetric part of the strain-energy function is changed, replacing these two variables will modify the material tangent and EQ-stress sufficiently.

```
C     VARIABLES
C
      vN=DvN
      chhi=chi
      BI1=BBTOT(1,1)+BBTOT(2,2)+BBTOT(3,3)
      fvisc=(LOG(ONE-ONE/DETTOT)*DETTOT+ONE-vN+chi/DETTOT
     1       -BmukT*DETTOT)/vN
      gvisc=(LOG(ONE-ONE/DETTOT)*DETTOT+DETTOT/(DETTOT-1)-chi/DETTOT
     1       -BmukT*DETTOT)/vN
C
C     CALCULATE EQ CAUCHY-STRESS
C
      sig(1,1) = DNKT*(BTOT(1,1)+fvisc)/DETTOT
      sig(1,2) = DNKT*BTOT(1,2)/DETTOT
      sig(1,3) = DNKT*BTOT(1,3)/DETTOT
      sig(2,1) = DNKT*BTOT(2,1)/DETTOT
      sig(2,2) = DNKT*(BTOT(2,2)+fvisc)/DETTOT
      sig(2,3) = DNKT*BTOT(2,3)/DETTOT
      sig(3,1) = DNKT*BTOT(3,1)/DETTOT
      sig(3,2) = DNKT*BTOT(3,2)/DETTOT
      sig(3,3) = DNKT*(BTOT(3,3)+fvisc)/DETTOT
C
```

From an initial state of zero mechanical load $\boldsymbol{C}_i = \boldsymbol{I}$ so the variables STATEV(4-9) is defined at the first step in the first increment forming an array of ones and zeros to make $\boldsymbol{C}_i^{-1} = \boldsymbol{I}$ (*CiINV0*) at this increment. The subroutine *BECALCMOD* calculates the NEQ Kirchhoff stress $\boldsymbol{\tau}_{NEQ}$ and the elastic left Cauchy-Green strain tensor $\boldsymbol{b}_e$ as well as the vectors and tensors used to calculate the NEQ spatial tangent modulus $\mathbb{c}_{NEQ}$ as covered in section 2.4.3 and 2.4.4. The subroutine *DNEQTANGENT* calculates the NEQ spatial tangent modulus and returns the tangent modulus $\mathbb{C}^{ABA}$ used in *ABAQUS/Standard* as a 6 by 6 matrix (Voigt form) by using the output from *BECALCMOD*. The state-variables are then updated with the new values of $\boldsymbol{C}_i^{-1}$ after the local iteration.

```
C     DEFINE INITIAL STATE-VARIABLE, INV(Ci)
C
      IF (KSTEP.EQ.1 .AND. KINC.EQ.1) THEN
       STATEV(4)=ONE
       STATEV(5)=ONE
```

```
        STATEV(6)=ONE
        STATEV(7)=ZERO
        STATEV(8)=ZERO
        STATEV(9)=ZERO
      END IF
C
      CiINV0(1,1)=STATEV(4)
      CiINV0(1,2)=STATEV(7)
      CiINV0(1,3)=STATEV(8)
      CiINV0(2,1)=STATEV(7)
      CiINV0(2,2)=STATEV(5)
      CiINV0(2,3)=STATEV(9)
      CiINV0(3,1)=STATEV(8)
      CiINV0(3,2)=STATEV(9)
      CiINV0(3,3)=STATEV(6)
C
C     CALCULATE Be, NEQ KIRCHOFF STRESS AND NEQ MATERIAL TANGENT
C
      DTID=DTIME
        CALL BECALCMOD (DvN, DkTV, chi, BmukT, BETA,NDI,NSHR,
     1              VISCdev, VISCvol, DTID,
     1              DFTOT, CiINV0, Be, TAUNEQ, TAUVEC, DLTR, DPVEC, CALG)
C
C
        CALL DNEQTANGENT (DETTOT, TAUVEC, DLTR, DPVEC,
     1                        CALG, TAUNEQ, DDSDDE2)
C
C     UPDATE STATE-VARIABLE
C
      CALL M33INV(Be, BeINV, FLAG)
      CiTEMP=MATMUL(BeINV,DFTOT)
      Ci=MATMUL(TRANSPOSE(DFTOT),CiTEMP)
      CALL M33INV(Ci, CiINV1, FLAG)
C
      STATEV(4)=CiINV1(1,1)
      STATEV(5)=CiINV1(2,2)
      STATEV(6)=CiINV1(3,3)
      STATEV(7)=CiINV1(1,2)
      STATEV(8)=CiINV1(1,3)
      STATEV(9)=CiINV1(2,3)
C
```

The variables f and g in the subroutine *BECALCMOD* is also defined by equation (3.52) and (3.56) and may be modified without changing the rest of the code (note that $y = J_e$).

```
      do K3=1,175,1
C
CCC   Explanation of the variables
CCC   DETE:=Je CC Q0(A):=Lambda^2_A CC DEVA:=dev(Be_A)
CCC   TR3:=tr(Be)/3 CC f:=f(y) CC g:=g(y)
CCC   ETRIAL(A):=epsilon^tr_Ae CC E0(A):=epsilon_Ae at step k
C
        DETE=(Q0(1)*Q0(2)*Q0(3))**(1.0D0/2.0D0)
        TR3=(Q0(1)+Q0(2)+Q0(3))/3.D0
        DEV1=(2.D0*Q0(1)-Q0(2)-Q0(3))/3.D0
        DEV2=(2.D0*Q0(2)-Q0(1)-Q0(3))/3.D0
        DEV3=(2.D0*Q0(3)-Q0(1)-Q0(2))/3.D0
        f=(LOG(1.0D0-1.0D0/DETE)*DETE+
     1     1.0D0-DvN+CHI/DETE-DMUKT*DETE)/DvN
        g=(LOG(1.0D0-1.0D0/DETE)*DETE+
     1     DETE/(DETE-1.0D0)-CHI/DETE-DMUKT*DETE)/DvN
        E0(1)=1.D0/2.D0*LOG(Q0(1))
        E0(2)=1.D0/2.D0*LOG(Q0(2))
        E0(3)=1.D0/2.D0*LOG(Q0(3))
C
```

Appendix B

Relation of the spatial and material tangent modulus

Given the material tangent modulus $\mathbb{C}$ defined from

$$\dot{\boldsymbol{S}} = \mathbb{C} : \dot{\boldsymbol{E}} = \mathbb{C} : (\boldsymbol{F}^T \cdot \boldsymbol{d} \cdot \boldsymbol{F})$$

and the time derivative of the Kirchhoff stress $\boldsymbol{\tau}$ given in terms of the second Piola-Kirchhoff stress as

$$\begin{aligned}\dot{\boldsymbol{\tau}} = \overset{\cdot}{\overline{\boldsymbol{F} \cdot \boldsymbol{S} \cdot \boldsymbol{F}^T}} &= \boldsymbol{l} \cdot (\boldsymbol{F} \cdot \boldsymbol{S} \cdot \boldsymbol{F}^T) + (\boldsymbol{F} \cdot \boldsymbol{S} \cdot \boldsymbol{F}^T) \cdot \boldsymbol{l}^T + \boldsymbol{F} \cdot \dot{\boldsymbol{S}} \cdot \boldsymbol{F}^T \\ &= \boldsymbol{l} \cdot \boldsymbol{\tau} + \boldsymbol{\tau} \cdot \boldsymbol{l}^T + \boldsymbol{F} \cdot \dot{\boldsymbol{S}} \cdot \boldsymbol{F}^T.\end{aligned}$$

Combining the two equations then leads to

$$\begin{aligned}\dot{\boldsymbol{\tau}} &= \boldsymbol{l} \cdot \boldsymbol{\tau} + \boldsymbol{\tau} \cdot \boldsymbol{l}^T + \boldsymbol{F} \cdot \Big(\mathbb{C} : (\boldsymbol{F}^T \cdot \boldsymbol{d} \cdot \boldsymbol{F})\Big) \cdot \boldsymbol{F}^T \\ &= \boldsymbol{l} \cdot \boldsymbol{\tau} + \boldsymbol{\tau} \cdot \boldsymbol{l}^T + \Big(\boldsymbol{F} \cdot \boldsymbol{F} \cdot \mathbb{C} \cdot \boldsymbol{F}^T \cdot \boldsymbol{F}^T\Big) : \boldsymbol{d} \\ &= \boldsymbol{l} \cdot \boldsymbol{\tau} + \boldsymbol{\tau} \cdot \boldsymbol{l}^T + J\mathbb{c} : \boldsymbol{d}\end{aligned}$$

where $\mathbb{c}$ is the spatial tangent modulus.

Frame indifference of the Jaumann-rate

Starting with the Lie-derivative of the Kirchhoff stress-tensor, it can be shown that frame indifference is satisfied. $\boldsymbol{F}$, $\boldsymbol{\tau}$ and $\boldsymbol{d}$ are frame indifferent such that

$$\begin{aligned}\boldsymbol{F}^* &= \boldsymbol{Q} \cdot \boldsymbol{F} \\ \boldsymbol{\tau}^* &= \boldsymbol{Q} \cdot \boldsymbol{\tau} \cdot \boldsymbol{Q}^{\boldsymbol{T}} \\ \boldsymbol{d}^* &= \boldsymbol{Q} \cdot \boldsymbol{d} \cdot \boldsymbol{Q}^{\boldsymbol{T}}.\end{aligned}$$

The rotation tensor $\boldsymbol{Q}$ have the following properties

$$\begin{aligned}\boldsymbol{Q} \cdot \boldsymbol{Q}^T &= \boldsymbol{I} \\ \overset{\cdot}{\overline{\boldsymbol{Q} \cdot \boldsymbol{Q}^{\boldsymbol{T}}}} = \dot{\boldsymbol{I}} = \boldsymbol{0} &= \dot{\boldsymbol{Q}} \cdot \boldsymbol{Q}^{\boldsymbol{T}} + \boldsymbol{Q} \cdot \dot{\boldsymbol{Q}}^{\boldsymbol{T}} = \boldsymbol{0}.\end{aligned}$$

The velocity gradient under a change of observer is

$$\boldsymbol{l}^* = \dot{\boldsymbol{F}}^* \cdot (\boldsymbol{F}^*)^{-1} = (\dot{\boldsymbol{Q}} \cdot \boldsymbol{F} + \boldsymbol{Q} \cdot \dot{\boldsymbol{F}}) \cdot (\boldsymbol{F}^{-\boldsymbol{1}} \cdot \boldsymbol{Q}^{\boldsymbol{T}})$$

$$= \dot{\boldsymbol{Q}} \cdot \boldsymbol{Q^T} + \boldsymbol{Q} \cdot (\dot{\boldsymbol{F}} \cdot \boldsymbol{F^{-1}}) \cdot \boldsymbol{Q^T} = \dot{\boldsymbol{Q}} \cdot \boldsymbol{Q^T} + \boldsymbol{Q} \cdot \boldsymbol{l} \cdot \boldsymbol{Q^T}$$

while the time-derivative of $\boldsymbol{\tau}^*$ is

$$\dot{\boldsymbol{\tau}^*} = \dot{\boldsymbol{Q}} \cdot \boldsymbol{\tau} \cdot \boldsymbol{Q^T} + \boldsymbol{Q} \cdot \dot{\boldsymbol{\tau}} \cdot \boldsymbol{Q^T} + \boldsymbol{Q} \cdot \boldsymbol{\tau} \cdot \dot{\boldsymbol{Q^T}}.$$

By applying these properties to the Lie-derivative of Kirchhoff stress during a change of observer

$$\begin{aligned}
\boldsymbol{\pounds_v \tau^*} &= \dot{\boldsymbol{\tau}^*} - \boldsymbol{l^*} \cdot \boldsymbol{\tau^*} - \boldsymbol{\tau^*} \cdot (\boldsymbol{l^*})^T \\
&= \dot{\boldsymbol{Q}} \cdot \boldsymbol{\tau} \cdot \boldsymbol{Q^T} + \boldsymbol{Q} \cdot \dot{\boldsymbol{\tau}} \cdot \boldsymbol{Q^T} + \boldsymbol{Q} \cdot \boldsymbol{\tau} \cdot \dot{\boldsymbol{Q^T}} \\
-(\dot{\boldsymbol{Q}} \cdot \boldsymbol{Q^T} + \boldsymbol{Q} \cdot \boldsymbol{l} \cdot \boldsymbol{Q^T}) \cdot (\boldsymbol{Q} \cdot \boldsymbol{\tau} \cdot \boldsymbol{Q^T}) &- (\boldsymbol{Q} \cdot \boldsymbol{\tau} \cdot \boldsymbol{Q^T}) \cdot (\boldsymbol{Q} \cdot \dot{\boldsymbol{Q^T}} + \boldsymbol{Q} \cdot \boldsymbol{l^T} \cdot \boldsymbol{Q^T}) \\
= \boldsymbol{Q} \cdot (\dot{\boldsymbol{\tau}} - \boldsymbol{l} \cdot \boldsymbol{\tau} - \boldsymbol{\tau} \cdot \boldsymbol{l^T}) \cdot \boldsymbol{Q^T} &+ \dot{\boldsymbol{Q}} \cdot \boldsymbol{\tau} \cdot \boldsymbol{Q^T} - \dot{\boldsymbol{Q}} \cdot \boldsymbol{\tau} \cdot \boldsymbol{Q^T} + \boldsymbol{Q} \cdot \boldsymbol{\tau} \cdot \dot{\boldsymbol{Q^T}} - \boldsymbol{Q} \cdot \boldsymbol{\tau} \cdot \dot{\boldsymbol{Q^T}} \\
&= \boldsymbol{Q} \cdot \boldsymbol{\pounds_v \tau} \cdot \boldsymbol{Q^T}
\end{aligned}$$

it can be concluded that the Lie-derivative of the Kirchhoff stress is frame indifferent.

Finally the Jaumann rate is defined as,

$$\boldsymbol{\tau}^{\Delta J} = \dot{\boldsymbol{\tau}} - \boldsymbol{w\tau} - \boldsymbol{\tau w^T} = \dot{\boldsymbol{\tau}} - \boldsymbol{(l-d)\tau} - \boldsymbol{\tau (l-d)^T} = \boldsymbol{\pounds_v \tau} + \boldsymbol{d\tau} + \boldsymbol{\tau d}$$

and with the change of observer,

$$\begin{aligned}
\boldsymbol{\tau^*}^{\Delta J} &= \boldsymbol{\pounds_v \tau^*} + \boldsymbol{d^* \tau^*} + \boldsymbol{\tau^* d^*} \\
= \boldsymbol{Q} \cdot \boldsymbol{\pounds_v \tau} \cdot \boldsymbol{Q^T} &+ (\boldsymbol{Q} \cdot \boldsymbol{d} \cdot \boldsymbol{Q}^T) \cdot (\boldsymbol{Q} \cdot \boldsymbol{\tau} \cdot \boldsymbol{Q^T}) + (\boldsymbol{Q} \cdot \boldsymbol{\tau} \cdot \boldsymbol{Q}^T) \cdot (\boldsymbol{Q} \cdot \boldsymbol{d} \cdot \boldsymbol{Q^T}) \\
&= \boldsymbol{Q} \cdot \boldsymbol{\tau}^{\Delta J} \cdot \boldsymbol{Q^T}
\end{aligned}$$

which concludes that the Jaumann, rate which is implemented in the Abaqus *UMAT*-subroutine, is indeed frame indifferent.

Exponential mapping of a tensor in $SO(3)$

Given a tensor $\boldsymbol{\Lambda}$ where:

$$\underbrace{\boldsymbol{\Lambda}(\ ;\eta)}_{\boldsymbol{\Lambda}_\eta} \in \mathbb{R}^3 \times S0(3) \ \ \eta \in \mathbb{R} \tag{7.8}$$

the variation of $\delta\boldsymbol{\Lambda}$ is defined as:

$$\delta\boldsymbol{\Lambda} = \frac{d}{d\eta}\boldsymbol{\Lambda}_\eta\Big|_{\eta=0} \tag{7.9}$$

Note that $\delta\boldsymbol{\Lambda} \in so(3)$, where so(3) is the set of linear spaces (tangent spaces of SO(3)) while SO(3) is the manifold group (see figure below). Given the relation:

$$\frac{d\mathbf{\Lambda}_\eta}{d\eta} = \boldsymbol{B}\mathbf{\Lambda}_\eta \tag{7.10}$$

Exponential mapping between so(3) and SO(3) can be performed such that:

$$\mathbf{\Lambda}_\eta = exp\big[\eta \boldsymbol{B}\big]\mathbf{\Lambda}_{\eta=0} \tag{7.11}$$

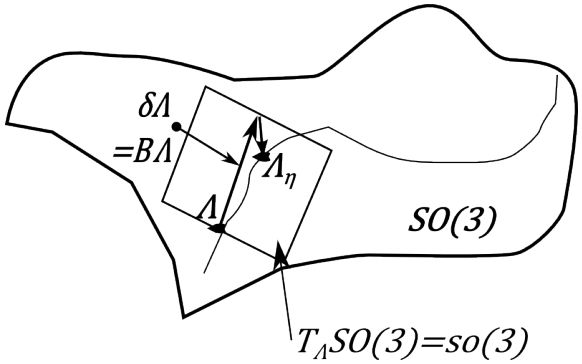

Sketch of the exponential mapping of the variation $\boldsymbol{\delta\Lambda}$ from so(3) to SO(3)

References:
Weisstein, Eric W. ”Exponential Map.” From MathWorld–A Wolfram Web Resource. http://mathworld.wolfram.com/ExponentialMap.html